
Report No. BD545 RPWO #39
FINAL REPORT

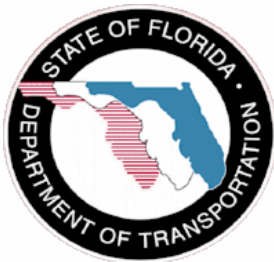
Date: March 2009

Contract Title: Stiffness Evaluation of Neoprene Bearing Pads Under Long-Term Loads
UF Project No. 00051121
Contract No. BD545 RPWO #39

STIFFNESS EVALUATION OF NEOPRENE BEARING PADS UNDER LONG TERM LOADS

Principal Investigator:	Ronald A. Cook, Ph.D., P.E.
Graduate Research Assistant:	Damon T. Allen
Project Manager:	Marcus H. Ansley, P.E.

Department of Civil & Coastal Engineering
College of Engineering
University of Florida
Gainesville, Florida 32611



DISCLAIMER

The opinions, findings, and conclusions expressed in this publication are those of the authors and not necessarily those of the Florida Department of Transportation.

SI* (MODERN METRIC) CONVERSION FACTORS

APPROXIMATE CONVERSIONS TO SI UNITS

SYMBOL	WHEN YOU KNOW	MULTIPLY BY	TO FIND	SYMBOL
LENGTH				
in	inches	25.4	millimeters	mm
ft	feet	0.305	meters	m
yd	yards	0.914	meters	m
mi	miles	1.61	kilometers	km
AREA				
in ²	square inches	645.2	square millimeters	mm ²
ft ²	square feet	0.093	square meters	m ²
yd ²	square yard	0.836	square meters	m ²
ac	acres	0.405	hectares	ha
mi ²	square miles	2.59	square kilometers	km ²
VOLUME				
fl oz	fluid ounces	29.57	milliliters	mL
gal	gallons	3.785	liters	L
ft ³	cubic feet	0.028	cubic meters	m ³
yd ³	cubic yards	0.765	cubic meters	m ³
NOTE: volumes greater than 1000 L shall be shown in m ³				
MASS				
oz	ounces	28.35	grams	g
lb	pounds	0.454	kilograms	kg
T	short tons (2000 lb)	0.907	megagrams (or "metric ton")	Mg (or "t")
TEMPERATURE (exact degrees)				
°F	Fahrenheit	5 (F-32)/9 or (F-32)/1.8	Celsius	°C
ILLUMINATION				
fc	foot-candles	10.76	lux	lx
fl	foot-Lamberts	3.426	candela/m ²	cd/m ²
FORCE and PRESSURE or STRESS				
lbf	poundforce	4.45	newtons	N
lbf/in ²	poundforce per square inch	6.89	kilopascals	kPa

APPROXIMATE CONVERSIONS FROM SI UNITS

SYMBOL	WHEN YOU KNOW	MULTIPLY BY	TO FIND	SYMBOL
LENGTH				
mm	millimeters	0.039	inches	in
m	meters	3.28	feet	ft
m	meters	1.09	yards	yd
km	kilometers	0.621	miles	mi
AREA				
mm ²	square millimeters	0.0016	square inches	in ²
m ²	square meters	10.764	square feet	ft ²
m ²	square meters	1.195	square yards	yd ²
ha	hectares	2.47	acres	ac
km ²	square kilometers	0.386	square miles	mi ²
VOLUME				
mL	milliliters	0.034	fluid ounces	fl oz
L	liters	0.264	gallons	gal
m ³	cubic meters	35.314	cubic feet	ft ³
m ³	cubic meters	1.307	cubic yards	yd ³
MASS				
g	grams	0.035	ounces	oz
kg	kilograms	2.202	pounds	lb
Mg (or "t")	megagrams (or "metric ton")	1.103	short tons (2000 lb)	T
TEMPERATURE (exact degrees)				
°C	Celsius	1.8C+32	Fahrenheit	°F
ILLUMINATION				
lx	lux	0.0929	foot-candles	fc
cd/m ²	candela/m ²	0.2919	foot-Lamberts	fl
FORCE and PRESSURE or STRESS				
N	newtons	0.225	poundforce	lbf
kPa	kilopascals	0.145	poundforce per square inch	lbf/in ²

Technical Report Documentation Page

1. Report No. BD545 RPWO #39		2. Government Accession No.		3. Recipient's Catalog No.	
4. Title and Subtitle Stiffness Evaluation of Neoprene Bearing Pads Under Long-Term Loads				5. Report Date March 2009	
				6. Performing Organization Code	
7. Author(s) R. A. Cook and D. Allen				8. Performing Organization Report No. 00051121	
9. Performing Organization Name and Address University of Florida Department of Civil Engineering 345 Weil Hall / P.O. Box 116580 Gainesville, FL 32611-6580				10. Work Unit No. (TRAIS)	
				11. Contract or Grant No. BD545 RPWO #39	
12. Sponsoring Agency Name and Address Florida Department of Transportation Research Management Center 605 Suwannee Street, MS 30 Tallahassee, FL 32301-8064				13. Type of Report and Period Covered Final Report	
				14. Sponsoring Agency Code	
15. Supplementary Notes					
<p>16. Abstract</p> <p>The objective of this project was to evaluate the interaction between the shear modulus of steel reinforced neoprene bearing pads and shear strain rate. The following interactions related to variations in the shear modulus were investigated for pads with various shape factors: product approval strain rates vs. short-term field strain rates, short-term field strain rates vs. long-term field strain rates, reduction in shear modulus due to load cycles, and effects of compressive stress.</p> <p>Forty-two tests were performed using test equipment designed to apply a shear strain at a variety of rates (50% shear strain at rates from 45 seconds to 90 days) while applying a sustained compressive load. Test results indicated: the shear modulus reduced on average 7% when tests were performed using the short-term field strain rates of 50% over 12 hours instead of the product approval strain rates of 50% over 30-60 seconds, there was essentially no reduction in shear modulus using long-term field loading rates of 50% over durations up to 90 days vs. short-term field strain rates, the shear moduli for pads that had never been load cycled were approximately 12% higher than cycled pads, and the effect of compressive stress agrees with previous work (i.e., the shear modulus decreases with increased compression particularly for bearings with low shape factors).</p> <p>Recommendations for upper and lower limits on the shear modulus to be used in design are included.</p>					
17. Key Word Neoprene, bearing, time, shear, bridge			18. Distribution Statement No restrictions		
19. Security Classif. (of this report) Unclassified		20. Security Classif. (of this page) Unclassified		21. No. of Pages 145	22. Price

STIFFNESS EVALUATION OF NEOPRENE BEARING PADS UNDER LONG TERM LOADS

Contract No. BD545 RPWO #39
UF No. 00051121

Principal Investigator: Ronald A. Cook, Ph.D., P.E.
Graduate Research Assistant: Damon T. Allen
FDOT Technical Coordinator: Marcus H. Ansley, P.E.

Engineering and Industrial Experiment Station
Department of Civil and Coastal Engineering
University of Florida
Gainesville, Florida

March 2009

ACKNOWLEDGMENTS

The authors acknowledge and thank the Florida Department of Transportation for providing the funding for this research project. The success of this project is owed in large part to facility and staff at the University of Florida and information provided by experts from Figg Engineering Group and Finley Engineering Group. Special thanks are extended to Dr. Cesar Fernandes, P.E. of Figg Engineering as well as to Jerry Pfuntner, P.E., of the Finley Engineering Group

EXECUTIVE SUMMARY

The objective of this research project was to evaluate the affect of shear strain rate on the shear modulus in steel reinforced neoprene bearing pads. Since neoprene is viscoelastic, it is possible that under strain rates typical in highway applications the shear modulus is less than what current product approval tests predict. The areas investigated were:

- Product approval strain rates vs. short-term field strain rates
- Short-term field strain rates vs. long-term field strain rates
- Reduction in shear modulus due to load cycles
- Effects of compressive stress

Forty-two tests were performed using test equipment designed to apply a shear-strain at various rates while maintaining a constant compression. Test results indicated:

- The shear modulus reduced on average 7% when tests were performed using the short- term field strain rates of 50% over 12 hours instead of the product approval strain rates of 50% over 30-60 seconds
- There was essentially no reduction in shear modulus using long-term field loading rates of 50% over durations up to 90 days vs. short-term field strain rates.
- Shear moduli for pads that had never been load cycled were approximately 12% higher than cycled pads (for 50 durometer hardness material).
- The effect of compressive stress conforms to previous work; the shear modulus decreases with increased compression particularly for bearings with low shape factors.

Based on the results of this study, the variation in shear strain rate, in highway applications has a negligible effect on shear modulus. However, it is recommended that upper and lower tolerance values for the shear modulus be used for calculations instead of a single value. Current product approval tests permit +15% to – 15% of the specified shear modulus, however this range should be adjusted up by at least 5% to account for the net effects of the lack of cycling (+12%) and the reduced strain rates (-7%) that exist in the field. The recommended values are +20% and -20% of a specified shear modulus. Furthermore, these values can be decreased due to dead load's effect on the shear modulus.

TABLE OF CONTENTS

CHAPTER	page
1.0 INTRODUCTION	1
1.1 General Concept	1
1.2 Objectives	2
2.0 LITERATURE REVIEW	3
2.1 Codes, Specifications and Design Guidelines	4
2.1.1 AASHTO Design Requirements	4
2.1.2 Shear Modulus Test AASHTO Designation: M 251-06	7
2.1.3 Shear Modulus Test ASTM D 4014 ANNEX-A	8
2.1.4 Florida Department of Transportation	10
2.1.5 Applications in FDOT Projects	11
2.2 Reviewed Literature	13
2.2.1 General Background on Elastomeric Bearings and Elastomers	13
2.2.1.1 Performance of elastomeric bearings: NCHRP report 298	13
2.2.1.2 Comparing the time and rate dependent mechanical properties of elastomers	16
2.2.1.3 Engineering with rubber	18
2.2.1.4 Neoprene elastomer bearings – ten years experience proves their importance	19
2.2.1.5 State-of-the-art elastomeric bridge bearing design	20
2.2.1.6 Elastomeric bearing research NCHRP report 109	20
2.2.1.7 Additional design data based on full-size bridge bearing pads of neoprene	24
2.2.1.8 Construction and design of prestressed concrete segmental bridges	24
2.2.1.9 Design of elastomer bearings	24
2.2.1.10 Summary of general background	25
2.2.2 Test Methods for Elastomeric Bearings and Complications	25
2.2.2.1 Test method for determining the shear modulus of elastomeric bearings	25
2.2.2.2 Elastomeric bridge bearings: recommended test methods: NCHRP report 449	26
2.2.2.3 On highly compressible helical springs and rubber rods, and their application for vibration-free mountings	27
2.2.2.4 Elastic stability of rubber compression springs	27
2.2.2.5 An experimental study of elastomeric bridge bearings with design recommendations	28
2.2.2.6 Slippage of neoprene bridge bearings	29
2.2.2.7 Elastomeric bearings: background information and field study	29
2.2.2.8 Neoprene bearing pad slippage at Louisiana bridges	30
2.2.2.9 Summary of test methods and complications	30
2.2.3 General Background and Models of Viscoelastic Material	30
2.2.3.1 Basic continuum models	30

2.2.3.2	Molecular theory	31
2.2.3.3	An engineering theory of nonlinear viscoelasticity with applications	32
2.2.3.4	Constitutive modeling of the large strain time-dependent behavior of elastomers	32
2.2.3.5	A three-dimensional constitutive model for the large stretch behavior of rubber elastic materials	33
2.2.3.6	The behavior of rubberlike materials in moderately large deformations	34
2.2.3.7	Constitutive model for stretch-induced softening of stress-stretch behavior of elastomeric materials	34
2.2.3.8	Nonlinear finite element analysis of elastomers—technical paper	34
2.2.3.9	Summary of models of viscoelastic material	34
2.2.4	Possible Temperature Effects	35
2.2.4.1	Viscoelastic properties of polymers	35
2.2.4.2	Low temperature behavior and acceptance criteria for elastomeric bridge bearings: NCHRP report 325	35
2.2.4.3	Performance of elastomeric bridge bearings at low temperatures	36
2.2.4.4	Summary of temperature	37
2.2.5	Summary of Literature Review	37
3.0	METHODOLOGY	38
3.1	Developing the Samples	38
3.2	Test Program	40
3.2.1	Strain Rates	41
3.2.2	Mullins Effect	42
3.2.3	Multiple Compressive Stresses	44
3.3	Design of Test Apparatus	44
3.4	Major Components of the Test Apparatus	47
3.4.1	Compression Mechanism	47
3.4.2	Long-Term Shear Loading Mechanism	50
3.4.3	Short-Term Shear Loading Mechanism	51
3.4.4	Instrumentation	52
3.5	Procedure	52
3.5.1	Compression	52
3.5.2	Shearing	54
3.6	Temperature Factors	54
4.0	TEST RESULTS	55
4.1	Sample Data	55
4.2	Determination of Shear Modulus	58
4.3	General Results	60
5.0	DISCUSSION OF RESULTS	62
5.1	Variations in Shear Modulus	62
5.1.1	Initial Change due to Strain Rate	62

5.1.2 Changes due to Short Term Field Loading vs. Long Term Field Loading	64
5.1.3 Changes due to the Number of Loading Cycles	64
5.1.4 Changes due to the Compressive Stress	66
5.1.5 Temperature	69
5.1.6 Final Analysis of Strain Rate	70
5.2 Summary	72
6.0 CONCLUSION	75
APPENDIX	
A RESEARCH DATA	77
B ADDITIONAL LITERATURE REVIEW	119
B.1 Additional Literature Summary	119
B.1.1 Elastomeric bearings: state-of-the-art	119
B.1.2 Effect of bearing pads on prestressed concrete bridges	119
B.1.3 Restraint effect of bearings	120
B.1.4 Load-deformation characteristics of elastomeric bridge bearing pads	120
B.1.5 Rotational effects on elastomeric bearings	121
B.1.6 Influence of compression upon the shear properties of bonded rubber blocks ...	121
B.1.7 Compression, bending, and shear of bonded rubber blocks	123
B.1.8 Behavior of elastomeric bridge bearings: computational results	124
B.1.9 The compression of bonded rubber blocks	124
B.1.10 Engineering with rubber	125
B.1.11 Stress analysis of rubber blocks under vertical loading and shear loading	127
B.1.12 Hydrostatic tensile fracture of a polyurethane elastomer	127
B.1.13 Steel bridge bearings	127
B.1.14 Earthquake isolation	127
B.1.15 Effects of axial load on elastomeric isolation bearings	128
B.1.16 Stability of elastomeric isolators: critical load tests and computations	128
B.1.17 Evaluation of low-temperature test methods for elastomeric bridge bearings ..	128
B.1.18 Parameters influencing performance of elastomeric bearings at low temperatures	128
B.1.19 Elastomeric bearing design, construction, and materials	129
B.1.20 Natural rubber structural bearings	129
C RECOMMENDED ADDITIONAL AASHTO LANGUAGE	130
LIST OF REFERENCES	131

CHAPTER 1 INTRODUCTION

Highway bridges are supported on bearings that reduce the forces in the substructure caused by translations due to creep, shrinkage, and uniform temperature change of the bridge superstructure. Different types of bearings are available for this function ranging from metal rocker and roller bearings to neoprene and PTFE (Teflon) bearings. Neoprene, invented in 1930 by the DuPont Company, became a popular type of bearing material in the 1950s when steel reinforced neoprene bearings were introduced. Due in part to the reduced need for maintenance, neoprene bearing pads are now often used in the support of bridge superstructures.

Unlike idealized roller bearings which are used for simplifying structural calculations, most real bearings, including neoprene bearing pads, exert a lateral force as a reaction to lateral movement in the system (see Figure 1-1). The magnitude of this force directly impacts both the design of the substructure of a bridge and the design of the superstructure.

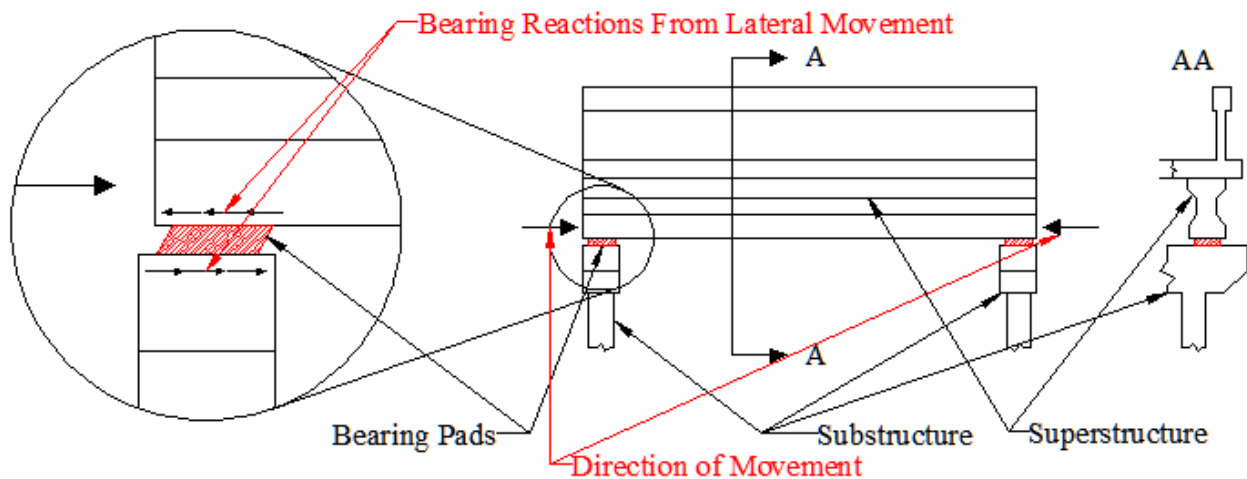


Figure 1-1 Bearing pad in bridge

1.1 General Concept

Vulcanized elastomeric material, specifically neoprene, has a tendency to creep over time under a sustained load. For displacements that are applied at a relatively slow rate, it is thought that the resulting reactions would be lower than if they had been applied faster. This is

particularly the case with neoprene since it is modeled as elastic material that has properties based on material tests conducted at a rapid displacement rate. The implications of this means that the forces induced in bridge structures due to translations from creep, shrinkage, and uniform temperature change are not really as high as they are currently predicted.

1.2 Objectives

Currently, the shear modulus of neoprene is measured with a short-term test and the strain rate of this testing is closer to the strain rate due to a braking car than the strain rate due to daily temperature change in most bridges. Results based on this short-term testing are supposed to be used by designers to calculate the stiffness for all loads, short and long term alike. Since most shear loads that bridge substructures experience due to these bearings are applied more slowly than the current test rate (which ranges from 50% stain in 30 to 60 seconds) a relationship between shear stiffness and rate of loading (i.e., rate of shear strain) needs to be determined. The objective of this project is to quantify the relationship between shear stiffness and the rate of shear strain for steel reinforced neoprene bearing pads.

CHAPTER 2 LITERATURE REVIEW

This chapter covers information found during the background review into neoprene bearing pads and serves as a basis of understanding for this project. It contains what was found in codes, design guides, literature, and information obtained from design professionals.

In order to provide some understanding into the subject mater of this chapter and neoprene an introduction to the concept of viscoelasticity is necessary. Viscoelastic behavior in the broadest sense is a combination of both elastic behavior and viscous behavior. Stress in a viscoelastic material is dependant on both strain and the rate that strain is applied.

Additionally, it is important to discuss some terminology at this point. The shape factor (denoted as SF in this report) is used in the American Association of State Highway and Transportation Officials^[1,2] (AASHTO) bearing design specifications, FDOT specifications^[3,4] and is found in many other studies on elastomeric bearing pads. Because of its prevalent use in code and research, the definition is presented here.

The shape factor is used to describe the geometric characteristics of a layer of an elastomer used in a bridge bearing. These bearings are essentially stub columns made of a flexible material that is expected to undergo large horizontal strains. Since elastomers have a Poisson's ratio of nearly 0.5, under compressive loading they experience significant transverse straining. With substantial compressive loads on a material with a low Young's modulus the typically neglected effects of end restraint on transverse straining become an important consideration when calculating the compressive deflection and capacity of these materials. The shape factor is a ratio of restrained surface area to the unrestrained surface areas and is used to account for the end restraint effect. In practice, the shape factor is used to try to capture the effect of the geometry of

the elastomeric layer on the compression strain, shear strain and both compression, and shear capacity of a bearing pad.

The shape factor is calculated by dividing the plan area by the area free to bulge in a layer. As an example, a 1 inch thick unreinforced pad that is 12 inch x 12 inch has a SF of 3, and a 2 inch thick unreinforced pad that is 18 inch x 36 inch also has a SF of 3. The shape factor is calculated for each individual layer for reinforced pads, i.e. a pad that consists of two layers 12 inch x 12 inch x 1 inch with a reinforcing plate between them would still have a SF of 3. An example calculation is shown below in Figure 2-1. For bearings with multiple layers the shape factor of the thickest layer controls.

$$\text{Plan Area} = (12'') (12'') = 144 \text{ in}^2$$

$$\text{Bulge Area} = 4 (12'') (1'') = 48 \text{ in}^2$$

$$\text{ShapeFactor} = \frac{\text{PlanArea}}{\text{BulgeArea}} = 3$$

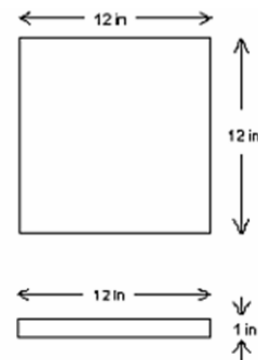


Figure 2-1. Shape factor calculation example

2.1 Codes, Specifications and Design Guidelines

2.1.1 AASHTO Design Requirements

The American Association of State Highway and Transportation Officials (AASHTO) publishes guidelines for the design of highways that include design specifications for bridge bearing pads. The sections of the AASHTO LRFD Bridge Design Specifications^[1] on elastomeric bearing pads treat elastomers as a homogeneous material but allow for bearings that are designed to act in a composite manor. Composite pads, also known as reinforced pads, are made by bonding layers of an elastomeric material with layers of reinforcement typically

consisting of either fiberglass, cotton-duck (cotton canvas), or thin steel plates. The reinforced pads that carry the greatest vertical loads are typically designed with steel reinforcement.

There are two methods that can be used to design steel reinforced elastomeric bearings in AASHTO Specifications; these are referred to as Method A and Method B. Of the two, Method B is the method most recently added to the specifications. The Commentary of the AASHTO Specifications states that Method B typically results in a higher bearing capacity as well as smaller horizontal forces. These smaller horizontal forces result from a reduced shear stiffness due to the reduction in size of the pads from the higher allowed compression capacity permitted by Method B. This higher compression capacity is only allowed with additional testing and quality control of the bearings. The alternative and more conservative approach, Method A, can be used for all types of reinforced and unreinforced elastomeric bearing pads as well as steel reinforced bearing pads.

In Method B of the AASHTO Design Specifications^[1], the limit for the average compressive stress under service loading for bearings subject to shear is calculated as follows in Equation 2-1 and Equation 2-2.

$$\sigma_s \leq 1.66 G S \leq 1.6 \text{ ksi} \tag{2-1}$$

$$\sigma_L \leq 0.66 G S \tag{2-2}$$

where

σ_s is the service average compressive stress due to the total load (ksi)

σ_L is the service average compressive stress due to live load (ksi)

G is the shear modulus of elastomer (ksi)

S is the shape factor of the thickest layer of the bearing

The shear modulus of the neoprene is found in AASHTO with the aid of Table 14.7.5.2-1 reproduced below as Table 2-1. This table allows the designer to specify a hardness value rather than a shear modulus.

Table 2-1. Shear modulus AASHTO table 14.7.5.2-1^[1]

	Hardness (shore A)		
	50	60	70
Shear modulus @ 73°F (ksi)	0.095-0.130	0.130-0.200	0.200-0.300
Creep deflection @ 25 years divided by instantaneous deflection	0.25	0.35	0.45

Note: (Source: pp. 14-53)

One of the restrictions of Method B is that an elastomer's shear modulus is required to fall in the range of 80 to 175 psi^[1]. The use of Method B also requires that the summation of the individual elastomer layer heights in a bearing pad be a minimum of twice the maximum shear displacement to which the bearing will ever be subjected. If the minimum height is selected, this is the same as having a maximum permitted shear strain of 50%. The shear strain, along with the shape factor and compressive stress make up the three key factors used to scale the bearing pad samples in this project.

The bearings are additionally specified by their temperature grade. The performance specifications for these grades are defined in Section 18 of the AASHTO LRFD Bridge Construction Specifications^[2]. The temperature grade required is shown in Table 14.7.5.2-2 in Section 14 of the AASHTO LRFD Bridge Design Specifications^[1]. This table has been reproduced here in Table 2-2. These grading specifications are used as guidelines for manufactures in supplying neoprene pads that resist stiffening at to low temperatures.

Table 2-2. Elastomer grade AASHTO table 14.7.5.2-2^[1]

Low-temperature zone	A	B	C	D	E
50-Year low temperature (°F)	0	-20	-30	-45	<-45
Maximum number of consecutive days when the temperature does not rise above 32°F	3	7	14	N/A	N/A
Minimum low-temperature elastomer grade	0	2	3	4	5
Minimum low-temperature elastomer grade when special force provisions are incorporated	0	0	2	3	5

Note: (Source: pp. 14-54)

2.1.2 Shear Modulus Test AASHTO Designation: M 251-06

The document cited in AASHTO LRFD Bridge Construction Specifications^[2] that covers the material requirements and test procedures for accepting elastomeric bridge bearings has the AASHTO Designation: M 251-06^[5]. This document includes the use of an inclined compression test to calculate shear modulus, as shown in Figure 2-2. In the inclined compression test, the surface slope can vary between 1:10 and 1:20. This style of testing results in the compression varying linearly with shear. M 251-06 also allows for the use of ASTM D 4014 ANNEX-A1^[6] with modifications that include shearing the samples to 70% strain and calculating the shear modulus with a secant modulus through the stress at 50%.

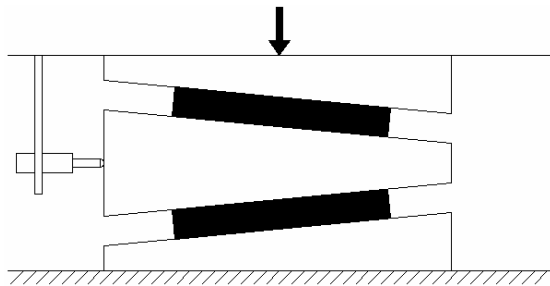


Figure 2-2. Inclined shear test setup

In addition to tests for calculating a typical shear modulus, AASHTO M 251-06^[5] contains a method for calculating the shear modulus as a function of time. This shear modulus is found in section A2 “A Test Method for Creep and Shear Bond in Elastomeric Bearings” and the test setup is shown in Figure 2-3. The testing method specifies that the samples measuring 51 mm by 51 mm are to be either hot or cold bonded to the steel plates shown. Once the bonds have reached sufficient strength the samples are then strained in shear 10 times at a rate of one percent per second to 50% then finally loaded to 50% shear strain in one second. This final 50% strain is held constant for a minimum of 6 hours and the load is recorded after the first half of an hour then every five minutes for the remainder of the testing period. The method for calculating the shear modulus is shown in Equation 2-3.

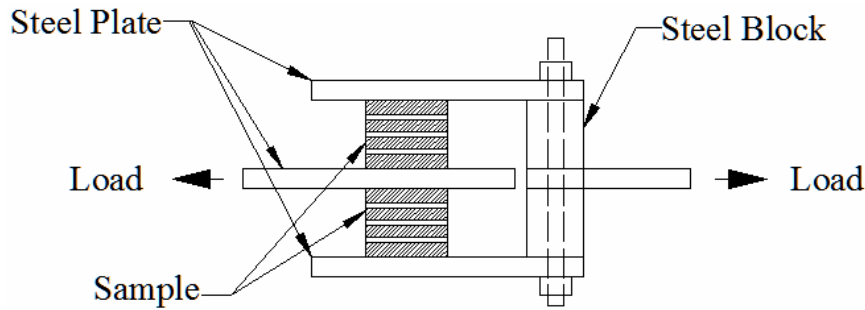


Figure 2-3. Shear creep test setup.^[5] (Source: Figure A2-1 pp. M 251-11)

$$G(t) = \frac{\text{load}(t)}{51 \times 51 \times 2 \times 0.5} \quad (2-3)$$

where

load(t) is the load at time t (min)

G(t) is the shear modulus (MPa) at time t

The (51 x 51) is the area of the sample in mm², the number 2 is to account for the pair of samples and the 0.5 is the 50% shear strain. Section A2.4.6 of AASHTO M 251-06^[5] states that the shear modulus can be predicted for any future time conservatively using a power law equation with coefficients calculated using a least-squares method regression analysis of the data obtained over the six hour period of testing. This power law equation is in the form shown below.

$$G(t) = at^b \quad (2-4)$$

To estimate the creep deflection at time T of a full size bearing the shear modulus relationship found using the regression analysis is used in the equation below.

$$\text{Creep}(\%) = \left(\frac{G(60)}{G(T)} - 1 \right) \times 100 \quad (2-5)$$

2.1.3 Shear Modulus Test ASTM D 4014 ANNEX-A

In the background research, AASHTO^[2, 5] references the current ASTM specification for finding the shear modulus of an elastomer, ASTM D 4014 ANNEX-A^[6]. The ASTM test

procedure requires the samples, shown in Figure 2-4, to be shear strained from 0 to 50% for six cycles while taking from 30 seconds to 60 seconds to reach 50% shear strain each cycle.

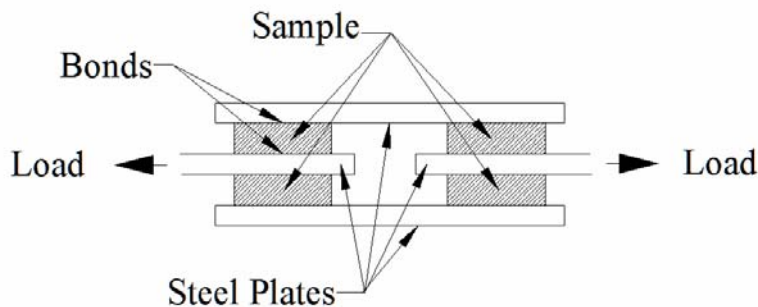


Figure 2-4. Test setup ASTM D 4014 ANNEX-A.^[6] (Source: Figure A1.1 pp. 5)

In the ASTM test, the purpose of first five cycles is to stabilize the stress-strain behavior of the elastomer and the additional sixth cycle is used to find the value of the shear modulus. The first five cycles of the ASTM test used for conditioning the sample minimize a transitory effect known as thixotropic or the Mullins effect which is discussed in more detail later. In this ASTM standard the shear modulus is calculated by taking the secant modulus on the stress-strain graph from the point of 2% of maximum stress to the point at 25% shear strain beyond this point (Figure 2-5). It should be noted that no compressive stress is required in this specification and in order for a reaction to be developed the samples are bonded to both the ridged outer plates and center shearing plates.

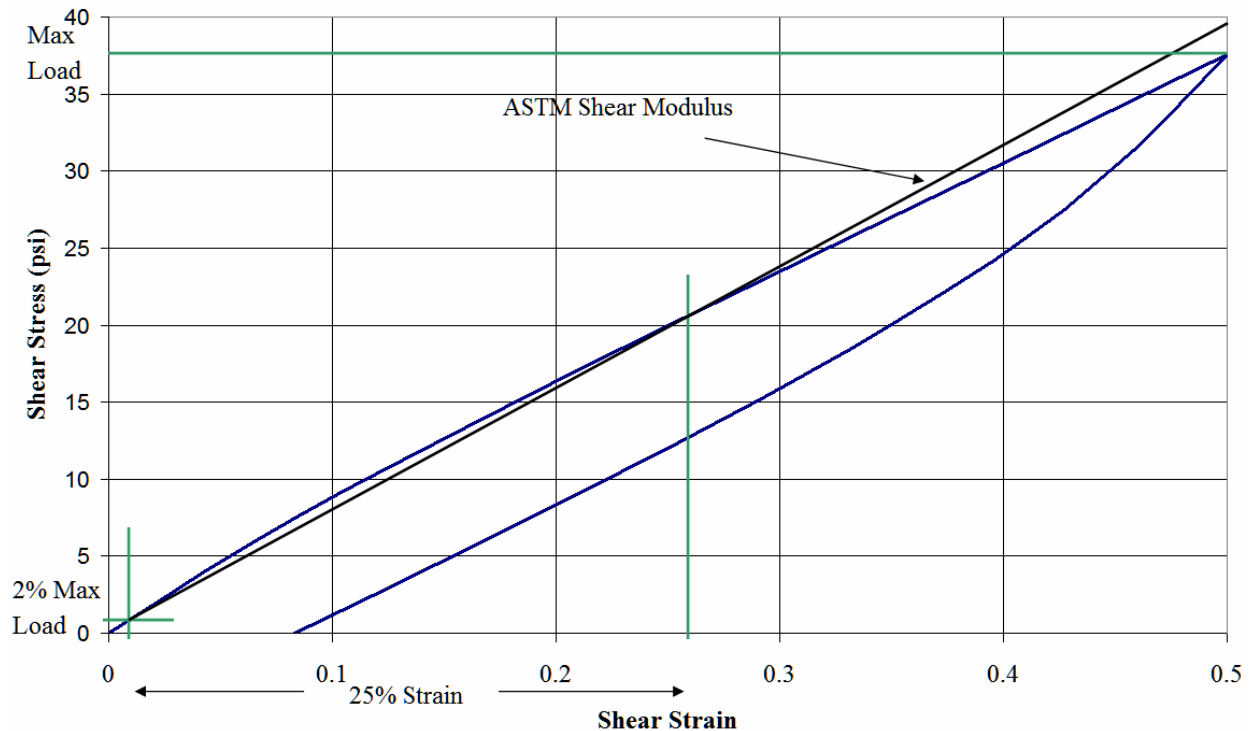


Figure 2-5. Example of ASTM D 4014 shear modulus determination from the sixth cycle

If a sample is being checked for a specific shear modulus a certain variation is allowed by the ASTM specifications. The ASTM specification states the following:

The shear modulus of the elastomer determined in accordance with Annex A1 shall not differ by more than $\pm 15\%$ from the required shear modulus of the elastomer.

This means a sample modulus could be from 85 to 115% of the specified value.

2.1.4 Florida Department of Transportation

The Florida Department of Transportation (FDOT) specifications^[3, 4] were reviewed to determine the sizes, design requirements and material grades that are currently used. Bridge bearing pads based on these standards typically have plan dimensions that range from less than one foot to 4 feet depending on the compression loads and the beam configuration being carried. Some of these combinations are shown in Table 2-3 which comes from the FDOT Standard Drawings^[4]. These dimensions are for pads made up of ½ inch thick elastomer layers and are designed to support Type II to VI (AASHTO) beams in prestressed bridges.

Table 2-3. Steel reinforced elastomer FDOT bearing pad dimensions for AASHTO beams^[4]

Pad type	Beam type	Bearing pad dimension		Shape factor	Number of layers
		L	W		
A	II (AASHTO)	1'-0"	1'-2"	6.46	3
	III (AASHTO)	10"	1'-6"	6.43	3
	IV (AASHTO)	10"	1'-10"	6.88	3
	V & VI (AASHTO) and Florida bulb-T's	11"	2'-0"	7.54	3
	II (AASHTO)	1'-4"	1'-2"	7.47	4
B	III (AASHTO)	1'-2"	1'-6"	7.88	4
	IV (AASHTO)	1'-0"	1'-10"	7.76	4
	V & VI (AASHTO) and Florida bulb-T's	1'-2"	2'-0"	8.84	4

Table 2-4 contains the standard properties for neoprene that design engineers working in the state of Florida are to use if they are specifying the bearing pads by durometer hardness instead of shear modulus.

Table 2-4. Neoprene properties FDOT^[3]

Durometer Hardness	50	60	70
Shear modulus at 73°F [23°C]	85-110 psi [0.59 to 0.76 MPa]	120-155 psi [0.83 to 1.07 MPa]	160-270 psi [1.10 to 1.86 MPa]
Creep deflection at 25 years instantaneous deflection	25%	35%	45%

Note: (Source: pp. 8)

2.1.5 Applications in FDOT Projects

A professional bridge engineer was contacted in order to obtain additional values of shape factors and typical compressive loads used in the design of segmental bridges. The information provided included the expected compressive stress, shape factor, the number of neoprene layers used, the size of the steel reinforcement and which design methodology was typically used. This information, along with the design guidelines given in the FDOT Standard Specifications,^[3] is listed in Table 2-5.

Table 2-5. Typical bearing pad properties

Property	Value, range or method
Maximum compressive stress	From 1.0 to 1.6 ksi with 1.0 ksi FDOT standard (unless stated otherwise) ^[3]
Durometer hardness	50 to 70 with 50 being FDOT standard (unless stated otherwise) ^[3]
Shear modulus	85 to 110 psi shear modulus being FDOT standard ^[3] for a hardness of 50 or $\pm 15\%$ of the shear modulus specified ^[6]
Shape factor range	From 6 to 9 for standard AASHTO beam sizes From 12 to 28 in segmental bridges examples
Number of layers	From 2 to 15 layers in segmental bridge examples
Steel thickness	1/16 inch with 14 – gauge specified by FDOT ^[3]
Method used	AASHTO LRFD Section 14.7.5 Steel Reinforced Bearing Method B (also used in FDOT Design Examples) ^[1]

Since AASHTO and FDOT currently have no guidelines for dealing with reduced strain rates, current practices involve a certain amount of engineering judgment. In particular, another professional bridge engineer provided the following procedure that is used for dealing with long term loading on neoprene bearing pads, such as seasonal temperature change, concrete creep and shrinkage. The shear modulus for neoprene of a given hardness is found by calculating the average of the values listed in the governing specification such as in Table 14.7.5.2-1 of AASHTO (reproduced as Table 2-1) or in the FDOT^[3] specification shown in Table 2-4. The corresponding creep deflection at 25 years (taken from the same tables) is used to determine the adjusted shear modulus for long term loads by assuming an inversely proportional relationship between shear modulus and deflection. For example, as shown in Table 2-1 and Table 2-4, a 50 durometer pad has a total deflection (initial instantaneous plus creep) at 25 years equal to 1.25 times the initial instantaneous deflection. This would indicate a shear modulus for long term loads equal to 0.8 or $1/1.25$ times the initial shear modulus.

2.2 Reviewed Literature

A literature review was conducted in order to find pertinent information about shear stiffness reductions for long term loads. This review produced information about short-term experiments that were similar to this proposed research. However, only limited information on long-term experimental testing pertaining to the shear stiffness of neoprene bearing pads was found. The majority of long-term experimental testing pertained to compressive behavior, not shear behavior.

2.2.1 General Background on Elastomeric Bearings and Elastomers

This section covers the research that went into the section of the AASHTO specifications that covers steel reinforced neoprene bearings. It also covers research into the basic viscoelastic properties of neoprene. Lastly, it covers the research that provided the motivation of this current research project.

2.2.1.1 Performance of elastomeric bearings: NCHRP report 298

This report compiled by Roeder, Stanton and Taylor^[7] describes Phase II of the National Cooperative Highway Research Program (NCHRP) Project 10-20. Phase I of the Project was a comprehensive state-of-the-art review of neoprene bearing pads. It was initiated in 1981 to update the AASHTO Specifications for Highway bridges. The report resulted in the proposal for “Method B” discussed in AASHTO Design Requirements of elastomeric bridge bearing design.

Phase II research findings fell into six categories: low temperature behavior, compression loading, rotation, shear and combined loading, stability and fatigue. These categories are briefly discussed below.

The effects of low temperature on the shear modulus of an elastomer are only pronounced near the crystallization temperature which was indicated to typically be below 32 degrees Fahrenheit. Below the crystallization temperature elastomers become much stiffer. This effect

on shear modulus was studied in detail by Roeder and Stanton(1989) during Phase III. Since Florida experiences only brief periods below the crystallization temperature it was deemed that, at this time, it unnecessary consider the effects of low temperature on shear stiffness.

In the NCHRP Report 298 the limiting compressive stress of 1600 psi, now used in the AASHTO specification, was determined based on when debonding occurred in the specimens. The debonding, which actually appeared as cracking or tearing in the elastomer near the steel elastomer interface, began at compressions greater than 2500 psi. It was limited by applying a factor of safety of approximately 1.6 to the compressive stress to this failure stress.

The effects of end rotation of the beam were considered an extension of the theories of compression. Rotations were looked at with respect to moment-rotation relationships and to the compression and tensions developed in the pads. In the conclusion, it was noted that the moment rotation curves were mainly linear. These results and additional tests were conducted by Stanton, Roeder and Mackenzie-Helnwein in NCHRP Report 12-68^[8].

The test procedure used in Phase II of this research for shear was similar to that of ASTM D 4014 ANNEX-A. During the tests conducted in shear it was noted that the corners of the bearings rolled over if the shear strains exceeded 50%. This rolling of the corners was believed to pose a risk to the reinforcement and could result in tearing of the elastomer. For these reasons the shear deformations are limited to 50% in AASHTO Method B.

In Appendix E of the NCHRP report, the relationship between shear force and compressive strain was presented for an elastomeric bearing pad as follows:

$$V = \frac{\phi \Delta_s G A_{s0}}{h_{cr0} (1 - \epsilon_c)^2} \quad (2-6)$$

where

V is shear force

ϕ is the ratio of total combined thickness to elastomer thickness in a reinforced bearing

Δ_s is the shear displacement

A_{s0} is the shear area of the uncompressed pad

h_{cr0} is the total thickness of all elastomer layers in a reinforced bearing in the unloaded state (not including the reinforcement thickness)

ϵ_c is the compressive strain

This relationship takes into account an increased shear area due to parabolic bulging and the effect of decreased height due to the compression of the elastomers. The implication is that as compression is increased the required shear force for a given displacement also increases, thus increasing the effective shear modulus.

In Appendix B of the report the relationship between compressive stress and strain for bonded elastomer pads was given as follows:

$$\sigma_c = E_c \epsilon_c = E f_c \epsilon_c \quad (2-7)$$

where

E_c is the effective compressive modulus

E is the Young's modulus

f_c is a conversion factor

$$f_c = A_c + B_c S^2 \quad (2-8)$$

where

A_c is a dimensionless constant reported as ranging from 0 to 1.33

B_c is a dimensionless constant dependant of the shape of the layer and the ratio of the Young's modulus to the bulk modulus

S is the shape factor of the pad

It was reported that researchers have used values of A_c ranging from 0 to 1.33.

Additionally it was noted that for practical shape factors B_c is much more important due to the S^2 term.

This report mentions decreased shear stiffness due to a tendency for elastomeric pads to buckle in shear as the shear displacement increases under a compressive load. Though this is mentioned no equation was presented to express the shear stiffness in terms of this effect.

It was also mentioned that during testing corrections for bulging and buckling stability did not account for all of the test data scatter.

2.2.1.2 Comparing the time and rate dependent mechanical properties of elastomers

Meinecke^[9] described three important load responses that must be accounted for in modeling the behavior of elastomers: instantaneous response; transient viscoelastic response; and permanent viscoelastic response. These three factors provide a description of the elastic response, creep and creep recovery in an elastomer. To illustrate these concepts, Meinecke provides expected displacement curves based on the response to various types and durations of loading. Meinecke also provides a basic rheological linear model that accounts for the behavior of elastomers.

The elements of a linear model are linear springs and linear viscous dashpots; these elements represent aspects of the material behavior of a dimensionless elastomeric sample. A linear spring is used to represent the elastic part of stiffness in an elastomeric sample i.e. the stress versus elastic strain of the sample as shown in Figure 2-6. Similarly, a linear viscous dashpot is used to represent the viscous response of the elastomeric sample response divided by the loaded area of the sample as shown in Figure 2-6.

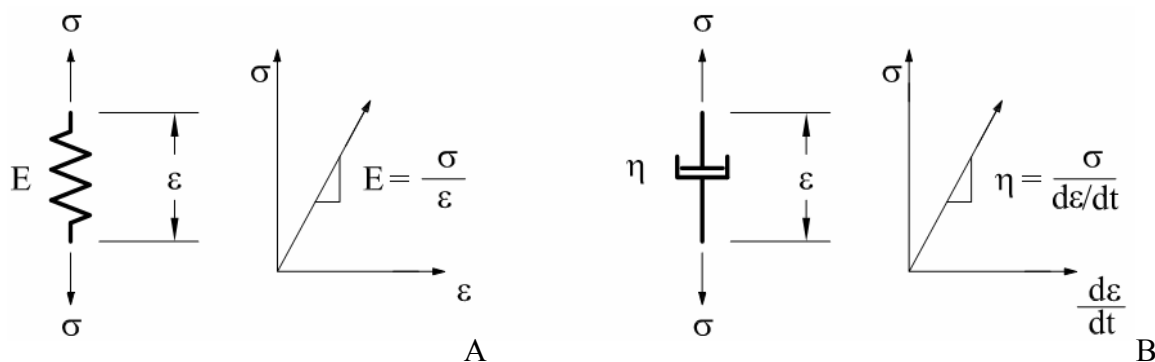


Figure 2-6. Examples of model elements. A) Spring element. B) Dashpot element.

The basic model, illustrated in Figures 2-7, 2-8 and 2-9, shows the expected response to a pulse load, neglecting inertial dynamic effects. At the time the load is applied there is an instantaneous elastic strain. This is followed by both a transient and a permanent viscoelastic response that superimpose on the elastic response. When the load is removed the same elastic

response is shown in the opposite direction followed by the relaxing of the transient response.

However, there is a permanent set in the material that is not recovered.

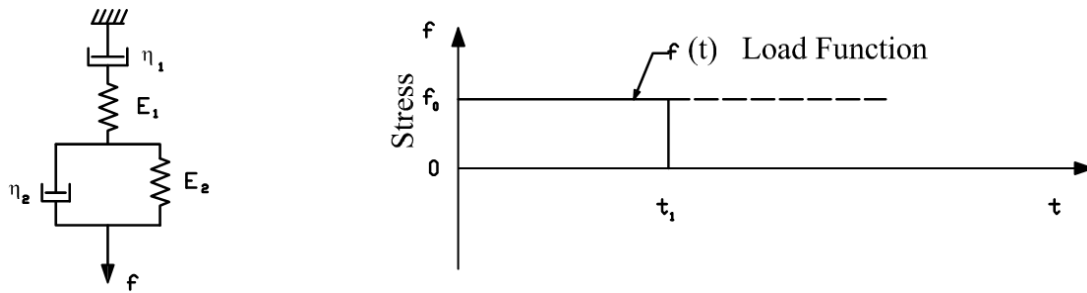


Figure 2-7. Four parameter viscoelastic model and pulse load.^[9] (Source: Figure 1 pp. 1146)

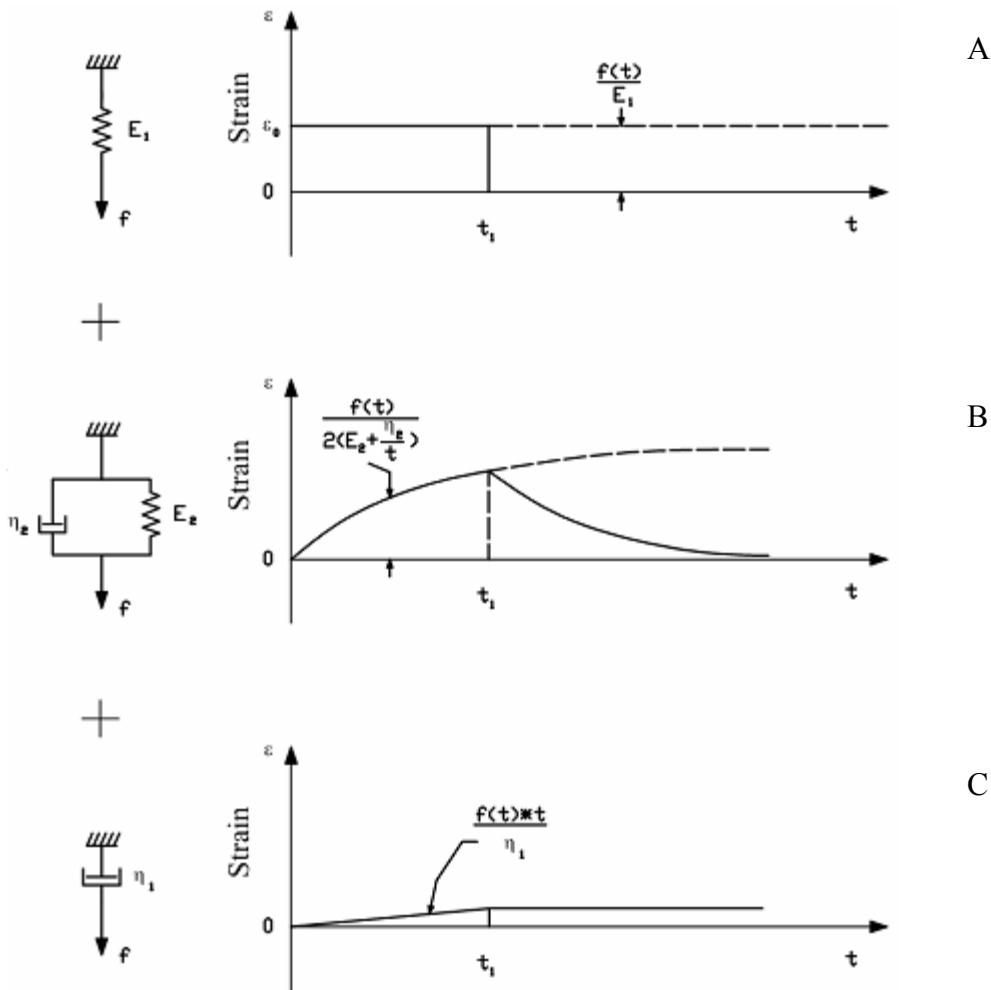


Figure 2-8. Piecewise strain vs. time response.^[9] A) Elastic response. B) Viscoelastic response. C) Permanent set. (Source: Figure 1 pp. 1146)

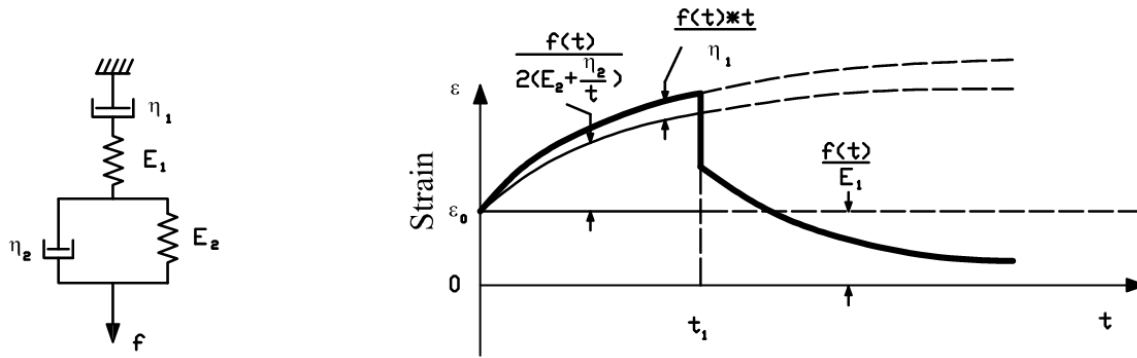


Figure 2-9. Superposition of strain vs. time response.^[9] (Source: Figure 1 pp. 1146)

In the Figures 2-7, 2-8 and 2-9 the dashed lines show what would have happened if the load had not been removed. Meinecke cautions that this is an over-simplified model and the value of η_1 , the value of the viscous response, is not actually a constant.

2.2.1.3 Engineering with rubber

Mullins^[10] reviews information on the “Mullins effect” which is a phenomenon where the shear stiffness of a bearing pad seems to reduce with repeated straining. The reduction in stiffness due to this effect quickly levels off, usually after the first three or four cycles of straining. This phenomenon is mainly found in material with large filler content, typically around 30% by volume, the most common filler being carbon black. Carbon black is a substance that comes from the incomplete combustion of petroleum and is similar to soot.

The Mullins effect is thought to be a product of changes occurring in the molecular structure, which consists of long carbon chains which are bonded to sulfur atoms and the molecules of the filler material. The bonds to the filler material are weak, and when the material is first strained part of the force needed achieve a particular level of strain is due to the breaking of the bonds between the carbon chains and the filler material. Once these bonds are broken and the carbon chains can rearrange, the force required to strain the pad to any strain level less than the previous maximum strain is not as great. It is important to note that if strains exceed the

previous maximum the stress strain relationship will pick back up on its original, uncycled, trend.

2.2.1.4 Neoprene elastomer bearings – ten years experience proves their importance

Maguire^[11] wrote this article in 1967 approximately ten years after the first use of neoprene bridge bearings in the United States. Published in ASCE's Civil Engineering Journal it championed the use of neoprene bearings with a brief history and recommended changes to the AASHTO specifications. The history included the original uses of the bearings stating they were first used shortly after WWII in France and England for railroad bridges. It points out the following failings of the specifications at the time:

- There was no rule for the length of bearing in relation to the width of the beam except that it needs to fit under the beam.
- The stress limits were too stringent.
- There were no reasons given for choosing one hardness level over another.
- No standard sizes had been established increasing the cost of the bearings since manufactures had to retool for each new set of pads.

Changes that were recommended:

- Shape factors should be above 5 to limit the vertical deflections to 7% or less with the compressive stress limit.
- Eliminate the requirement of the use of adhesives or mechanical fasteners to secure the bearings in exchange for a minimum compressive stress.
- Set a total load deflection limit.
- Require manufactures to place trademarks on the bearings for positive identification.
- Require testing of samples of the bearing materials during the production run.
- Eliminate the tear test required then.
- Add 50 durometer physical properties to the list of properties that included only 60 and 70 durometer hardnesses.

Pare advocated these changes to increase the usefulness of neoprene bearings and concludes stating that over the ten previous years the neoprene bearings that had been in service had performed with little or no deterioration. Since then other reports have continued to tout the virtues of neoprene as a bridge bearing material and push the limits of its use.

2.2.1.5 State-of-the-art elastomeric bridge bearing design

Roeder and Staton^[12] reported on compression load failures as well as the standards current as of 1991. The modes of compressive failure included both yielding failures of the reinforcement and delamination of the neoprene layers. The reported delamination compressive stresses ranged up to 8500 psi but were scattered and no apparent correlation to the shape factor was found. All but one of the delamination failures were above 2300 psi. It was noted that a failure due to delamination does not result in immediately disastrous consequences for a bridge or building but does reduce the service life of the bearing by accelerating the fatigue process.

Fatigue failure modes were mentioned, but it was reported that limits to the compressive stress and shear strain were sufficient to prevent this mode. Specifically, shear strains of no more than 50% were said to effectively control failure by fatigue.

The article also mentioned that holes in the reinforcing layers resulted in stress concentrations that reduced the capacity of the neoprene bearing pads.

The intent of the article was to eliminate the misunderstandings that were restricting the use of neoprene bearings and allow for the use of additional capacity.

2.2.1.6 Elastomeric bearing research NCHRP report 109

The NCHRP Report 109^[13] is one of the most similar projects to this one and it presents information on stress relaxation of the shear modulus of neoprene bearings. Stress relaxation is the reduction of stress over time as displacement is held constant. In order to test the stress relaxation of neoprene, samples were created by gluing together a sandwich of two steel

compression plates, two pieces of neoprene with a SF of 2, and a center steel shear plate as shown in Figure 2-10.

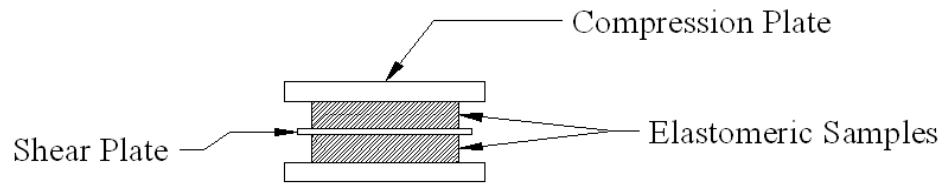


Figure 2-10. Sample for relaxation testing NCHRP 109^[13]

In order to conduct the test, the sample was first compressed approximately 10% of the sample thickness (0.10 in/in) over a period of about 5 minutes. The pads were then loaded in shear four times to approximately 50% shear strain at a rate of 8% per minute. The multiple cycles were used to condition the neoprene pads. After conditioning the pads were loaded to 50% shear strain and held in this position for 22 hours while shear load readings were taken every 2 minutes for the first 10 minutes, then at the half hour mark followed by readings at 1 hour, 3 hours, 5 hours, and 22 hours. An example of the data collected is shown in Figure 2-11.

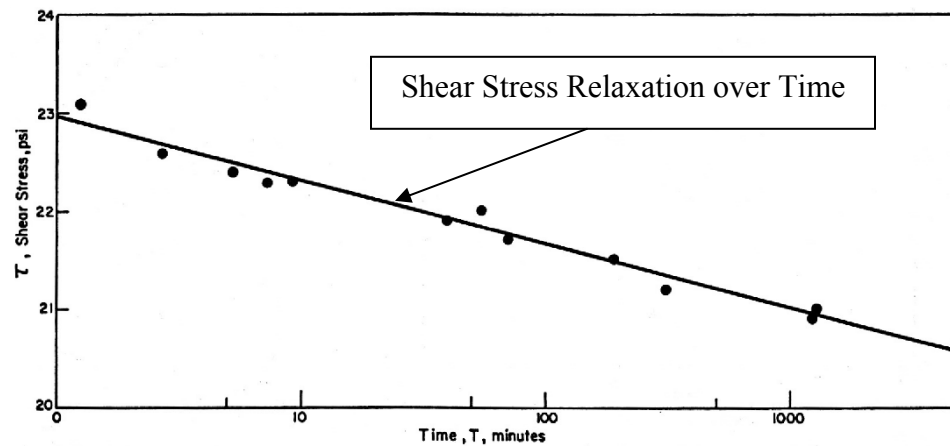


Figure 2-11. Typical shear stress – time graph constant 50% shear strain NCHRP 109^[13] (Source: Figure A-10 pp. 21)

The data in Figure 2-11 and data like it was used to generate Figure 2-12 which displays short-term shear modulus vs. percent relaxation per decade of time in minutes. A decade of time is defined as the log of time in minutes, i.e. 10 minutes is one decade, 100 minutes is two decades and 1000 minutes is three decades.

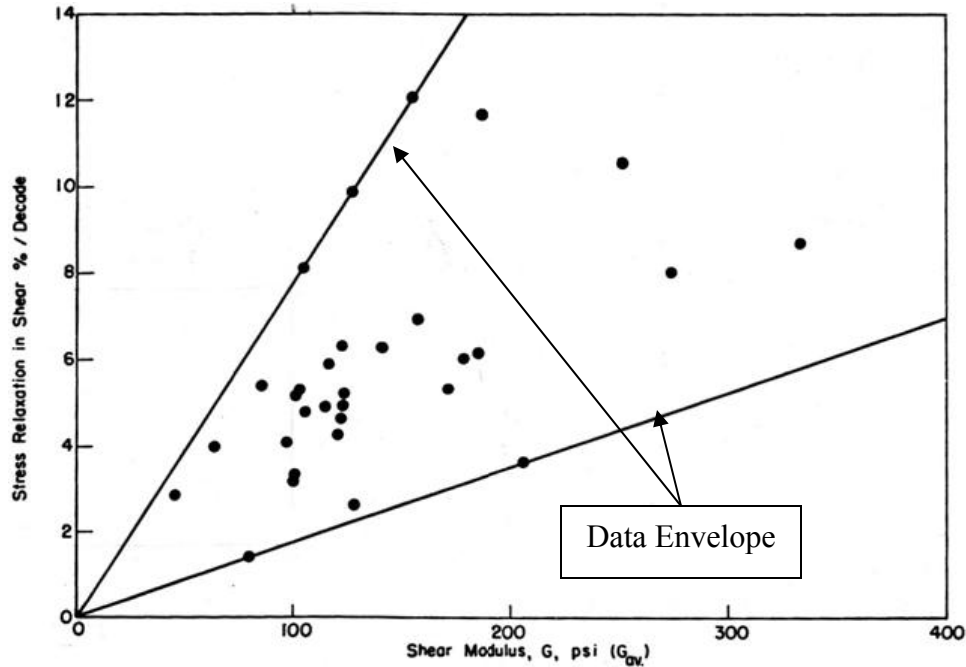


Figure 2-12. Shear modulus (G_{ave}) vs. stress relaxation per decade of time NCHRP 109^[13]
 (Source: Figure A-13 pp. 23)

The calculation for converting Figure 2-11 to a data point in Figure 2-12 is shown in Equation 2-9 and is plotted against the average of shear modulus of the first five conditioning cycles.

$$\text{Stress_Relaxation} = \frac{(r_1 - r_n)(100)}{(r_1)(n)} \quad (2-9)$$

where

r_1 is the shear stress at 1 minute (psi)

r_n is the shear stress after n decades of time (psi)

n is the number of decades of time

The trend in Figure 2-12 shows that as the values for shear modulus become greater, the scatter in the percent relaxation per decade of time increases. For 100 psi shear modulus material the percent relaxation ranges from 1.7% to 7.8% per decade of time. This would translate to a 1.7% to 7.8% reduction in the force required to hold a displacement after 10 minutes. After 100 minutes there would be an additional reduction of 1.7% to 7.8% in the force. An example of this calculation is found in Table 2-6.

Table 2-6. Relaxation examples

Number of decades (n)	Time in minutes	Time in days	Shear modulus G (psi) based on reductions	
			1.7% loss / decade	7.8% loss / decade
0	1	6.94 E-4	100	100
1	10	6.94 E-3	98.3	92.2
2	100	6.94 E-2	96.6	85.0
3	1000	0.694	95.0	78.4
4	10000	6.94	93.4	72.3

The longest stress relaxation test reported in NCHRP 109^[13] study was only 22 hours, which is not as long as it takes to apply loads such as those due to seasonal temperature change and prestressed concrete shrinkage. Table 2-7 shows the values of shear modulus based on the same calculations in Table 2-6 taken to time periods beyond their original test duration. In the NCHRP 109 research, all shear strain takes place in six minutes and then held constant for the duration of the test. In this study, the shear strain is applied in a linear fashion over the entire test period. Even though these experiments were conducted using different approaches, a direct comparison between this current project and the results in NCHRP 109 did provide a starting point for this investigation.

Table 2-7. Extended relaxation example

Number of decades (n)	Time in minutes	Time in days	Shear modulus G (psi) based on reductions	
			1.7% loss / decade	7.8% loss / decade
4.64	43200	30	92.1	63.8
5.11	129600	90	91.3	60.1
5.72	525600	365	90.3	55.4

2.2.1.7 Additional design data based on full-size bridge bearing pads of neoprene

This article^[14] presents data generated by E. I. Du Pont De Nemours and Company in 1981. The pad designs tested were fiberglass reinforced, steel reinforced and plain pads. The data reported was for compressive strain vs. stress for shape factors ranging from 3 to 20 for hardnesses of both 50 and 60 durometer. Additionally, tests were conducted to evaluate the ultimate load of some of the pads. The steel reinforced pads were reported to have failed in debonding above 5000 psi with two pads failing above 10000 psi.

2.2.1.8 Construction and design of prestressed concrete segmental bridges

Podolny and Muller^[15] provided a guide for engineers, architects and contractors for the design and construction of prestressed concrete segmental bridges. This guideline mentions that the shear modulus of neoprene is dependent on the rate of loading. Podolny and Muller provide a table that contains a list of recommended elastic constants based on hardness, however, they recommend that the values listed be doubled for instantaneous (i.e., impact) loading (Table 2-8).

Table 2-8. Elastic constants^[15]

Hardness (IRHD ±4)	Young's modulus E (N/mm ²) / ((psi))	Shear modulus G (N/mm ²) / ((psi))
45	1.80 / (261)	0.54 / (78.3)
50	2.20 / (319)	0.64 / (92.8)
55	3.25 / (471)	0.81 / (117)
60	4.45 / (645)	1.06 / (154)
65	5.85 / (848)	1.37 / (199)

Note: (Source: Table 5.1 pp. 246)

2.2.1.9 Design of elastomer bearings

This article was published in the PCI Journal in October of 1964^[16], Rejcha describes the considerations that need to be accounted for during the design process of an elastomeric bearing, presents some recommendations and provides a design example. The recommendations made by Rejcha about Elastomer Shear Modulus include the following:

For permanent forces, a considerable relaxation takes place. Therefore, a reduced modulus, $G' = 0.5G$, should be considered. The above is related to the effect of shrinkage and creep of a concrete girder, the vertical shortening under dead load, etc.

This particular interpretation was a major motivation of this research project since no additional justification was given.

2.2.1.10 Summary of general background

There is some misunderstanding as to the behavior of neoprene under long term loading and there needs to be some clarification as to what is the shear modulus of neoprene and if there is a lower limit to it. Additionally, steel reinforced neoprene bearings seem to have a reserve capacity for compression above the limits imposed by AASTHO.

2.2.2 Test Methods for Elastomeric Bearings and Complications

This section includes research on methods for finding the properties of elastomers as well as some of the complications that arise while conducting tests on elastomers. These complications include interactions between compression and shear as well as problems that might arise due to the manufacturing process.

2.2.2.1 Test method for determining the shear modulus of elastomeric bearings

Topkaya and Yura^[17] reviewed the accepted test methods for determining the shear modulus of neoprene pads and introduced a new method. The new method involved the use of inclined plates to simultaneously compress and shear the pads being tested.

Quad-shear tests (Figure 2-4) and tests using full size bearings were run along side the proposed inclined compression tests (a 1:10 slope and a 1:20 slope) shown in Figure 2-2, to compare the effectiveness of the new test. The compression using the 1:10 slope is 10 times greater than the shear force imparted while the 1:20 slope has compression 20 times greater than the shear force. This paper suggests cycling tests repeatedly until a repeatable result can be obtained before calculating the shear modulus.

During testing Topkaya, and Yura^[17] found that a change in loading rate from 50% shear strain in 2 minutes vs. 14 minutes resulted in a 5% drop in shear modulus for neoprene with a specified shear modulus of 200 psi. The change was less pronounced, only 2%, in neoprene with a shear modulus of 100 psi.

In a section of the paper titled “Future Research Needs” it was noted that there existed a need for a P-Δ correction factor for the test results. This factor was only recommended to be used for the samples not in bridge designs.

2.2.2.2 Elastomeric bridge bearings: recommended test methods: NCHRP report 449

The NCHRP Report 449^[18] reviewed several existing testing methods with the intention of simplifying and improving the AASHTO specifications. Tests for the following properties were examined.

- Hardness
- Shear Modulus
- Heat Resistance
- Ozone Resistance
- Low Temperature Behavior
- Creep and Compression Set

Yura, Kumar, Yakut, Topkaya, Becker, and Collingwood^[18] recommended the elimination of some of these tests, in particular the tests for hardness, heat resistance, ozone resistance, and compression set. These tests were reported to have limited or no practical value for neoprene bridge bearings. The report also recommended using the test method for determining the shear modulus of an elastomeric material that involved inclined plates that induced shear into samples placed under compression. It was also noted that shear modulus could be changed in an experiment by changing the loading rate from 30% shear in 2-3 minutes to 10 hours. This inclined shear test was not deemed suitable for this current research project due to the need to look at shear separate from compression.

2.2.2.3 On highly compressible helical springs and rubber rods, and their application for vibration-free mountings

Haringx^[19-21] developed a theoretical derivation of buckling in rubber rods and springs.

This differed from work done on rigid columns due to the low shear resistance of the material.

The derivation accounted for the shear strain contribution to buckling by treating it as an additional rotation.

2.2.2.4 Elastic stability of rubber compression springs

Gent^[22] reviewed research done by Haringx^[19-21] and experimented with the buckling of elastomeric columns investigating the shear effects. The buckling form of these elastomeric columns is due to the composite nature of the bearings. Because the compression and tension stiffnesses are so much greater than the shear stiffness the buckled shape includes shear deformations (Figure 2-13). Gent also examined the effect of compression on applied shear in these columns.

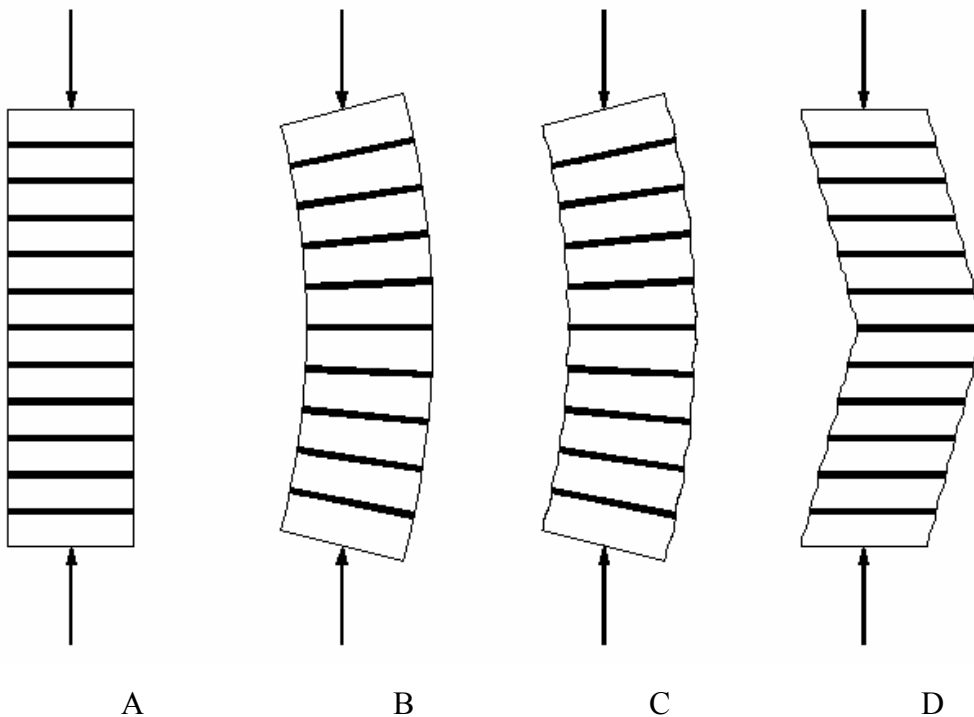


Figure 2-13. Shear buckling. A) Axially Loaded Bearing B) Euler Buckling C) Euler Buckling with Shear Contribution D) Pure Shear Buckling

2.2.2.5 An experimental study of elastomeric bridge bearings with design recommendations

Yura and Muscarella^[23] analyzed elastomeric bearing performance of both tapered and flat bearings with the purpose of developing a design procedure for tapered bearings. This study also indicated that wax infusion to meet AASHTO^[1] ozone test requirement is unnecessary and even detrimental for neoprene.

In the investigation of inclined bearings Yura and Muscarella^[23] examined the effect of compression on shear stiffness due to the decrease in buckling stability. Since at the buckling load there would be no shear resistance Yura and Muscarella asserted that there was a linear relationship, shown in Equation 2-10, between the shear displacement and the remaining buckling capacity of a bearing under compression.

$$\Delta_{total} = \frac{\Delta_{initial}}{1 - \frac{P}{P_{cr}}} \quad (2-10)$$

where

$\Delta_{initial}$ is the shear deflection due to applied shear force

P is the applied compression load

P_{cr} is the buckling load (Equation 2-11)

The buckling equation used by Yura and Muscarella was based on work done by Gent^[22].

This equation is based on the assumption that the top and bottom surfaces of the bearing are parallel to each other and that the applied shear force is applied to one of these surfaces.

$$P_{cr} = \frac{\phi G_0 A_s}{2} \left\{ \sqrt{1 + \frac{4EI f_r}{G_0 A_s} \left(\frac{\pi}{\phi h_{rt}} \right)^2} - 1 \right\} \quad (2-11)$$

where

ϕ is the total bearing thickness (including steel) divided by total elastomer thickness h_{rt}

A_s is the shear area of bearing

f_r is the ending stiffness coefficient = $1.0 + 0.575 S^2$

G_0 is the shear modulus of the elastomer under no compression

E is the $3G_0$

The shear modulus of an elastomer under no compression can be defined as follows.

$$G_0 = \frac{Vh_{rt}}{\Delta A_s} \quad (2-12)$$

where

V is the force necessary to shear a sample through distance Δ

The effect of compression on shear modulus can be seen directly by rewriting Equation 2-10 in terms of the shear modulus in Equation 2-12 and an effective shear modulus based on the total displacement.

$$G_{eff} = G_0 \left(1 - \frac{P}{P_{cr}} \right) \quad (2-13)$$

where

G_{eff} is the shear modulus under compression

This is still subject to the assumptions of parallel surfaces and loads in the original buckling equation. By replacing P_{cr} and E with their equations and distributing G_0 throughout a linear relationship between G_{eff} and the compression load P is shown in Equation 2-14.

$$G_{eff} = G_0 - P \left(\frac{\phi A_s}{2} \left\{ \sqrt{1 + \frac{12If_r}{A_s} \left(\frac{\pi}{\phi h_{rt}} \right)^2} - 1 \right\} \right)^{-1} \quad (2-14)$$

2.2.2.6 Slippage of neoprene bridge bearings

McDonald, Heymsfield and Avent^[24] reviewed existing literature and did field surveys to determine the causes of slippage and conclude with strong recommendations to eliminate as much wax as possible from the bearing and their surfaces. These recommendations included relaxing the ozone protection requirements and scraping the surface of the bearings with razor blades.

2.2.2.7 Elastomeric bearings: background information and field study

English, Klingner and Yura^[25] conducted field surveys to investigate the tendency of bearings to move gradually parallel to the supported beam. In extreme cases the pads would

move partially off of their supports and would have eventually let the beam fall to the underlying support if not corrected. This movement of the elastomeric bearings was described as “walking out”. The behavior of the bearings was found to occur due to thermal movement of bridges. In the field survey the only bearings observed “walking out” were made from natural rubber.

2.2.2.8 Neoprene bearing pad slippage at Louisiana bridges

Heymsfield, McDonald and Avent^[26] report on the investigation of neoprene bearing pad slippage and conclude that the pads were “walking out” due to daily temperature fluctuations and wax being excreted from the pads lubricating their surfaces.

2.2.2.9 Summary of test methods and complications

There seems to be some relationship between compression and shear modulus for elastomeric pads, and even though the relationship is not entirely clear it should be observed over the range of stresses allowed by AASHTO. Additionally, the manufacturing process of neoprene bearings includes the use of wax, which can cause problematic slippage during the service life of these bearings.

2.2.3 General Background and Models of Viscoelastic Material

This section covers research that uses models and modeling techniques for elastomeric behavior in an effort to account for the viscoelastic properties of elastomers. The most recently developed of these models tries to take into account the Mullins effect as well as the viscoelastic properties.

2.2.3.1 Basic continuum models

References Malvern^[27] and Findley, Lai and Onaran^[28] review the time dependent properties of viscoelastic materials. A variety of models are covered including the standard linear model or Kelvin Model shown in Figure 2-14.

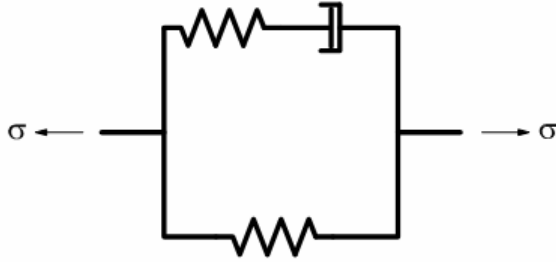


Figure 2-14. Standard linear model

This standard model is made up of spring elements and a dashpot which are shown in Figure 2-6. The combination of a spring element and dashpot in series is also known as a Maxwell element, shown in Figure 2-15 with its governing differential equation. Other models that are examined by References Malvern^[27] and Findley, Lai and Onaran^[28] include using an infinite number of Maxwell elements in parallel with the standard linear model.



$$\varepsilon = \frac{1}{2k} \sigma + \frac{1}{2\eta} \sigma'$$

Figure 2-15. Maxwell element

2.2.3.2 Molecular theory

References Smith^[29], Yin and Pariser^[30], Ronan, Alshuth and Jerrams^[31], Green and Tobolsky^[32] and Adkins^[33] all look at viscoelastic behavior from the perspective of molecular physics. Using molecular physics to describe the effect of loading rate and the effect of temperature on elastomeric materials requires the use of the random movement of the molecules due to internal heat (Brownian motion) and a temperature scale based on absolute zero. Many of the following papers are based on these concepts.

2.2.3.3 An engineering theory of nonlinear viscoelasticity with applications

Schapery^[34] discusses relatively simple stress-strain equations developed for nonlinear isotropic viscoelastic material at constant temperature. The equations Schapery used are based on Boltzmann's linear thermodynamic theory and they describe the post Mullins behavior. The equations account for all three dimension however they only cover unreinforced behavior and would have to be modified to take into account compatibility when looking at compression of reinforced pads. The shear equation is shown in Equation 2-15.

$$Q = \int_0^t G(t-\tau) \frac{d\gamma}{d\tau} d\tau$$
$$G(t) = G_e + \sum_s G_s e^{-\lambda_s t} \quad (2-15)$$

where

Q is the total shear stress

γ is the shear strain

τ is a dummy time variable

t is time

G_e is the elastic shear modulus ($G_e \geq 0$)

G_s is shear storage modulus series ($G_s \geq 0$)

λ_s storage exponential coefficient ($\lambda_s > 0$)

2.2.3.4 Constitutive modeling of the large strain time-dependent behavior of elastomers

Bergström and Boyce^[35] examined the response of carbon black filled chloroprene rubber. Polychloroprene, more commonly known as neoprene, is made from chains of chloroprene molecules (C_4H_5Cl). In the process of vulcanization these chains are linked or cross linked to one another with the addition of sulfur atoms. Bergström and Boyce use a model proposed by Arruda and Boyce^[36] consisting of 8 of these chains forming a network. Bergström and Boyce account for the time dependant behavior by leaving one chain “free”. Once the network has been deformed due to the application of stress this “free” chain is allowed to rearrange itself via Brownian motion. While the free chain rearranges itself the level of strain is held constant in the network and the rest of the network responds to the strain elastically. Eventually the “free” chain

will come to oscillate around a configuration that requires the least amount of energy to maintain, resulting in a level of stress in the sample equal to the elastic stress.

The experiments of Bergström and Boyce were conducted on samples that had the Mullins effect removed and their model mimicked the results of tests of samples placed into compression. One result of the model shown by Bergström and Boyce is that no matter how a sample was strained if held in a fixed position the stress would decay toward the elastic stress. This is shown in test data shown in Figure 2-16 (from Bergström and Boyce's paper). It is important to note in Figure 2-16 that after straining is resumed at the previous rate the stress strain relationship recovers to its previous trend. The standard linear model (Figure 2-14) was referenced to aid in the description of the observed behavior.

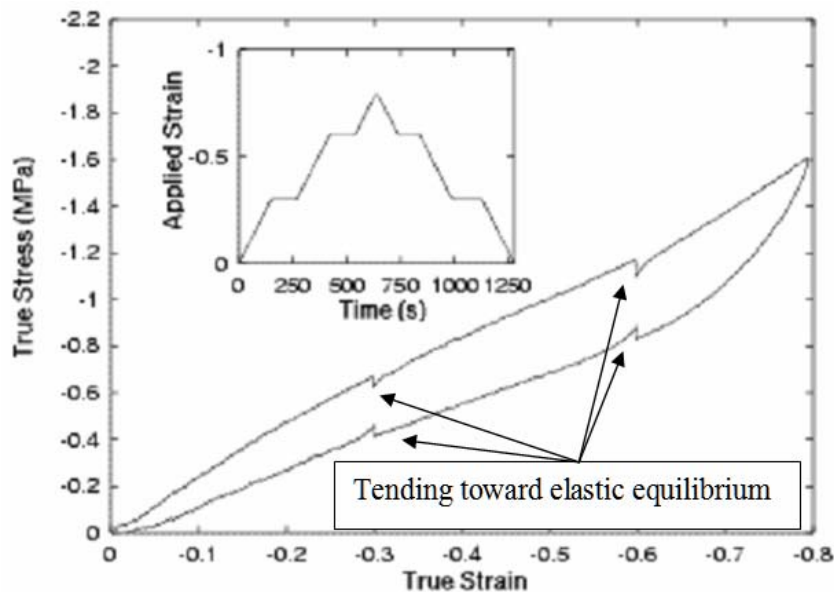


Figure 2-16. Test data from constitutive modeling of the large strain time-dependent behavior of elastomers.^[35] (Source: Figure 8 pp. 8)

2.2.3.5 A three-dimensional constitutive model for the large stretch behavior of rubber elastic materials

Arruda and Boyce^[36] present a model that successfully represents viscoelastic materials in uniaxial extension, biaxial extension, uniaxial compression, plane strain compression and pure shear. This is also the basis of Qi and Boyce's^[37] work.

2.2.3.6 The behavior of rubberlike materials in moderately large deformations

Bloch, Chang and Tscgoegl^[38] examined crosslinked rubberlike material with the use of relaxation modulus and strain energy functions. In this paper “moderately large deformations” referred to in the title refers to strains of up to 150%.

2.2.3.7 Constitutive model for stretch-induced softening of stress-stretch behavior of elastomeric materials

Qi and Boyce^[37] present a model of viscoelastic material behavior that includes the Mullins effect. This model describes the strain energy density function and how it relates to the strain softening of the viscoelastic material. This model bears consideration due to the fact that almost all bearing pads do not have the Mullins effect removed before they are put in service. Additionally, to account for the Mullins effect by testing is both cost prohibitive and technically difficult.

2.2.3.8 Nonlinear finite element analysis of elastomers–technical paper

MSC Software Corporation’s paper^[39] is on the capabilities of their finite element model software with respect to elastomeric modeling. Their paper included which variables their software took into account, and references some of the theory and equations behind the software.

2.2.3.9 Summary of models of viscoelastic material

There are theoretical models that can account for most of the behavior of neoprene. Using these models requires finding the required coefficients and knowing the displacement history that the bearings are going to go through. None of these models appear to have been validated for the type of long term loading to which bridge bearings are subjected.

2.2.4 Possible Temperature Effects

This covers research on what possible effects temperature could have during testing of samples. This predominately is to determine what actions can be taken to minimize these effects during the testing of elastomers for this report.

2.2.4.1 Viscoelastic properties of polymers

Ferry^[40] describes the glass transition temperature, which is approximately -58°F for neoprene, as the temperature at which the “free volume” in an elastomer first starts to increase. Glass transition temperature specifically refers to the fact that elastomers become brittle and can shatter below this temperature. The “free volume” made up of the voids in the molecular structure is used by the elastomer’s carbon chains to rearrange in response to an external stress. When the temperature rises above the glass transition temperature in a pure elastomer the volume of the voids increases proportionally to the change in temperature. This increase of volume makes it easier for the carbon chains to move and this increased mobility has the effect of softening the elastomer.

2.2.4.2 Low temperature behavior and acceptance criteria for elastomeric bridge bearings: NCHRP report 325

Roeder, Stanton, and Feller^[41] write about ways low temperatures stiffen elastomeric bearings. One reported way is crystallization; this refers to the increase of shear modulus over time due to the cooling of the molecular structure down to a point where the carbon chains begin to stick to each other between the sulfur bonds. They indicate that this only begins to occur below 50°F in neoprene. Instantaneous stiffening is another phenomena that is due to the reduction in internal energy in an elastomer. It is characterized as an immediately measureable stiffing when a sample has reached thermal equilibrium. They also mention that the glass

transition temperature is the temperature at which samples of elastomers may fracture in a brittle manor.

Roeder, Stanton, and Feller^[41] also developed design requirements and acceptance test procedures for low temperature elastomeric bridge bearings.

2.2.4.3 Performance of elastomeric bridge bearings at low temperatures

Yakut's^[42] dissertation formed the basis of Yakut and Yura's^[43] work. The dissertation shows more clearly exponential trends in shear modulus due to instantaneous stiffening for neoprene and natural rubber. When additional filler was used to increase the shear modulus of an elastomer the instantaneous stiffening became more pronounced with decreasing temperature. The neoprene samples had been specified to have shear moduli of 100 psi and 150 psi however, the actual shear moduli values were closer to 110 psi and 230 psi respectively. The trends in Yakut's data are shown in Figure 2-17.

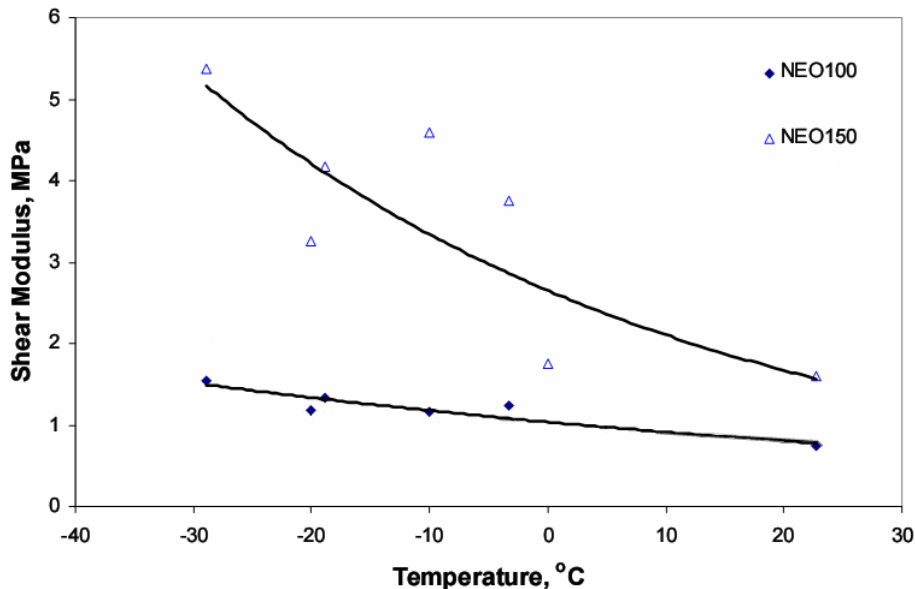


Figure 2-17. Elastomer shear moduli variation with temperature.^[42] (Source: Figure 5.28 pp. 106)

2.2.4.4 Summary of temperature

Neoprene behaves in a nonlinear fashion and temperature can play a roll in the stiffness of neoprene bearings. However, AASHTO requires the designer to select of a grade of neoprene that has been formulated to minimize this temperature effect and this selection criteria is shown in Table 2-2.

2.2.5 Summary of Literature Review

It should be noted that not all of the literature reviewed was directly related to the research objective and some was redundant. A summary of these references are in Appendix B. During the literature review for neoprene bearing pads, no models were found for steel reinforced neoprene bearings which were based on the strain rate in highway applications. However, as shown in the literature, reduced strain rate does result in a reduction in effective shear modulus. Because of this observation, it is necessary to investigate to what extent this occurs. The literature reviewed revealed that the critical parameters to monitor in the investigation were; shape factor, the effect of compression on shear modulus and cycling's effect on shear modulus. Additionally the literature reviewed provided insight into a potential testing problem related to pad slippage due to the addition of wax to the neoprene.

CHAPTER 3 METHODOLOGY

3.1 Developing the Samples

In order to develop a test program, a sample size needed to be chosen with consideration of both the design of pads for the field and pads used in previous research. The majority of the full size of steel reinforced pads used in bridges are too unwieldy for laboratory testing. It is also exceptionally difficult to reproduce loads due to the dead weight of a bridge superstructure for the larger pads in the lab. Therefore, the only viable alternative was to scale the bearing pads to a more manageable size.

Since a variety of shape factors are used in the field it was decided to have samples with a similar range of shape factors. The range of 8 to 24 was chosen as representative for larger bridges based on the values in Tables 2-3 and 2-4. It was also decided to use samples with grade 0 material which is what is typically used in Florida. The standard design shear modulus of neoprene specified in the FDOT Standard Specifications^[3] has a durometer hardness of 50 and approximately a 100 psi shear modulus. This is what was specified in the samples design.

A base line compression stress of 1.0 ksi was chosen for the majority of the tests in this study. However, FDOT^[3] and AASHTO^[1] provide an upper limit for a compressive stress of 1.6 ksi with additional testing, therefore the test apparatus was developed to be able to reproduce this stress.

A pad with eight steel reinforced layers was selected as a median representative based on the information provided. Once the number of layers was chosen the typical maximum compressive stress was used to calculate a bearing area. The sample size was chosen to be no larger than 12 inch x 12 inch due to concerns over high compressive loads. These concerns were primarily related to laboratory safety around high pressure hydraulic lines and concerns about

being able to produce those loads.. The layer thicknesses were varied to create the range of shape factors. Pads having uniform layer thickness from 1/8 inch to 3/8 inch were used to create shape factors ranging from 24 to 8, respectively. The thickness of the steel reinforcement was varied proportionately within the limits of the manufacturing process (Table 3-1). The manufacturer could not provide samples that contain steel thinner than 16 gauge sheet metal due to problems caused by the process of vulcanization. Table 3-1 lists the final properties and dimensions for the neoprene bearing pad samples and as an example drawing Figure 3-1 shows the design of the SF 24 sample. All of the other samples were similar in design with only the dimensions varying as noted in Table 3-1.

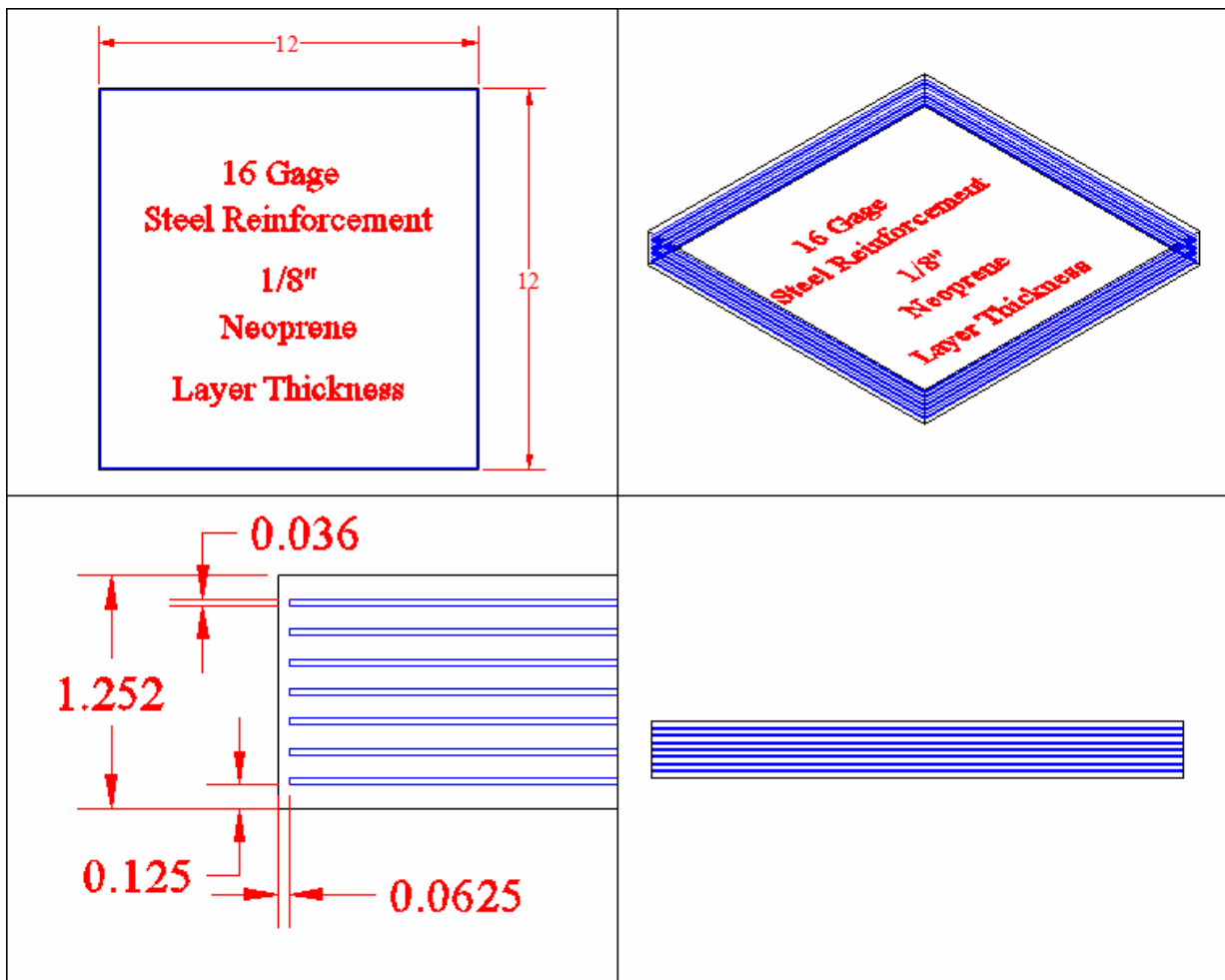


Figure 3-1. Pad design for shape factor of 24 (1 inch pad or SF-24 pad)

Table 3-1. Sample physical dimensions

Shape factor	Layer thickness (in)	Elastomer thickness (in)	Steel gage & thickness (in)	Number of neoprene layers	Overall dimensions (in)
8	0.375	3.0	12 – 0.1050	8	12 x 12 x 3.735
12	0.250	2.0	15 – 0.0670	8	12 x 12 x 2.469
16	0.1875	1.5	16 – 0.0598	8	12 x 12 x 1.919
24	0.125	1.0	16 – 0.0598	8	12 x 12 x 1.419

Note – The side cover for the steel in all of the pads is equal to 1/16th of an inch.

In the ordering of the samples, 100 psi shear modulus material was specified however, upon receipt of the specimens it was found that, 50 durometer hardness material was supplied instead. This information on the material status was supplied with the shipment of the samples. The manufacture chosen to make these samples is a regular supplier for FDOT projects and used the same process in their fabrication as typically used for FDOT. Because of the substitution of material, the samples were in compliance with FDOT and could have been placed into service in a Florida bridge.

3.2 Test Program

In order to determine the most relevant information for use of this research, the method typically used in the design of bridge bearings was referred to in the development of this test program. AASHTO^[1] specifies that the minimum elastomer thickness is twice the maximum shear displacement. This is equivalent to making the maximum shear strain allowed by AASHTO^[1] 50%. Since this value was also cited^[7] as a limiting factor in the serviceability of these bearings it was determined that this maximum shear strain would be the limit of these tests. Strain rates were chosen to determine the time dependent properties of the material and to provide a basis for establishing trends. In addition to variations in strain rates for different shape factors, the effects of initial “new” pad stiffness compared to pad stiffness after the removal of the Mullins effect, and the effects of different levels of compressive stress were also considered

in the test program. The determination of the change in stiffness due to the Mullins effect removal is particularly important owing to the fact that bearings in the field are not cycled prior to being placed into service.

3.2.1 Strain Rates

The strain rates for this study range from 50% shear strain in 45 seconds to 50% shear strain in 90 days. The rates were chosen to conform with those found in ASTM D 4014^[6], as well as conforming with strain rates that would reach 50% shear strain in 12 hours, a week and three months. These rates were chosen to correspond to daily, weekly, and seasonal temperature changes. All tests were conducted from zero to a maximum positive shear strain of 50% with the exception of the 18-minute cyclical test. The 18-minute cyclical test was conducted with strains that range from positive to negative 50%. In this report, tests are referred to by the time taken to go from 0 to 50% strain as shown in Table 3-2. For visualization purposes, Figure 3-2 depicts a scale representation of a 12 inch by 12 inch pad with 3 inches of neoprene in both the initial pre-strained configuration and how it appears at 50% shear strain. In the end a total of 45 tests were conducted; three of these tests were thrown out due to sensor malfunctions during testing.



Figure 3-2. Bearing deformation. A) Initial pad. B) Shear strained to 50%.

Table 3-2. Testing matrix

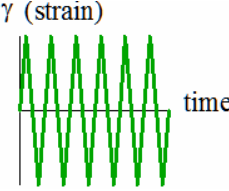
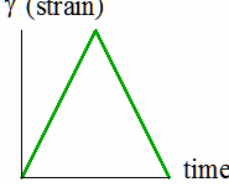
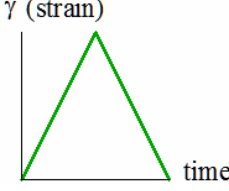
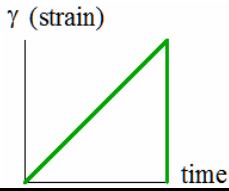
Duration / type	Shear strain vs. time 50% strain max.	Time from 0 to 50% shear strain
18 min / 2 way linear (6 cycle at 3 min each) (removing the Mullins effect)		45 seconds
24 hr / 2 way linear		12 hours
14 day / 2 way linear		7 days
90 day / linear		90 days

Table 3-3. Testing matrix: duration variation

Elastomer thickness (in)	Shape factor	Number of tests			
		45 seconds	12 hours	7 days	90 days
1	24	2	6		
1.5	16	2	10*	2	2
2	12	2	5		
3	8	2	7	1	1

* – A single test was conducted for 9.5 hrs and a single test was conducted at 7.2 hrs

3.2.2 Mullins Effect

Since some literature indicated the possibility that both transitory and permanent deformations could occur in the samples, the order of the tests and time between tests were chosen to minimize the impact of potential permanent deformations on the results. Although permanent deformations were not observed during the course of testing, another type of

permanent change was observed, the Mullins effect (stress softening). In order to quantify the Mullins effect, it was necessary to eliminate this effect in at least some of the samples. The Mullins effect was eliminated by using a short term 18 minute cyclic loading test; straining the samples to 50% shear strain multiple times prior to conducting other tests. To account for the fact that new bearing pads in the field will exhibit initial pad stiffness (i.e. Mullins effect is not removed) tests were run at various strain rates with and without elimination, of the Mullins effect.

Transitory deformations were found to dissipate upon the removal of the compression at the end of each test. As a result, tests were run in a sequence that let the pads rest after each test and recover from this transitory deformation.

The 18 minute test was chosen to match the loading rate in ASTM D 4014^[6] which was 0 to 50% shear strain over 30 to 60 seconds. Based on the ASTM rate a complete cycle is from 0 to +50% then to -50% and back to 0% shear strain should range from 2 to 4 minutes. Using six cycles at the average rate of 3 minutes per cycle the total duration of the test is 18 minutes.

The last 3 minute period of the 6 cycle test is the relevant test^[6] for certifying the shear modulus of an elastomeric sample with the Mullins effect removed. Since the first cycle of the 6 cycle test did not have the Mullins effect removed it was used to determine the initial shear modulus at this strain rate. For the purpose of this report an individual cycle will be referred to as a “45 sec.” test. Table 3-4 shows the number of tests that were conducted with and without the removal of the Mullins effect.

Table 3-4. Testing matrix: with and without Mullins effect removed

Elastomer thickness (in)	Shape factor	Number of tests							
		45 seconds		12 hours		7 days		90 days	
		w/	w/o	w/	w/o	w/	w/o	w/	w/o
1	24	1	1	6					
1.5	16	1	1	7*	3**	1	1	1	1
2	12	1	1	5					
3	8	2		6	1		1		1

* – A single test was conducted for 9.5 hrs

** – A single test was conducted for 7.2 hrs

3.2.3 Multiple Compressive Stresses

For the purpose of looking at the interaction between compressive stress and effective shear modulus some tests were conducted at multiple compressive stresses. To examine this relationship a series of 12 hour long tests were run at the compressive stresses of 0.5 ksi, 1 ksi, 1.2 ksi, and 1.5 ksi. The tests not included in Table 3-5 were all conducted at 1 ksi compression.

Table 3-5. Testing matrix: 12 hour compression variation

Elastomer thickness (in)	Shape factor	Number of tests			
		0.5 ksi	1 ksi	1.2 ksi	1.5 ksi
1	24	3	2		1
1.5	16	3	6		1
2	12	1	1		2
3	8	1	4	2	

3.3 Design of Test Apparatus

The testing process was accomplished with the aid of compression and friction. This was started by sandwiching a thin steel plate between two sample pads similar to what is shown in Figure 2-10 then compressing the samples between two thick steel plates. Once the samples reached the desired compressive load, the shear plate was displaced. In the initial testing, these steel plates were cleaned then roughened with a hammer. The smoothness of this surface was not considered a problem since the coefficient of friction of neoprene on steel was assumed to be greater than 0.05. This assumption proved to be incorrect due in part to wax that was infused

into the neoprene samples during the manufacturing process as previously noted^[23, 24, 26]. Once the samples were in compression this wax bloomed to the surface and resulted in pad slippage when the shear plate was loaded. The slippage was found to occur in the range of 15-25 psi shear stress for 12 hour tests and 35-40 psi for 45 second tests. In order to prevent slipping the surfaces of the plates were roughened to about the equivalent of Coated Abrasive Manufacturers Institute (CAMI) 30-50 grit sand paper with a pneumatic weld chipping hammer.

The compression loading was accomplished with a 400-ton double acting cylinder (Enerpac model number CLRG-4006). Once the samples reached the desired compressive stress the steel plate between the two samples was then either pushed or pulled at a controlled displacement rate, and the load required to hold this displacement was measured. With data on displacement, load, and given the geometry of the pads, the shear modulus of the material could be calculated.

In order to provide a correlation between the short-term stiffness, which was typically known, and the long-term stiffness both short-term and long-term tests were conducted on the same samples. To accommodate the range in loading rates, it was determined that two separate loading systems would be the most practical.

The short-term loading rate of 3 minutes per cycle was based on tests cited in the literature review. This relatively quick application of loading was accomplished with a 60-ton hydraulic double acting cylinder using an electronically controlled servo valve connected to a constant hydraulic pressure source. An electric hydraulic pump was used for this pressure source.

The slow rate of displacement needed in the long-term test was simulated by moving a ball-screw jack with a stepper motor controlled by a computer at the rate of 0.001 inch per cycle. This resolution translates to a strain rate of 0.002 in/in per cycle in the thinnest sample pad.

Figure 3-3 shows the testing apparatus with the short-term loading mechanism connected and the long-term loading mechanism disconnected. During normal operating conditions either the short-term or long-term loading system was connected, but not both.

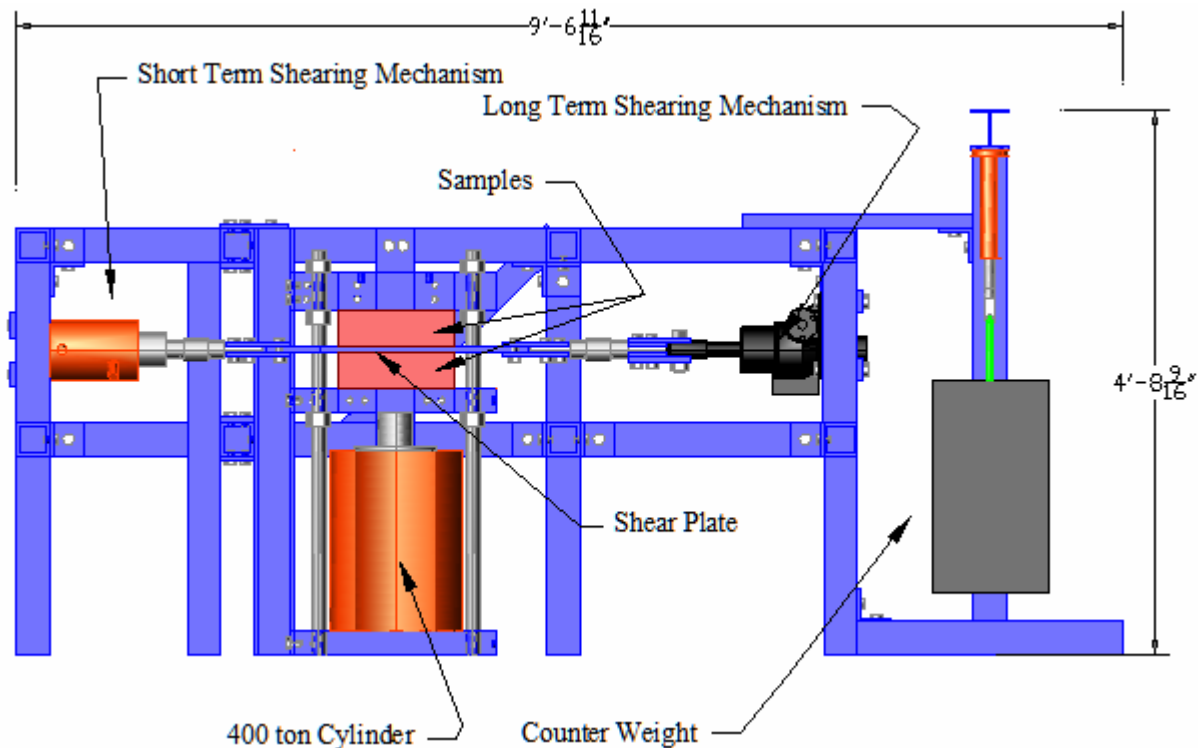


Figure 3-3. Test apparatus cross section

The loading jacks were connected to the central shearing plate through load cells with a 30 kip capacity. The shear displacement data was monitored with two potentiometers (POTs) which were read continually for the short-term tests and after every movement for the long-term tests. The control program used a calculated number of steps of the stepper motor to control the displacement rate of the samples during the long-term tests. Operating the system in this manner allowed for accurate movement without relying on fluctuating readings from the POTs. A photo of the test apparatus is shown in Figure 3-4.



Figure 3-4. Test apparatus photo

3.4 Major Components of the Test Apparatus

The test mechanism can be broken down into five major parts:

- Compression mechanism
- Long-term shear loading mechanism
- Short-term shear loading mechanism
- Reaction frame
- Instrumentation

3.4.1 Compression Mechanism

The compressive load in the sample bearings was applied with a 400-ton double acting cylinder Enerpac model CLRG-4006 pressurized by a 2/4-ton double acting cylinder Enerpac model number RD-46 (4 ton advancing, 2 ton retracting). The compressive load was measured by a 300 kip load cell. The hydraulic fluid in the 4-ton double acting cylinder was pressurized by suspending a weight from it. The pressurized side of the 4-ton cylinder was connected to the extension side of the 400-ton cylinder to compress the samples. In theory the two-jack system

shown in Figure 3-5 allows a constant pressure to be maintained as the sample pads creep under compression. An example of this method of constant pressure was found in the research by Muscarella and Yura^[23] done for the Texas Department of Transportation. Over typical short-term testing creep is not a factor, but with durations up to 90 days creep becomes a consideration.

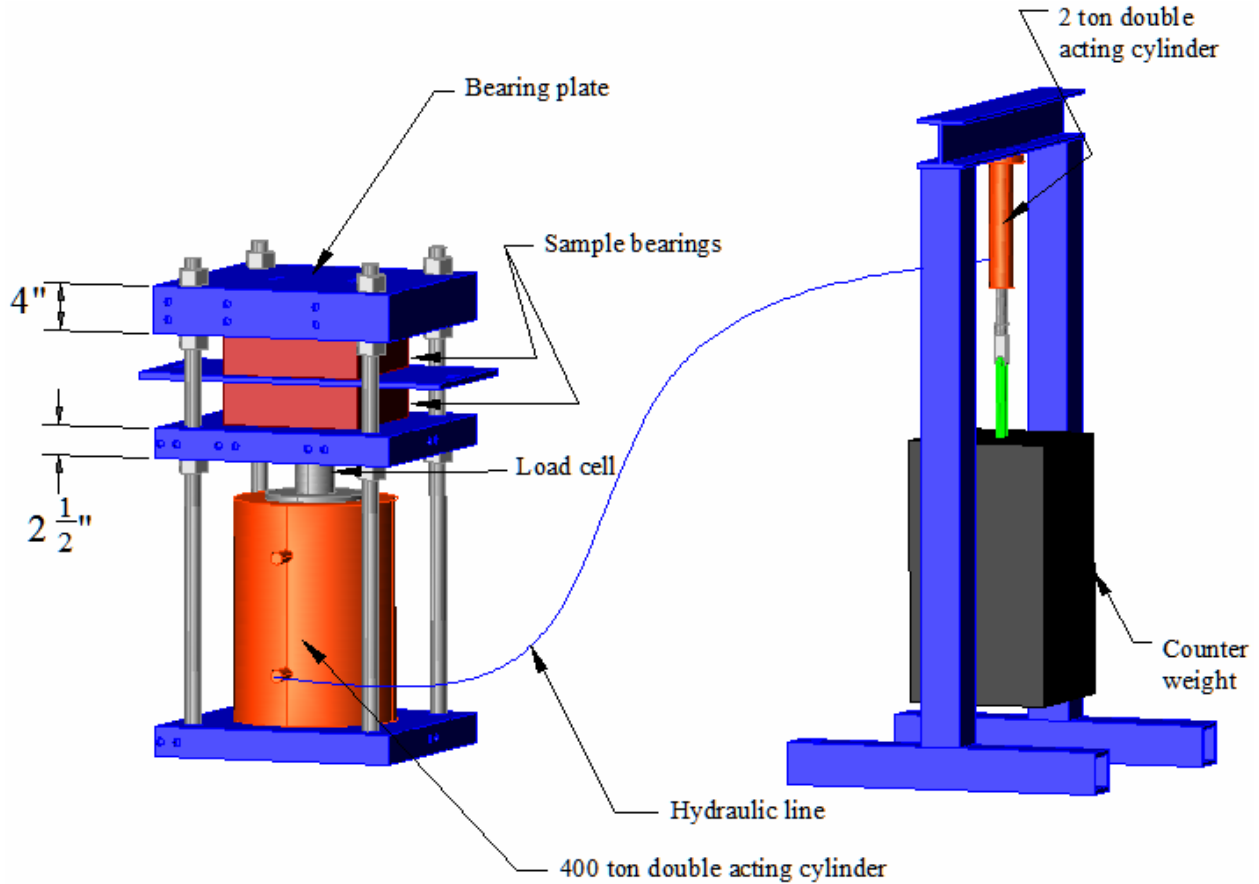


Figure 3-5. Compression mechanism

The combinations of cylinders available to produce the load required in testing are compared in Table 3-6. The two criteria for determining the combination of the two jacks was first, keeping the line pressure below 3000 psi, and second, minimizing the number of times the hydraulic system would need to be refilled based on the assumed maximum of 0.04 inch of compression creep in the thickest samples. A schematic of the hydraulic system is shown in

Figure 3-6. Some components rated at 10 ksi were chosen due to concerns over the high pressures in the hydraulic system.

Table 3-6. Cylinder combinations (based on 1.6 ksi compressive stress)

High load cylinder					Low load cylinder						Fluid needed for creep (in ³)	Travel for small of cylinder (in)	Number of strokes for refills	
Max cylinder cap. (tons)	Cylinder eff. area (in ²)		Stroke (in)	Line pressure (psi)	Max cylinder cap. (tons)	Cylinder eff. area (in ²)		Stroke (in)	Required weight (lbs)					
Adv.	Ret.	Adv.	Ret.		Adv.	Ret.	Adv.	Ret.						
250	104	56.8	23.7	11.81	4056	4	2	0.79	0.34	6.13	1379	2.41	7.10	1
300	100	70.7	23.5	11.81	3258	4	2	0.79	0.34	6.13	1108	3.00	8.83	1
400	138	86.79	29.99	11.81	2655	4	2	0.79	0.34	6.13	903	3.69	10.84	1
500	169	113.3	38.37	11.81	2034	4	2	0.79	0.34	6.13	692	4.81	14.15	2
600	207	132.6	45.79	11.81	1738	4	2	0.79	0.34	6.13	591	5.63	16.56	2
800	263	182.3	59.99	11.81	1264	4	2	0.79	0.34	6.13	430	7.74	22.78	3
1000	370	227.2	83.97	11.81	1014	4	2	0.79	0.34	6.13	345	9.65	28.38	4

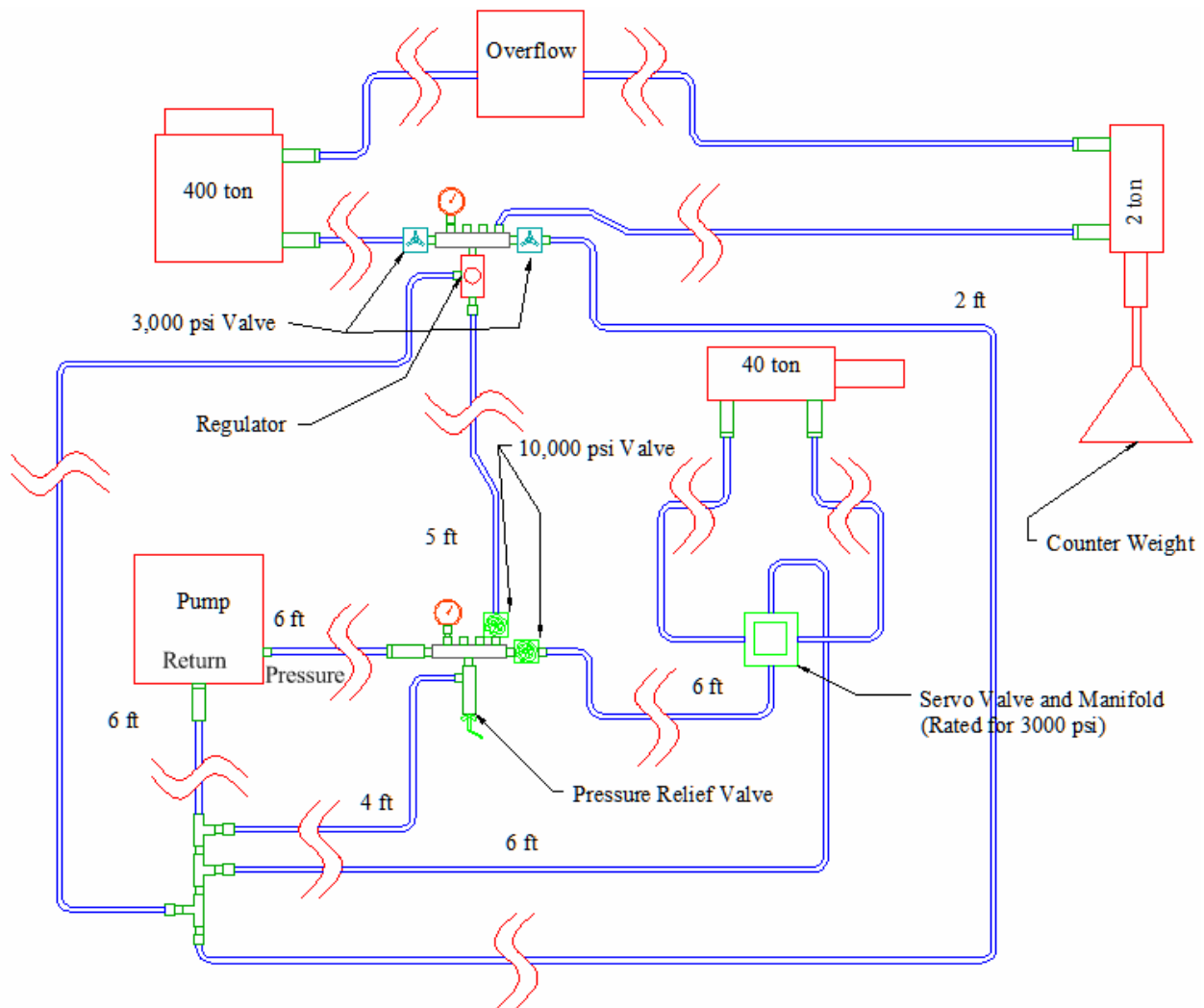


Figure 3-6. Hydraulic system diagram

The hydraulic system was designed so that the fluid reservoir in the 2/4 ton cylinder could be refilled since it was expected to drain down due to the compressive creep of the samples during long-term testing. The same pump used in the short-term testing hydraulic system was used to refill the compression mechanism.

3.4.2 Long-Term Shear Loading Mechanism

The long-term shearing mechanism was controlled by a computer due to the duration of the test. A hydraulic jack was ruled out for the long-term loading mechanism due to concerns over leaks. After investigating the operating capacity of a ball screw jack from Joyce/Dayton Corporation, a 10 ton jack with the addition of a 100:1 reducer was chosen. A ball screw model was picked due to its reduced internal friction; internal friction could cause the jack to only be able to move in jumps instead of a continuous motion. In combination with the reducer, the jack can be operated at a fine resolution of motion with a small motor. A stepper motor was chosen over a conventional motor to operate the jack because of its ability to be operated by a computer with precision control and then hold its position during possible power outages. Figure 3-7 shows the ball screw jack in position during operating.

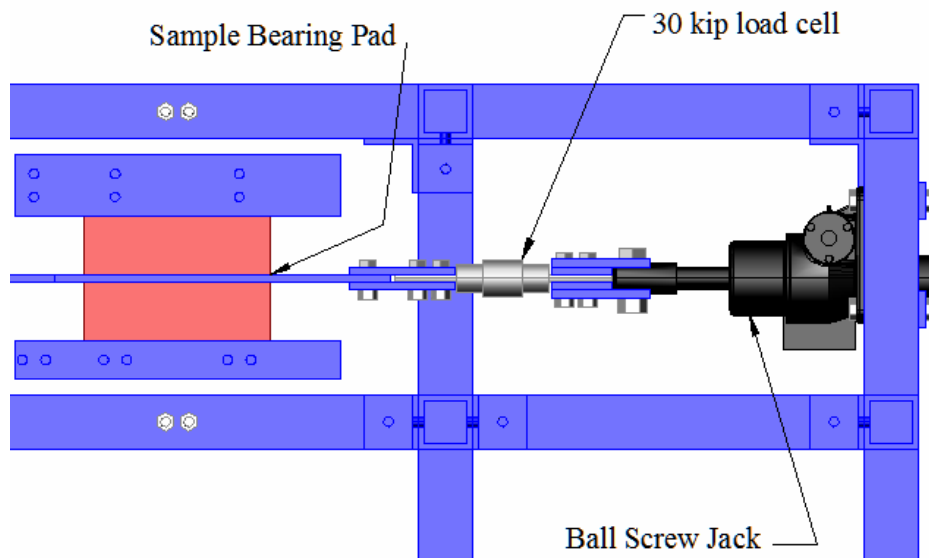


Figure 3-7. Long-term shear loading mechanism

3.4.3 Short-Term Shear Loading Mechanism

The short-term shearing mechanism was capable of moving the shear plate in a cyclic fashion with periods of approximately 3 minutes each. The load required to shear a pair of 144 in² bearing pads made from an elastomer with 100 psi shear modulus to 50% strain is 12 kips. A safety factor of 1.3 was used in the design calculations of the system. For the short-term shearing mechanism the controlling factor was the hydraulic pressure rating of 3 ksi for the servo valve used to control the hydraulic cylinder rather than any other load requirements. In order to create the 12 kip shear load and operate at or below the 3 ksi pressure limit a 60 ton cylinder was incorporated into the design.

Since the short-term loading system is idle for long periods of time, the section of the support frame housing the short-term loading system was made to be removable. The ability to remove the short-term loading system allows it to be used with multiple testing apparatuses if it became necessary. Figure 3-8 shows the 60 ton cylinder mounted and connected to the shear plate through a 30 kip load cell.

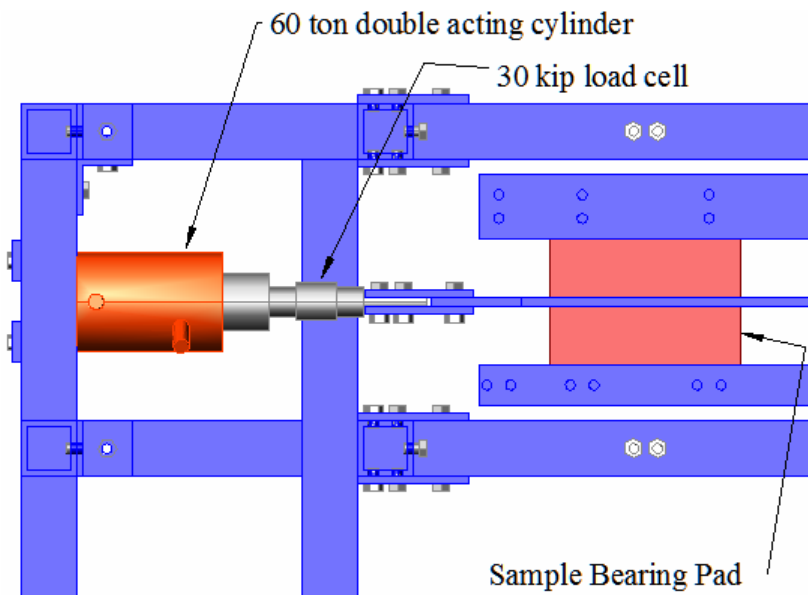


Figure 3-8. Short-term shear loading mechanism

3.4.4 Instrumentation

The test data was collected from two linear variable differential transformers (LVDTs), two potentiometers (POTs), three load cells, and a temperature sensor. Two POTs were used to measure the horizontal displacement of the shear plate and two LVDTs were used to monitor the vertical creep of the samples and the vertical rotation of the shear plate. Two load cells with a 30 kip capacity and were used to monitor shear forces during the short-term and long-term loading tests. Additionally the disconnected load cell signal was used as a baseline value to eliminate noise in the other two load cell signals. The final load cell with a 300 kip capacity and was used to monitor the compressive load applied by the 400 ton cylinder. The temperature sensor was used for monitoring fluctuations in ambient temperature.

3.5 Procedure

The procedure used to run these tests started with placing the pads in the test apparatus. The pads were centered over the 400 ton cylinder with the shear plate between them and then the 400 ton cylinder was raised so that the top pad was within 0.1 inches of the top reaction plate. The LVDT sensors were then lowered to a point where they are partially compressed to establish the starting position of the shear plate vertically. The Labview program was then started to begin collecting data as soon as the pads begin compressing.

3.5.1 Compression

It was initially thought that the counter weight system would be able to maintain a constant compressive stress during the stress relaxation of the pads but it was found that the 2/4 ton slave cylinder used for the compression system had a relatively high internal friction which prevented it from moving smoothly. Because of this high internal friction the compressive stress did not remain constant as stress relaxation occurred in the pads. This was accounted for by first over pressurizing the pads and then allowing them to rest prior to testing. The compressive stress

reached the target pressure by the time the sample reached maximum shear strain. The increase in compressive stress was around 20% of the target value for each test with this being reduced to about 10% by the time the shear load was applied. An example of the compressive stress load history is shown in Figure 3-9.

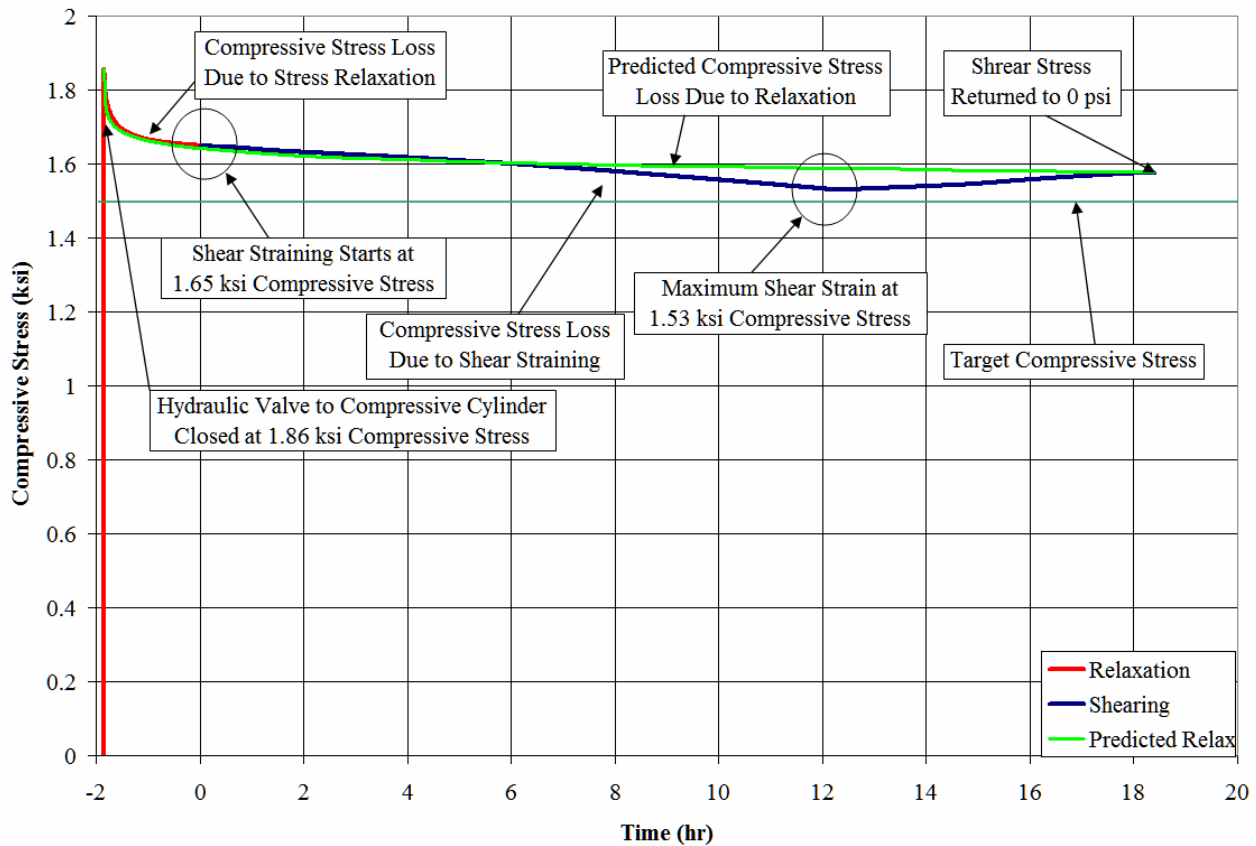


Figure 3-9. Compressive stress losses during SF 12, 1.5 ksi, 12 hour test

A slight additional loss in compression was observed during the shearing of the samples. This additional loss is thought to be due to the samples not undergoing pure shear but instead undergoing mostly shear with some bending.

Once the pads were brought up to the starting compressive load (20% higher than the target), the compressive hydraulic system was closed and allowed to set for around 2.5 hours. Using a targeted compressive stress rather than strain was used since both AASHTO and FDOT place limits on stress rather than strain.

3.5.2 Shearing

The shear loading was displacement controlled and as such there were certain parts of the computer program that monitors the readings of the POTs to control how fast the shearing jacks reached 50% shear strain. Additionally, this feed back determined when the shearing jacks' direction was to reverse. Throughout the testing, readings from the various sensors are recorded to a text file which can then be analyzed in a spreadsheet program.

3.6 Temperature Factors

Since all but one of the tests' average temperatures were within the allowable limits of the ASTM test^[6] and based on the trend exhibited by Yakut's^[42] data in conjunction with the reduced filler used in the samples the effect of temperature were expected to be negligible.

CHAPTER 4 TEST RESULTS

This chapter provides sample data from the test program, the methodology used to determine the shear modulus, and general results. A complete summary of all data is in Appendix A.

4.1 Sample Data

The displacement history from the 90 day test of the sample having a SF equal to 16 is shown in Figure 4-1. This test used a pair of bearing pads where each pad's total elastomer thickness was 1.5 inches and as such a 50% shear strain was equivalent to 0.75 inch of shear displacement. This test was conducted using approximately a 1 ksi compressive stress. The corresponding recorded shear force history is shown in Figure 4-2. This history consists of the total force applied to the top and bottom pads. The force history for an individual pad would show half of the load in Figure 4-2.

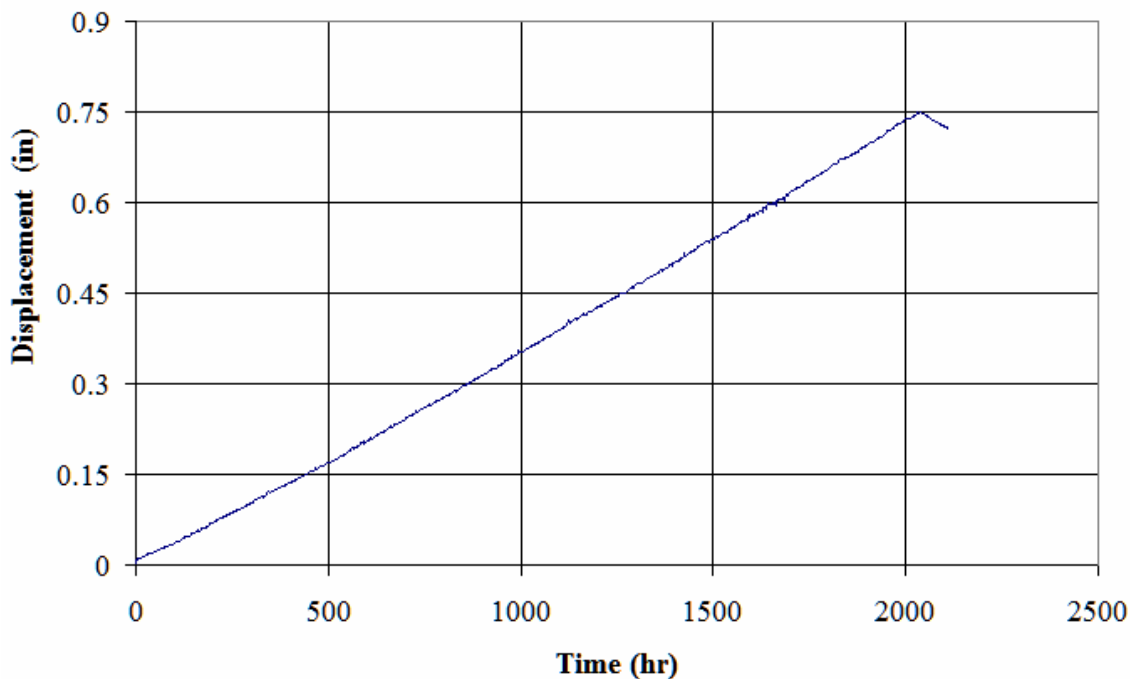


Figure 4-1. Displacement time history from 90 day test (SF = 16)

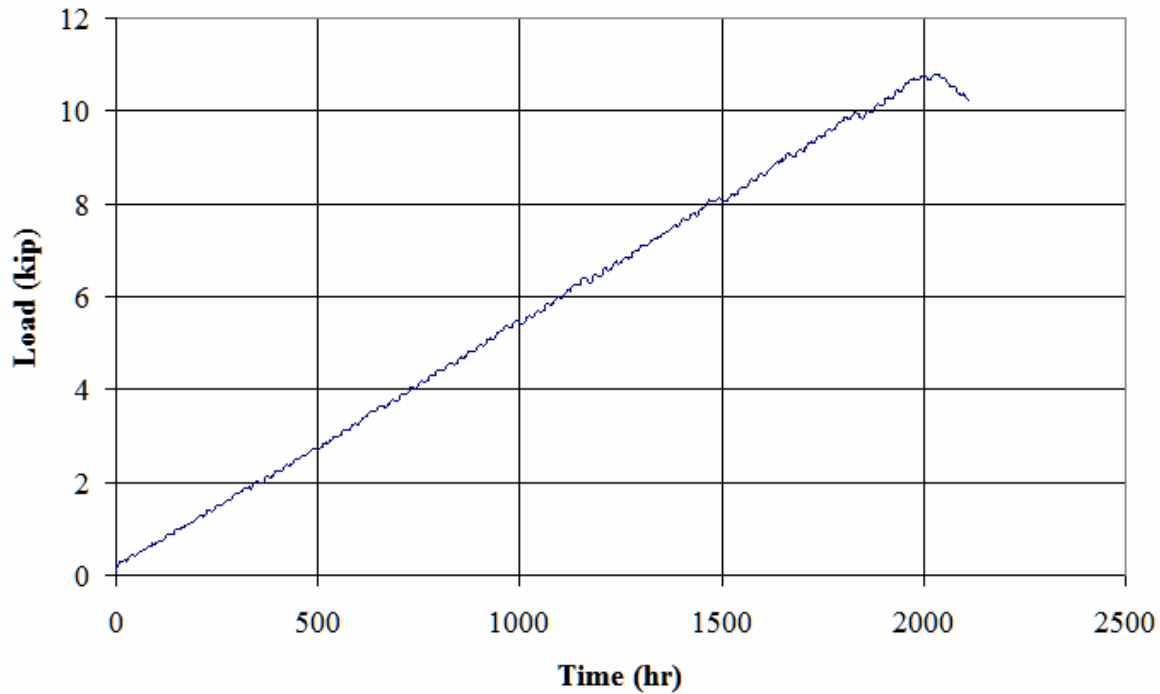


Figure 4-2. Load time history from 90 day test (SF = 16)

The histories shown in Figures 4-1 and 4-2 were used to generate the strain and stress histories shown in Figure 4-3 and 4-4 respectively. The shear strain shown in Figure 4-3 is calculated by dividing the horizontal displacement by the original height of an individual pads total elastomer thickness, in this case 1.5 inches. The shear stress is calculated by dividing the total load by two and then dividing the result by the loaded area.

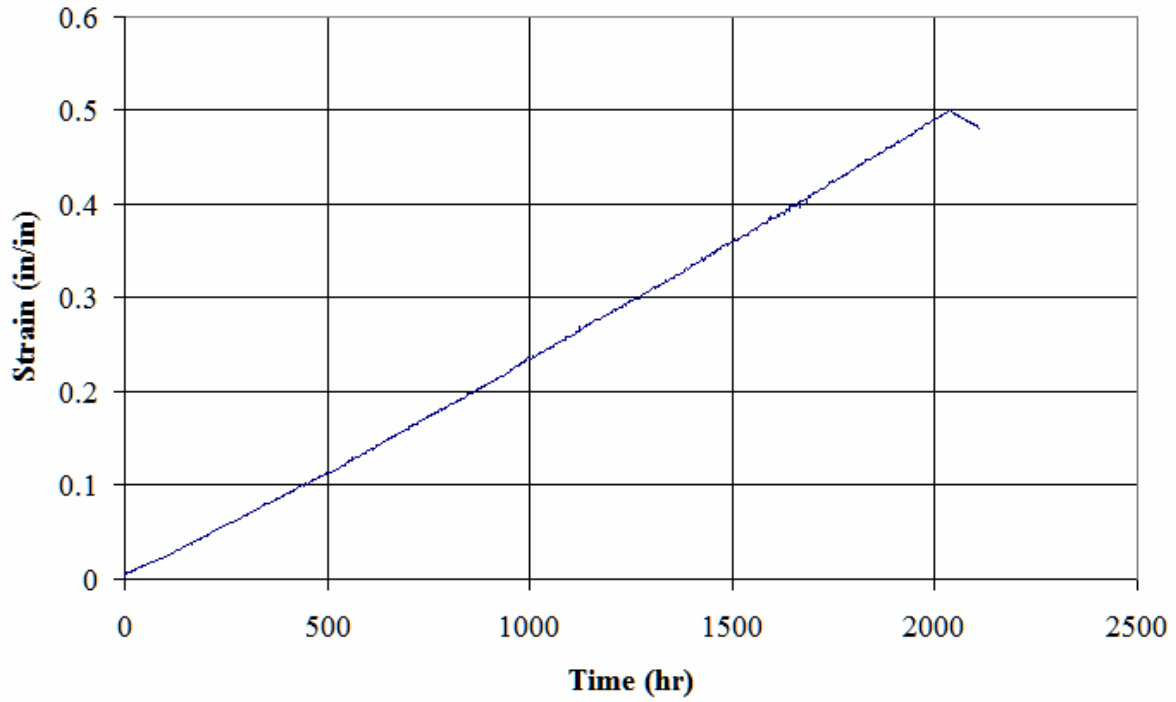


Figure 4-3. Strain history from 90 day test (SF = 16)

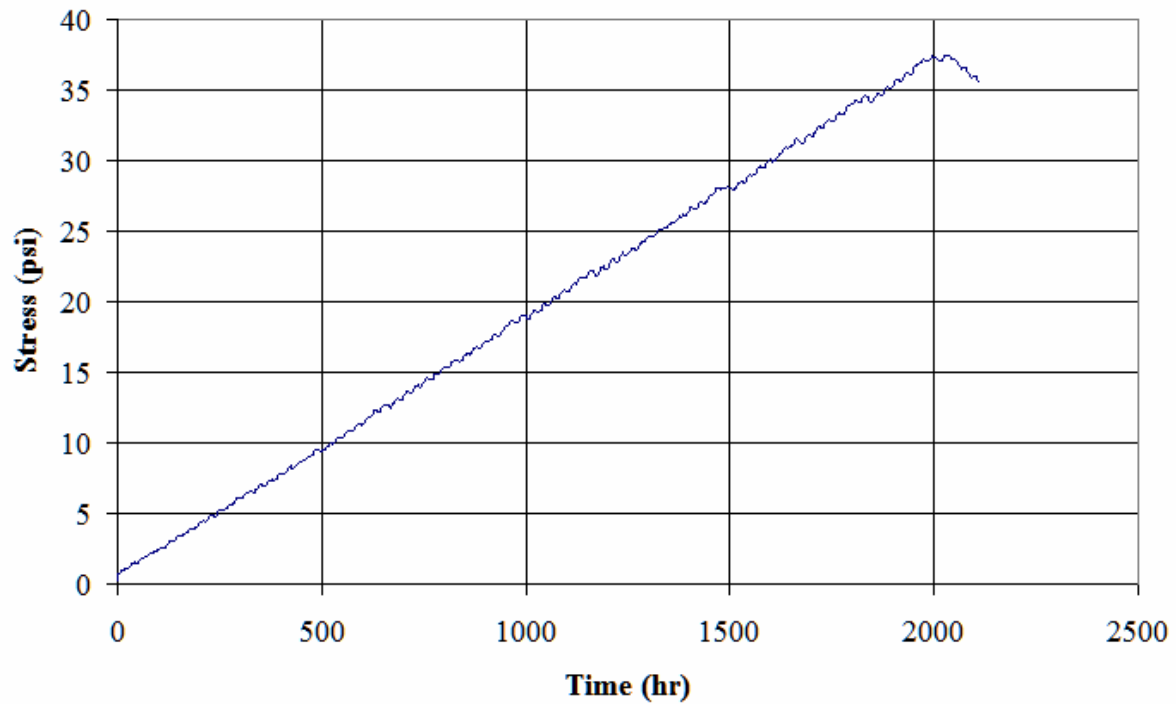


Figure 4-4. Stress history from 90 day test (SF = 16)

4.2 Determination of Shear Modulus

Figures 4-3 and 4-4 are combined to form Figure 4-5 which shows a shear stress-strain graph. In order to calculate a shear modulus similar to the ASTM modulus as shown in Figure 2-3 a second order curve was fit to the ascending portion of the stress-strain graph. This curve overlaid onto the graph and the corresponding points used to calculate the shear modulus are shown in Figure 4-6. Using a second order curve eliminates the fluctuation observed in the stress-strain graphs.

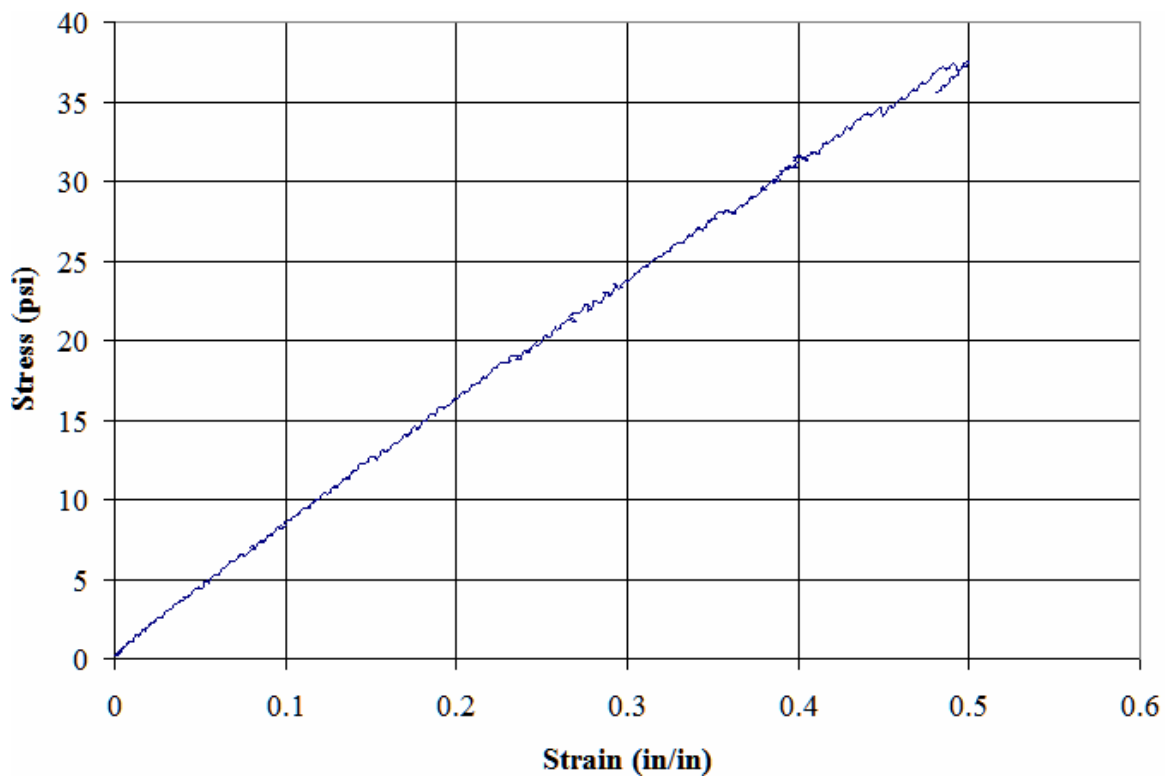


Figure 4-5. Stress-strain history from 90 day test (SF = 16)

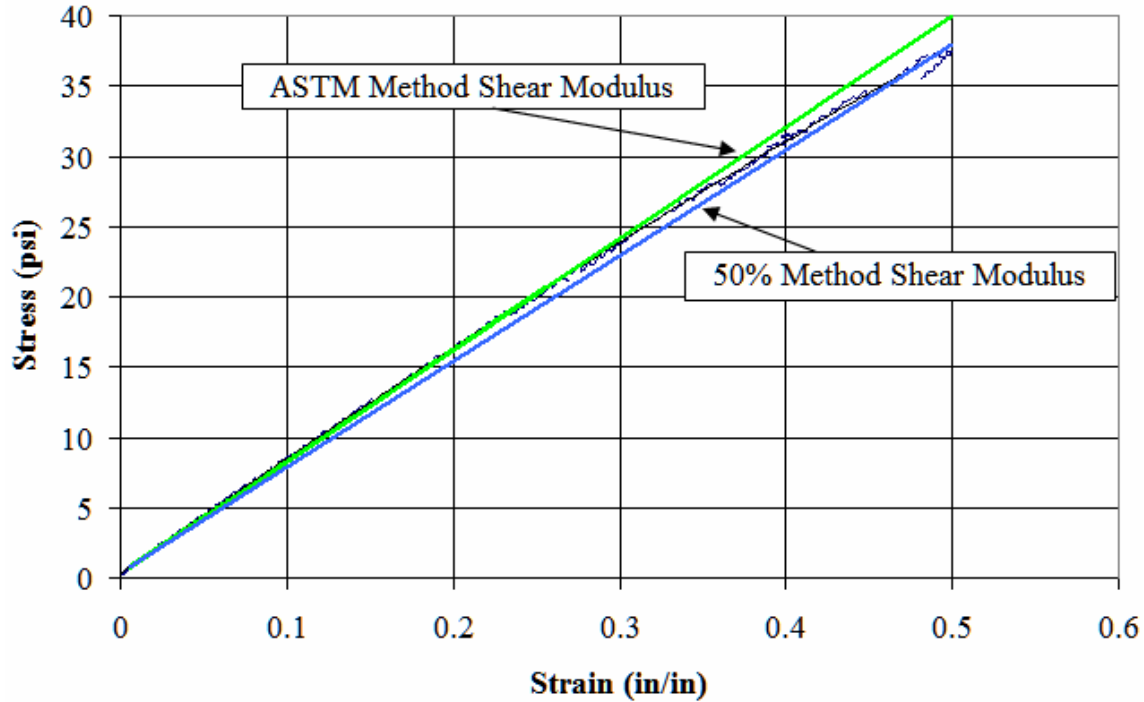


Figure 4-6. ASTM method shear modulus from 90 day test (SF = 16)

Calculating a shear modulus in the same manner as ASTM, i.e. the shear modulus is calculated by taking the secant modulus on the stress-strain graph from the point of 2% of maximum stress to the point at 25% shear strain beyond this point, will be called the “ASTM Method” in this report.

The ASTM method shear modulus for the 90 day SF 16 test is 79.3 psi. An alternative method for calculating a shear modulus used by Yura et al^[18, 23] is found using a secant modulus drawn through the origin (0 psi stress and 0% strain) and the value of stress at 50% strain. For this study a similar method was examined with the difference from previous studies is that instead of the origin used as a starting point, the first point will be the same one used in the ASTM method shear modulus calculation; this is shown in Figure 4-6. The value for the shear modulus calculated this way is 75.1 psi. The average ratio of the shear modulus from the 50% method to the shear modulus from the ASTM method for the tests shown in Table 4-1 is 92% and there is only a 3.7% coefficient of variation (COV) in this ratio. Since this is such a small

COV this report will only be referring to the shear modulus from the ASTM method from this point on. The shear modulus using the 50% method is 8% less than this.

4.3 General Results

A summary of the shear moduli from all of the tests is provided in Table 4-1. The values that are indicated as “New Pad” refer to pads that have not had the Mullins effect removed. Additionally, the “New Pad” values for “45 sec” tests refer to the first cycle of the six cycle test.

Table 4-1. Shear moduli result table

Sample thickness (in)	S F	Duration	Compression (ksi)	New pad	G _{ASTM} (psi)	G _{50%} (psi)	G _{50%} / G _{ASTM} (%)
1	24	45 sec	1	YES	102.7	90.1	87.8
1	24	45 sec	1	NO	95.5	85.4	89.3
1	24	12 hr	0.45	NO	87.2	75.5	86.6
1	24	12 hr	0.5	NO	85.8	75.2	87.6
1	24	12 hr	0.5	NO	85.1	74.7	87.8
1	24	12 hr	1	NO	83.3	77.3	92.8
1	24	12 hr	1	NO	85.2	74.9	88.0
1	24	12 hr	1.44	NO	82.0	74.8	91.2
1.5	16	45 sec	1	YES	101.0	87.6	86.7
1.5	16	45 sec	1	NO	91.5	84.3	92.1
1.5	16	7.2 hr	1.06	YES	95.4	88.0	92.2
1.5	16	9.5 hr	0.52	NO	93.8	83.2	88.7
1.5	16	12 hr	0.47	NO	93.0	81.9	88.1
1.5	16	12 hr	0.5	NO	93.8	82.6	88.1
1.5	16	12 hr	1	YES	98.0	90.1	91.9
1.5	16	12 hr	1	NO	79.9	75.6	94.6
1.5	16	12 hr	1	NO	84.1	80.6	95.8
1.5	16	12 hr	1	NO	82.8	74.8	90.4
1.5	16	12 hr	1.01	YES	96.2	89.2	92.8
1.5	16	12 hr	1.53	NO	86.3	80.3	93.0
1.5	16	7 day	1	YES	89.4	82.6	92.4
1.5	16	7 day	1	NO	81.3	77.1	94.9
1.5	16	90 day	1	YES	89.8	82.3	91.6
1.5	16	90 day	1.1	NO	79.3	75.1	94.8
2	12	45 sec	1	YES	97.3	85.1	87.5
2	12	45 sec	1	NO	85.7	79.5	92.7
2	12	12 hr	0.5	NO	84.7	74.5	88.0
2	12	12 hr	1	NO	78.1	73.7	94.4
2	12	12 hr	1	NO	76.9	69.2	90.0
2	12	12 hr	1.5	NO	68.0	62.1	91.3
2	12	12 hr	1.53	NO	70.2	65.4	93.0
3	8	45 sec	1	NO	69.5	68.9	99.1
3	8	45 sec	1	NO	66.9	65.6	98.0
3	8	12 hr	0.5	NO	77.2	68.1	88.2
3	8	12 hr	0.92	NO	65.7	62.6	95.3
3	8	12 hr	0.98	NO	74.8	71.6	95.7
3	8	12 hr	1	NO	73.4	71.2	97.0
3	8	12 hr	1.08	YES	77.0	71.1	92.4
3	8	12 hr	1.2	NO	61.6	58.6	95.1
3	8	12 hr	1.23	NO	57.5	53.0	92.1
3	8	7 day	1.08	YES	75.6	71.1	94.0
3	8	90 day	1	YES	77.8	73.0	93.9

CHAPTER 5 DISCUSSION OF RESULTS

This chapter covers variations in shear modulus with respect to short term product qualification loading and short term field loading (i.e. 50% strain in 45 seconds vs. 12 hours); short term field loading and long term field loading (i.e. 50% strain in 12 hours up to 90 days); the number of loading cycles (i.e. pre and post Mullins effect removal); and finally, the variation of shear modulus with compressive stress.

5.1 Variations in Shear Modulus

5.1.1 Initial Change due to Strain Rate

The ASTM 4014 ANNEX-A^[6] product qualification test for shear modulus requires the use of a strain rate in the range of 50% strain within 30 to 60 seconds and with the shear modulus determined using data gathered after the Mullins effect has been removed. Figure 5-1 shows the shear moduli for all of the shape factors tested at 1 ksi compressive stress (with the Mullins effect removed) having strain rates of 50% shear strain in 45 seconds and in 12 hours. The strain rate of 50% strain in 12 hours is representative of the quickest rate that pads would experience in the field.

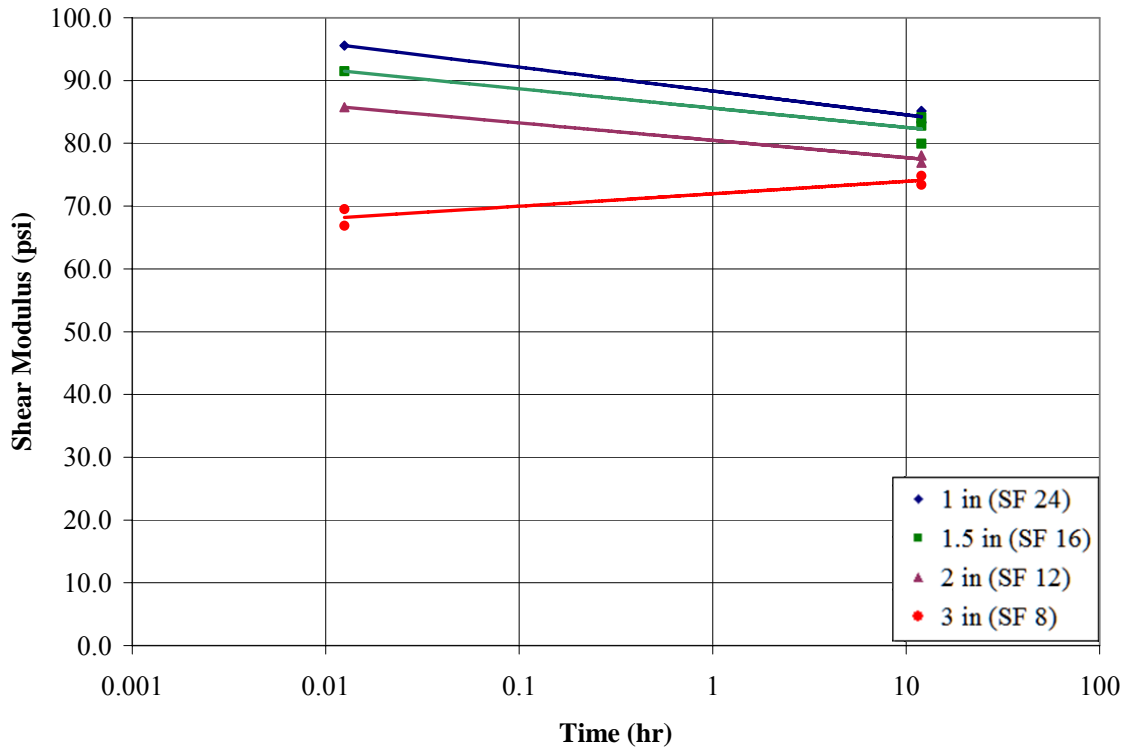


Figure 5-1. Mullins removed shear moduli (45 sec and 12 hr) of 1 ksi compression tests

Table 5-1 shows that a shear modulus found using the rapid strain rates in ASTM 4014 ANNEX-A^[6] should be reduced by about 7% to account for the lower in strain rate seen in the field.

Table 5-1. Initial shear modulus change due to reduced strain rate

SF	G _{ASTM} (psi)		Average G _{ASTM} (psi)		12 hr / 45 sec G (%)
	45 sec	12 hr	45 sec	12 hr	
24	95.5	85.2	95.5	84.2	88.2
	91.5	79.9			
16	85.7	78.1	91.5	82.3	90.0
	84.1	82.8			
12	66.9	65.7	85.7	77.5	90.4
	69.5	73.4			
8		74.8	68.2	71.3	104.6
Mean					93.3
Change					6.7
Standard deviation					7.59
COV					8.14

5.1.2 Changes due to Short Term Field Loading vs. Long Term Field Loading

Figure 5-2 shows the change in shear modulus over longer durations (i.e. slower) strain rates. This figure also includes shear moduli calculated using samples that have not had the Mullins effect removed prior to testing. The trends in this figure indicate that at strain rates at or below 50% in 0.5 days (12 hours) there is no significant change in the shear modulus. The change recorded was a maximum of 7.5% from 0.5 days to 90 days and a maximum of 3.7% from 7 days to 90 days.

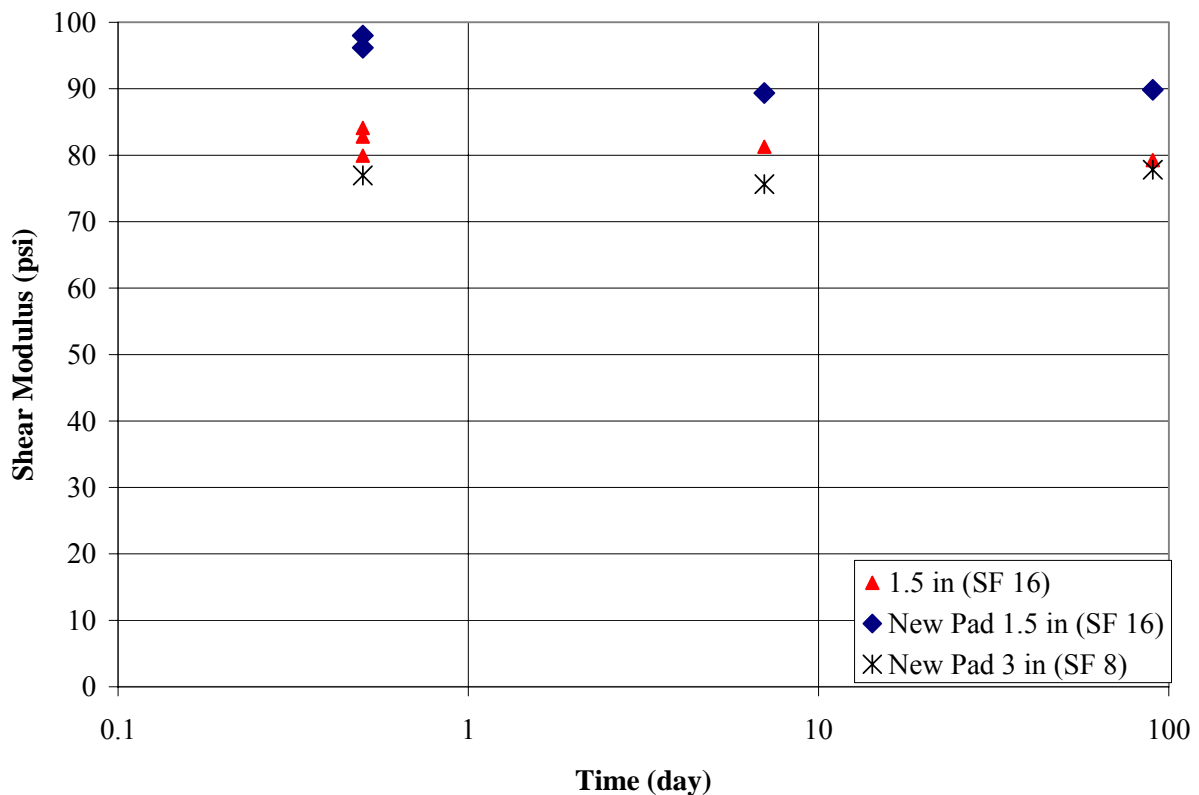


Figure 5-2. Long-term modulus change with duration

5.1.3 Changes due to the Number of Loading Cycles

The change due to of the Mullins effect is summarized in Table 5-2. This table indicates that for shear moduli calculated using the ASTM method (defined in Chapter 4) are on average 12% higher prior to the removal of the Mullins effect for 50 durometer harness material. This indicates that new pads in the field would be stiffer than expected since they would not have

experienced cycling prior to installation. Some samples were tested repeatedly under the identical conditions after being allowed to rest. Table 5-3 shows that the stiffness eliminated by cycling does not appear to recover with time.

Table 5-2. Mullins effect change

Duration	SF	G (psi)		G (psi)		Average change (%)
		Mullins removed		Average Mullins removed		
		w/o	w/	w/o	w/	
	24	102.7	95.5	102.7	95.5	107
	16	101.0	91.5	101.0	91.5	110
45 sec	12	97.3	85.7	97.3	85.7	113
	8	77.0	74.8			
	8		73.4			
	8		65.7	77.0	71.3	108
	16	98.0	79.9			
	16	96.2	84.1			
12 hr	16		82.8	97.1	82.3	118
7 day	16	89.4	81.3	89.4	81.3	110
90 day	16	89.8	79.3	89.8	79.3	113
Mean						112
Standard deviation						3.69
COV						3.31

Table 5-3. Recovery of Mullins effect with time

Date	Sample thickness (in)	G (psi)	Days from previous test	Change (%)
1/9/2007	1	83.3		
11/18/2007	1	85.2	313	2.2
1/16/2007	1.5	79.9		
2/1/2007	1.5	84.1	16	5.2
11/20/2007	1.5	82.8	292	-1.6
1/6/2007	2	78.1		
11/14/2007	2	76.9	312	-1.5
12/29/2006	3	74.8		
1/4/2007	3	73.4	6	-1.9
Mean				0.5
Standard deviation				3.1
COV				624

5.1.4 Changes due to the Compressive Stress

The effect of compression on shear modulus is shown in Figure 5-3. All of the shear moduli in Figure 5-3 are only for tests that had a strain rate of 50% over 12 hours. Figure 5-3 also shows trend lines based on to a least-error-squared fit to the moduli using a linear relationship between shear modulus and compressive stress. A linear relationship was chosen because Muscarella and Yura's model (Equation 2-14) indicated that the relationship between compressive stress and effective shear modulus was linear.

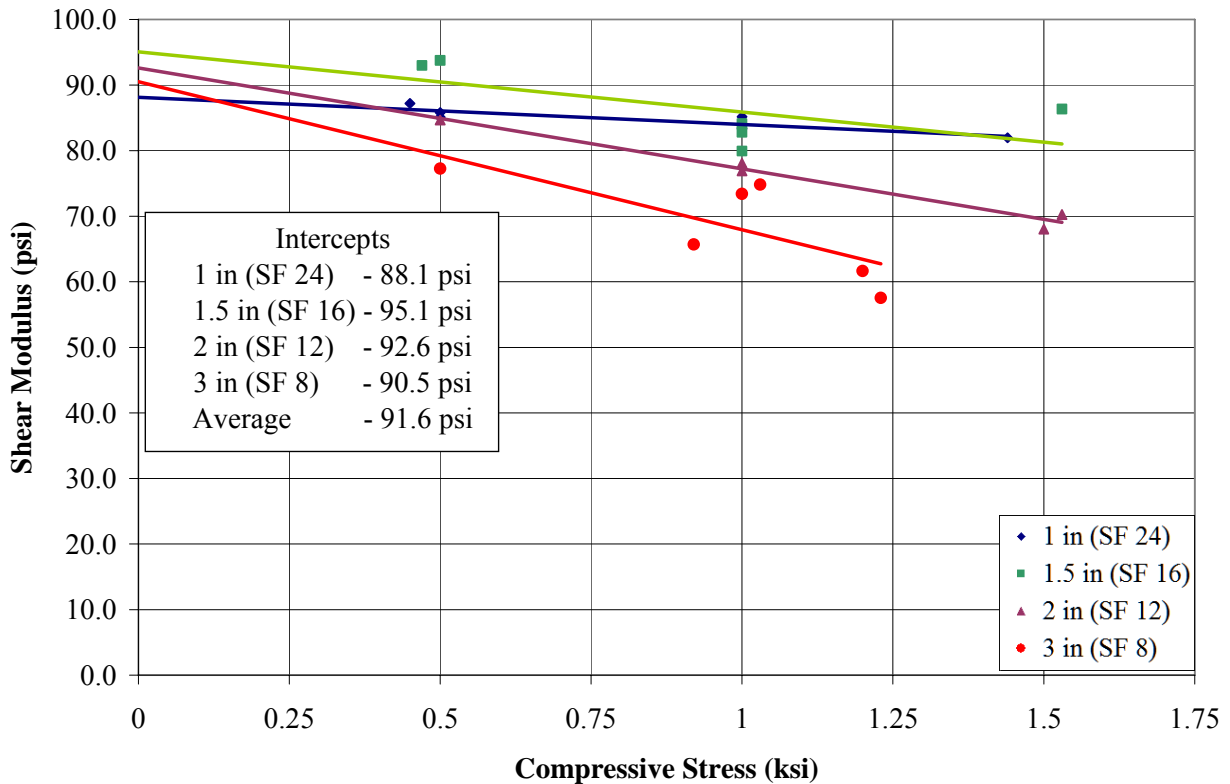


Figure 5-3. ASTM method 12 hr shear moduli vs. compression

ASTM 4014 ANNEX-A^[6] does not specify a compression stress and it requires that the samples are bonded to the reaction plates as well as the shear plates. This, in conjunction with the lack of a compression component in Figure 2-4, seems to indicate that no compression stress should be used during this type of testing. Due to this implication the trend lines in Figure 5-3 were extended through a point on the graph of 0 ksi compression in order to predict what the

average moduli of each shape factor would have been if the test was conducted without the use of compression.

ASTM 4014 ANNEX-A^[6] specifies a rate of strain such that straining from 0 to 50% is over 30 to 60 seconds. In order to compare the average of the intercepts in Figure 5-3 to the range of values found in the FDOT specifications^[3] the intercepts' average needed to be adjusted for the increased strain rate. This was accomplished by multiplying the average intercept value by the inverse of the average ratio of 12 hour test results to 45 second test results (the "Mean" found in Table 5-1, i.e. $1/_{93.3\%}$). This strain rate corrected value is shown in Equation 5-1. Recalling that the range of shear modulus for 50 durometer hardness neoprene in the FDOT Specifications^[3] is 85 psi to 110 psi, it seems that if these samples had been tested under no compression as in ASTM 4014^[6] they would have been certified acceptable.

$$G_{45\text{sec}} = \frac{G_0}{\text{Mean}} \quad (5-1)$$

$$G_{45\text{sec}} = \frac{91.6\text{psi}}{0.933} = 98.7\text{psi}$$

Table 5-4 shows the predicted values of effective shear modulus based on compressive stress using Equation 2-14 shown again below. These calculated values are based on the average shear modulus under no compression (Figure 5-3). Only tests longer than 45sec and with the Mullins effect removed were included in Table 5-4 to remove those contributions to the shear moduli.

$$G_{\text{eff}} = G_0 - P \left(\frac{\phi A_s}{2} \left\{ \sqrt{1 + \frac{12If_r}{A_s} \left(\frac{\pi}{\phi h_{rt}} \right)^2} - 1 \right\} \right)^{-1} \quad (2-14)$$

where

ϕ is the total bearing thickness (including steel) divided by total elastomer thickness h_{rt}

A_s is the shear area of bearing

f_r is the ending stiffness coefficient = $1.0 + 0.575 S^2$

G_0 is the shear modulus of the elastomer under no compression

G_{eff} is the shear modulus under compression
 I is the moment of inertia
 h_r is the total elastomer thickness

Table 5-4. Predicted compression adjusted shear modulus vs. measured

SF	σ (ksi)	G_{eff} (psi)	G measured (psi)	G_{eff} / G_{meas}
24	0.45	90	87.2	1.04
24	0.5	90	85.8	1.05
24	0.5	90	85.1	1.06
24	1	89	85.2	1.04
24	1	89	83.3	1.06
24	1.44	87	82.0	1.07
16	0.52	88	93.8	0.94
16	0.47	89	93	0.95
16	0.5	88	93.8	0.94
16	1	85	79.9	1.06
16	1	85	84.1	1.01
16	1	85	82.8	1.03
16	1.53	82	86.3	0.94
16	1	85	81.3	1.05
16	1.1	84	79.3	1.06
12	0.5	86	84.7	1.01
12	1	80	78.1	1.02
12	1	80	76.9	1.04
12	1.5	74	68.0	1.09
12	1.53	74	70.2	1.05
8	0.5	78	77.2	1.02
8	0.92	67	65.7	1.03
8	0.98	66	74.8	0.88
8	1	65	73.4	0.89
8	1.2	60	61.6	0.97
8	1.23	59	57.5	1.03
Mean				1.01
Standard Deviation				0.06
COV				6%

Figure 5-4 shows the trends from the value predicted by Muscarella and Yura's model and the measured values from Table 5-4. The trends in Figure 5-4 are very similar to those found in Figure 5-3 showing this is a good model.

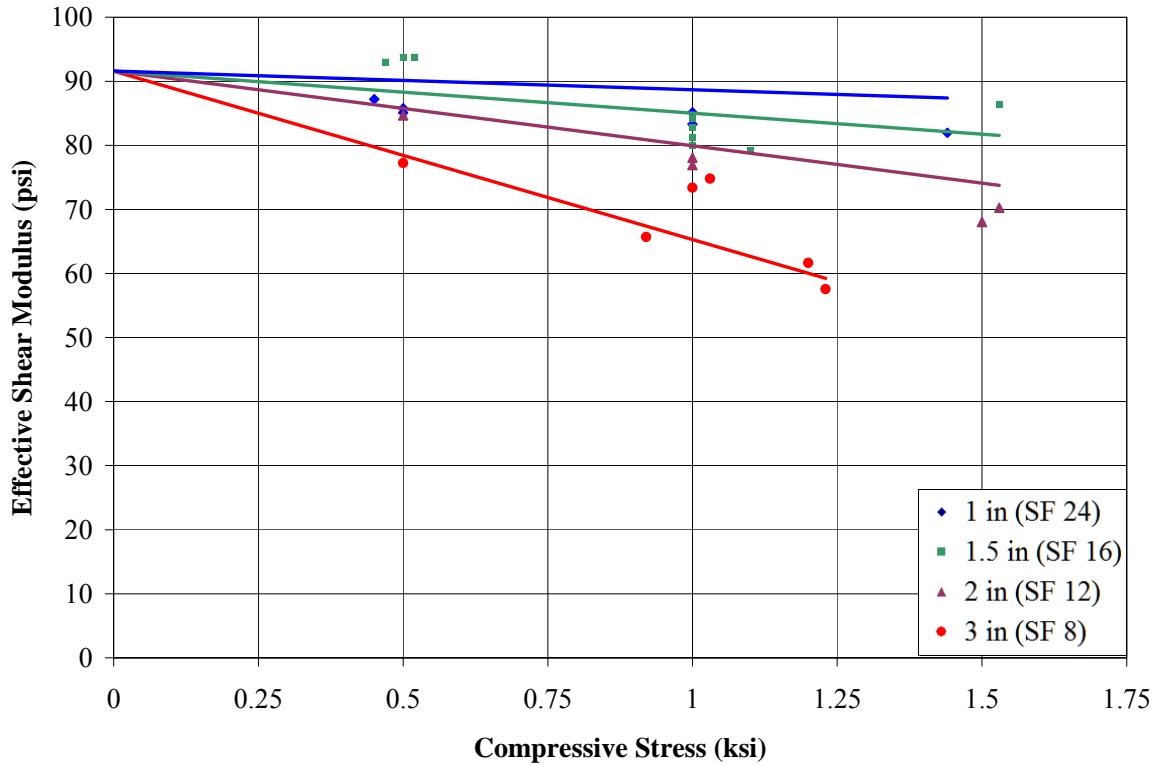


Figure 5-4. Shear moduli vs. compression with prediction by Yura and Muscarella^[23]

5.1.5 Temperature

The temperatures fluctuated during some tests, however, all but one test had the average temperature within the ASTM test accepted range. Equation 2-14 was used to calculate the values of the shear moduli at no compressive stress in order to verify that temperature had no effect on the shear modulus results of all of the shear moduli. After correcting them further for duration and the Mullins effect, the results were plotted in Figure 5-5. Figure 5-5 shows that the values of the shear moduli had no noticeable trend with respect to temperature.

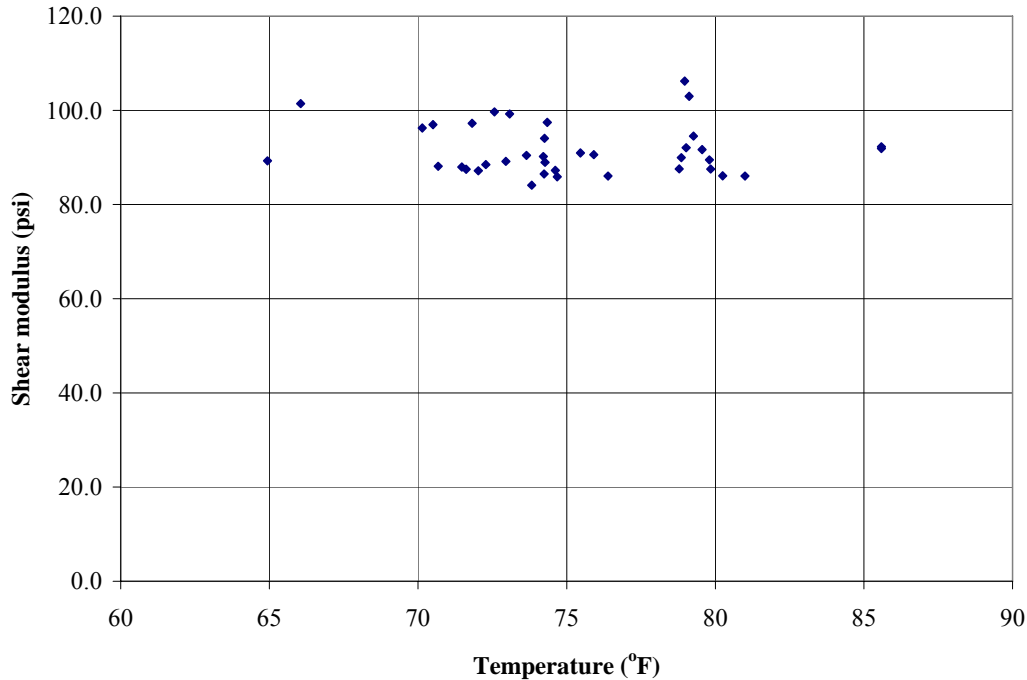


Figure 5-5. Shear modulus vs. temperature

5.1.6 Final Analysis of Strain Rate

Based on Muscarella and Yura's^[23] model and the analysis of the Mullins effect, a prediction can be made for the results of all of the tests if they had been conducted under no compression and had been cycled sufficiently to remove the Mullins effect. This calculation is performed by dividing the value of the shear moduli that did not have the Mullins effect removed by the average of the ratio of pre-removal to post-removal shear moduli, i.e. 1.12 for 50 durometer hardness material. Adjusting the shear modulus values with Mullins removed to a zero compression test state is accomplished with the use of Muscarella and Yura's model. This is accomplished by adding the reduction in shear moduli the model predicts for the compression under which each test was conducted to the resulting shear moduli. An example of these calculations is shown in Equations 5-2 and 5-3 for the test of a new pad with a shape factor of 16 under a compressive load of 144 kips with a measured shear modulus of 89.8 psi.

$$G_{6th} = \frac{G_{mea}}{1.12} \quad \text{(Mullins effect adjustment)} \quad (5-2)$$

$$G_{6th} = \frac{89.8 \text{ psi}}{1.12}$$

$$G_{6th} = 80.2 \text{ psi}$$

$$G_{adj} = \frac{G_{6th}}{\left(1 - \frac{P}{P_{cr}}\right)} \quad \text{(Compression loading adjustment)} \quad (5-3)$$

$$P_{cr} = 2,009 \text{ kip} \quad \text{(From Equation 2-11)}$$

$$G_{adj} = \frac{80.2 \text{ psi}}{\left(1 - \frac{144 \text{ kip}}{2,009 \text{ kip}}\right)}$$

$$G_{adj} = 86.4 \text{ psi} \quad \text{(Predicted post-cycled 0 ksi compression test result)}$$

With all of the data collected adjusted in this manner, a clear trend can be seen in the relationship between shear modulus and strain rate. The data resulting from these calculations is shown in Figure 5-6. It is important to note that these predictions conform to the ASTM standard testing method in compression and the removal of the Mullins effect.

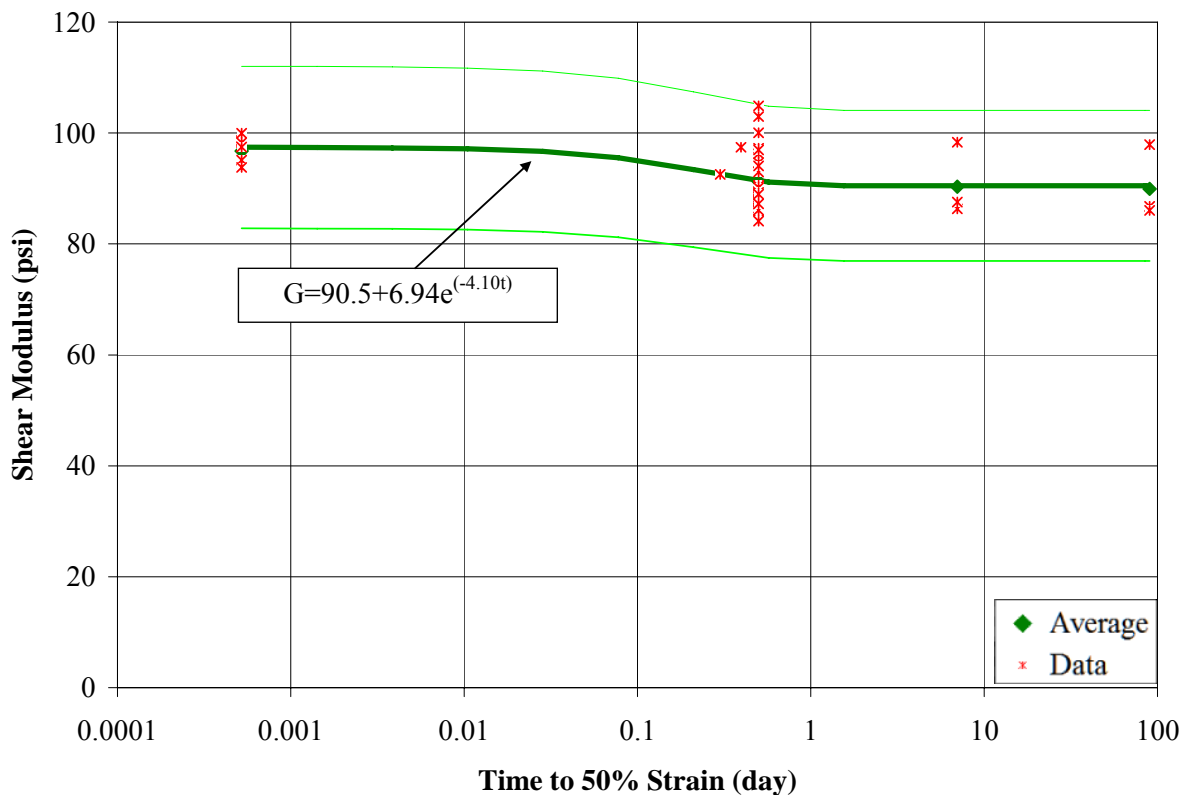


Figure 5-6. Strain rate data summary

From Figure 5-6 it can be seen more clearly that for strain rates that conform to highway bridge applications there is no substantial change in the shear modulus with strain rate. Additionally the only substantial change is approximately 7% change in shear modulus from the ASTM strain rate to the typical highway application strain rates. The form of the fitted trend line reflects an elastic structure within the neoprene samples combined with a viscous component which decays exponentially with decreasing strain rate. The trend eventually stabilizes around the elastic modulus value of the internal elastic structure.

Because of the negligible change in the shear modulus over the strain rates seen in the field it was not necessary to use one of the more complicated models encountered in the course of the literature review into this subject. However during the research program attempts were made to make use of these models. This was ultimately unable to be accomplished because of the lack of change in the shear modulus for different strain rates which led to the inability to accurately fit all of the coefficients necessary in these models.

5.2 Summary

The theory that neoprene softens as strain rate is reduced is generally supported by the trends shown in Figure 5-1 and Figure 5-6. However, research found in the literature review^[29-40] and the trend shown in Figure 5-6 indicate that there is a lower limit to this reduction in stiffness. The shear modulus found using ASTM 4014 ANNEX-A^[6] uses a strain rate of 50% strain over 30 to 60 seconds, which makes the reported modulus approximately 7% higher compared to the modulus resulting from field strain rate conditions.

This increase in reported shear modulus is offset by the fact that new pads in the field do not typically have the Mullins effect removed as is required in ASTM testing. This results in a 12% decrease in the reported results in the ASTM testing for shear modulus for 50 durometer

hardness material. The net effect is that for the same material new pads in the field are 5% stiffer than what would be expected based on ASTM tests.

Table 5-4 shows a correlation between observed shear moduli and the value predicted using Muscarella and Yura's model (Equation 2-14). These values fall within the $\pm 15\%$ range of error allowed by ASTM^[6] making the model a valid predictor of bearing shear behavior under compression.

The range of values for shear modulus found in the FDOT Specifications^[3] and AASHTO^[2] for 50 durometer hardness neoprene cover a spread of ± 12.5 psi and ± 17.5 psi respectively from the average values. In addition to this, the ASTM^[6] standard and FDOT Specifications^[3] allow a variation of $\pm 15\%$ of the target shear modulus in verifying the shear modulus of a sample. All of this adds to the uncertainty of the actual shear modulus of a pad in the field. This uncertainty along with the addition of the effect of compression encompasses all the variations observed in this study.

Because the shear modulus seems to stabilize at durations above 12 hours it is recommended that tests for bearing pads be conducted using a constant strain rate of 50 percent over a 12 hour duration. It is also recommended that these tests be conducted without the Mullins effect being removed first to find the stiffness that is initially present in the field, as well as conducting a 12 hour test after the Mullins effect is removed to find the final stiffness seen after repeated cycling of long term use. Additionally, it is recommended that the tests be conducted at the expected service dead load and using the appropriate shape factor and number of layers because of the influence of compressive stress on the shear modulus.

The original contribution of this research is the conclusion that the shear stiffness or effective shear modulus of steel reinforced neoprene bearing pads is essentially a constant value

for the strain rates occurring in highway applications. The only observed change in shear modulus due to strain rate, was the approximately 7% drop as the strain rate changed from that used in ASTM standard testing to the strain rates in typical highway applications. Additionally it was observed that the shear modulus reported using ASTM test procedures under estimates the shear modulus that would be present in a new pad by approximately 12% for 50 durometer hardness material due to the removal of a component of the original stiffness by repeated cycling of the material samples. Finally, the Yura and Muscarella^[23] model to account for the compression contribution to the reduction in effective shear modulus provided an excellent description for the behavior observed in flat steel reinforced neoprene bearings.

It should be noted that since the shear modulus in Figure 5-6 stabilizes after 12 hours, the procedure explained in section 2.1.5 of this report should not continue to be used. That procedure is based on using creep deflection estimates found in Table 14.7.5.2-1 of AASHTO (Table 2.1 in this report) to back-calculate an apparent long-term shear modulus. The values found in Table 14.7.5.2-1 of AASHTO (Table 2.1 in this report) were developed using both short-term shear modulus tests and creep tests under sustained load. AASHTO Table 14.7.5.2-1 does not purport to provide guidance on the behavior of the shear modulus with loads applied slowly over a long period of time. What it does provide is values for the short-term shear modulus and estimates of creep deflection under sustained load based on material hardness.

Appendix C of this report contains suggested language for an addition to Section 14.7.5.2 of the AASHTO LRFD Design Specifications regarding guidance on how typical shear loading rates, compression and cycling affect the shear modulus of neoprene bearings.

CHAPTER 6 CONCLUSION

The objective of this project was to evaluate the interaction between the shear modulus of steel reinforced neoprene bearing pads and shear strain rates of highway applications. The following interactions related to variations in the shear modulus were investigated for pads with various shape factors:

- Short term product qualification loading vs. short term field loading
- Short term field loading vs. long term field loading
- Number of loading cycles
- Effects of compressive stress

Forty-two tests were performed using test equipment designed to apply a shear strain at a variety of rates while applying a sustained compressive load. Test results indicated:

- There was an average 7% reduction in the shear modulus when it was observed at the strain rates typically seen in highway applications as opposed to shear moduli found using strain rates in the range required by ASTM D4014.
- There was a maximum of 7.5% reduction in shear modulus when comparing the higher shear modulus found using short term field loading (50% strain in 12 hours) to the shear modulus found using long term field loading (50% strain in 90 days). However, on average for typical highway application strain rates there is no significant change in the shear modulus.
- The shear modulus for new pads in the field that have not been subjected to repeated load cycles (i.e., removal of the Mullins effect) is approximately 12% higher for 50 durometer hardness material than that of the same pads after load cycling.
- In elastomeric bearings as compression increases, within the limit of AASHTO specifications, the shear modulus reduces, particularly for bearing pads with low shape factors. The trends seem to conform to previous work by Muscarella and Yura^[23] with the resulting shear moduli within the $\pm 15\%$ tolerance range allowed by ASTM^[6].

Based on the results of the forty-two tests conducted in this study, it is recommended that upper and lower tolerance values for the shear modulus be used for calculations instead of a single value. The limits in ASTM D 4014 are $\pm 15\%$ of the specified shear modulus. However,

the upper value of this range should be increased by 5% to account for the net effect of the lack of cycling (+12%) and the reduced strain rates (-7%) in the field. Since the cycling effect will eventually dissipate, the lower value of this range should be reduced by 7%. This results in values that are +20% and -22% of a specified shear modulus. To simplify calculations, the recommendation is to use $\pm 20\%$ of a specified shear modulus. For example, neoprene with a specified shear modulus of 100 psi, with tolerance values defined by ASTM of 85 to 115 psi, should actually be considered to be both 80 and 120 psi in calculations with no compression. Adjustments for compression should be in accordance with Equation 2-14 from Muscarella and Yura^[23].

The implication of these recommendations for a design engineer would mean that instead of one calculation based on the shear stiffness of the bearings there would be a minimum of two separate calculations, one for both the high and the low value of the range of shear moduli. Additionally, if a designer chooses multiple pads with smaller shape factors instead of one pad with a large shape factor, using the effect of shear modulus reduction due to compression (Equation 2-14) may result in smaller calculated forces than previously considered. The end result of these lower forces could be construction cost savings.

APPENDIX A
RESEARCH DATA

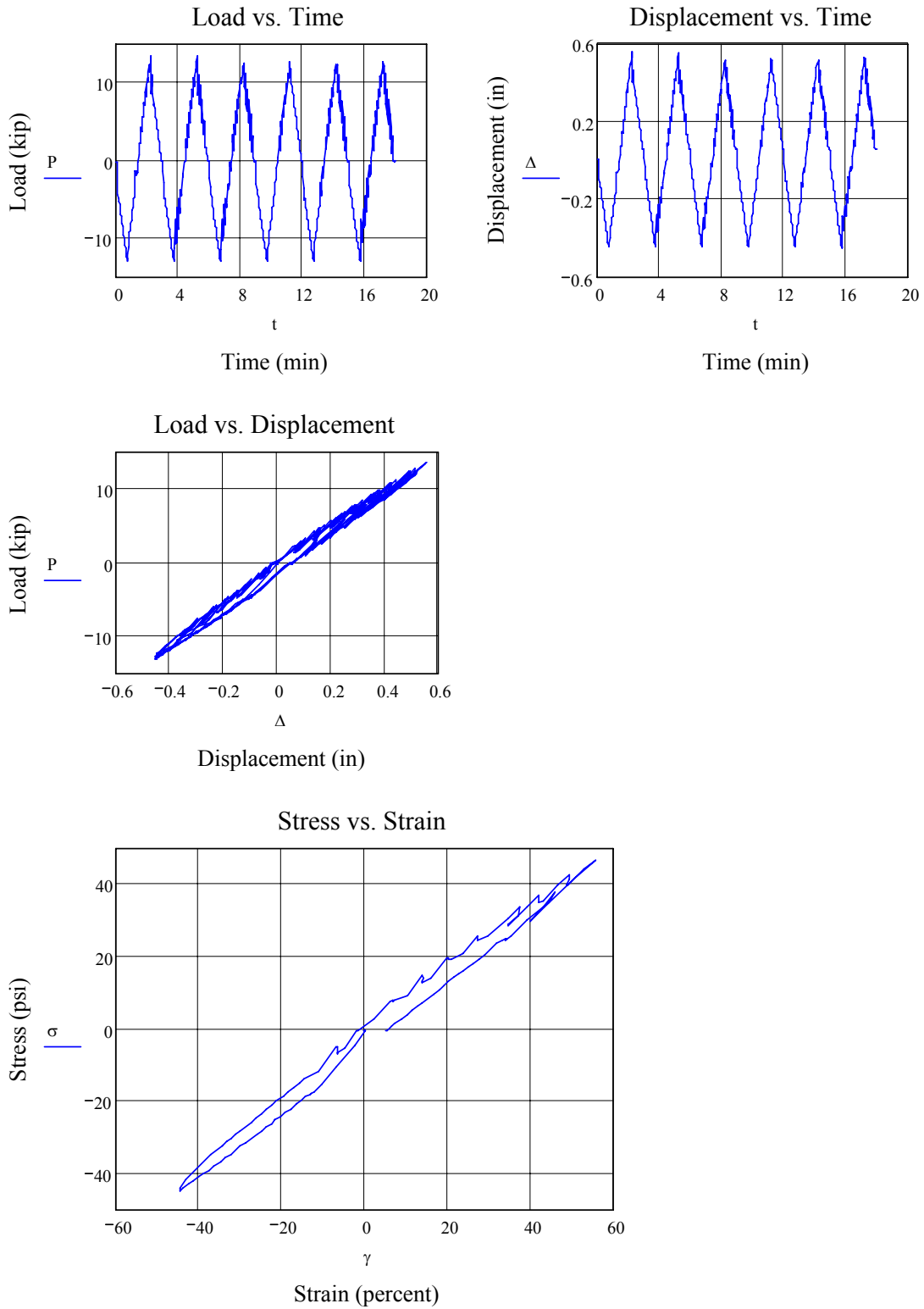


Figure A-1. Shape factor 24, 1.0 ksi compression, 45 second test new pad (start) data

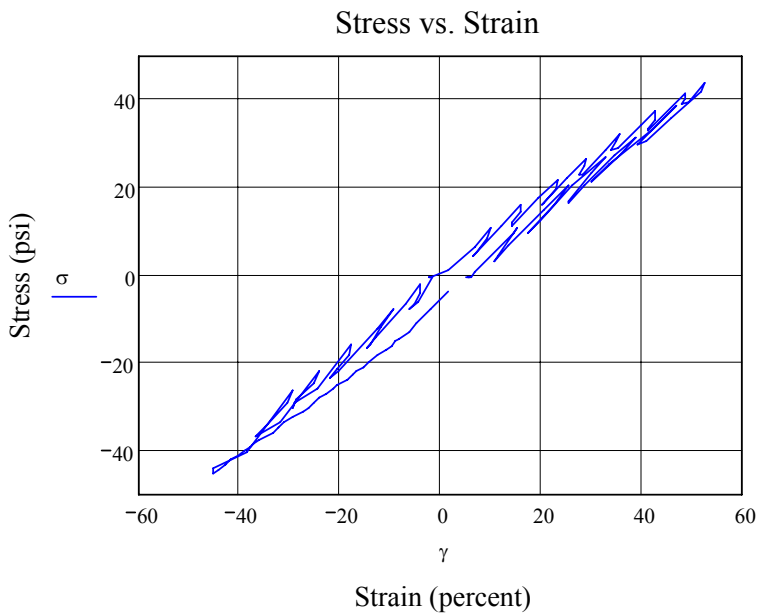
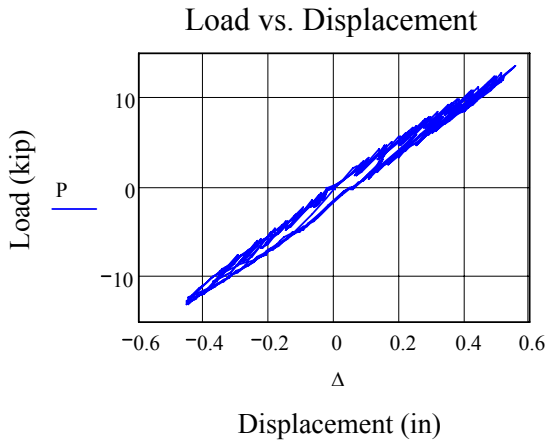
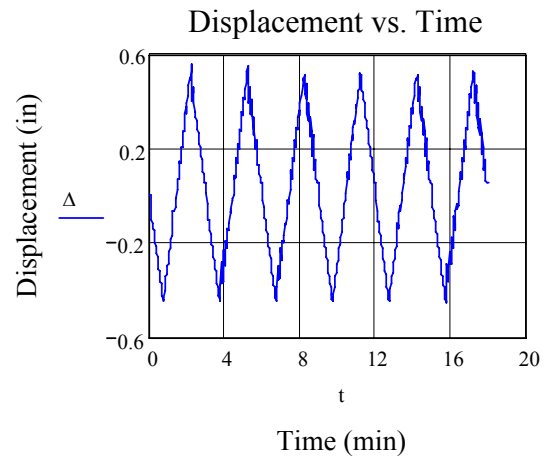
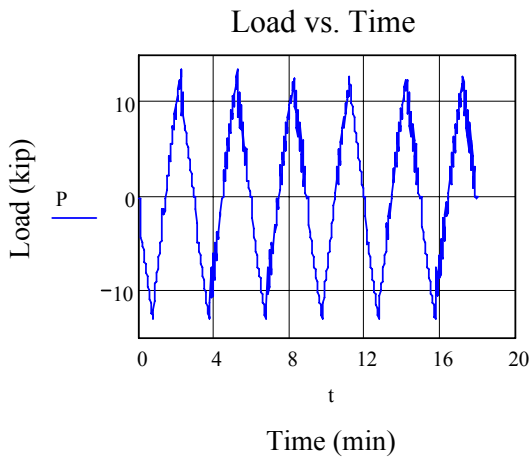


Figure A-2 Shape factor 24, 1.0 ksi compression, 45 second test (end) data

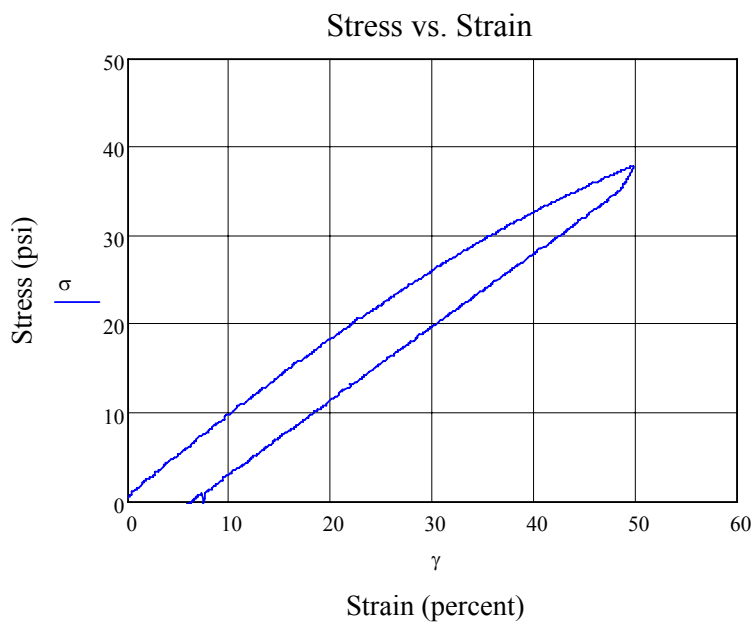
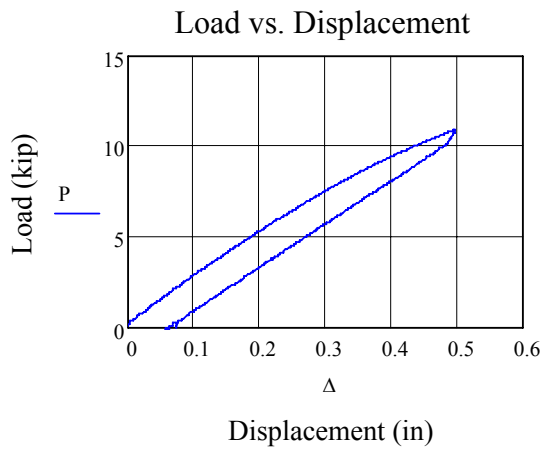
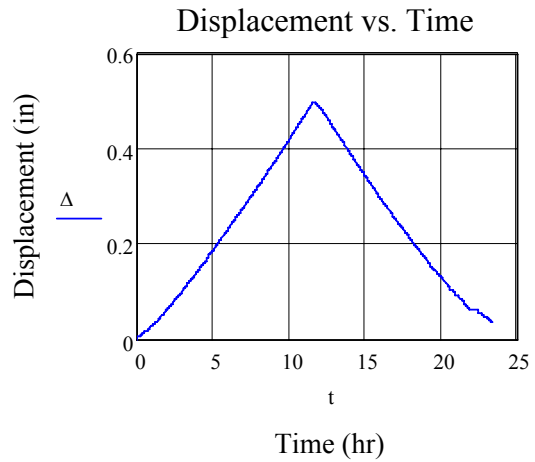
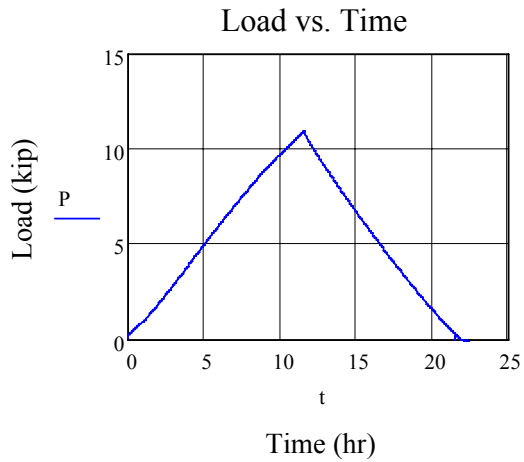


Figure A-3. Shape factor 24, 0.5 ksi compression, 12 hour test 1 data

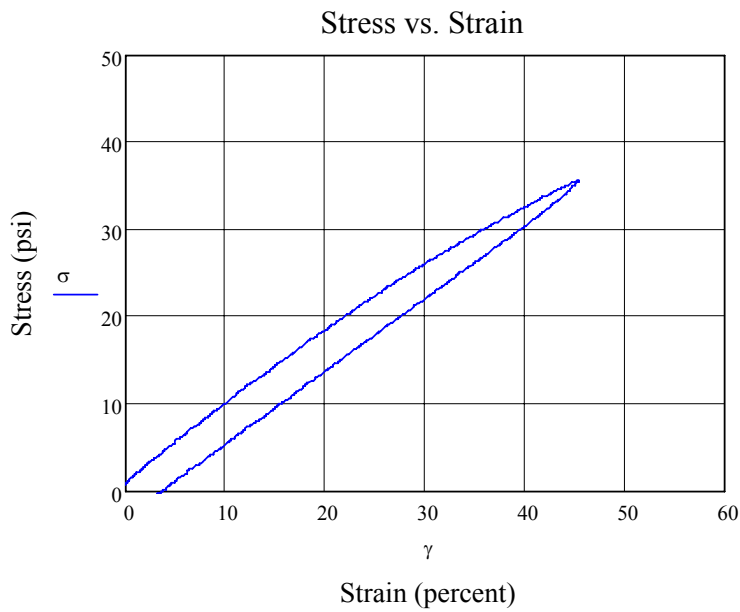
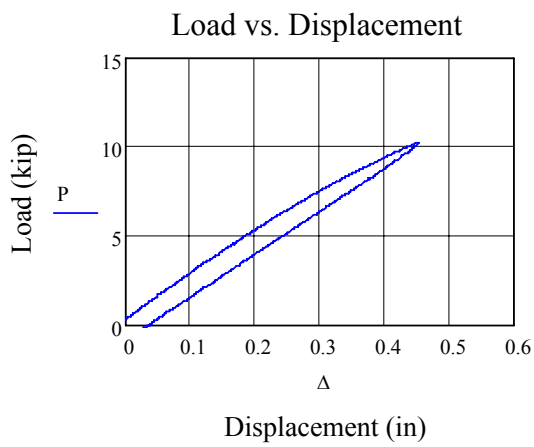
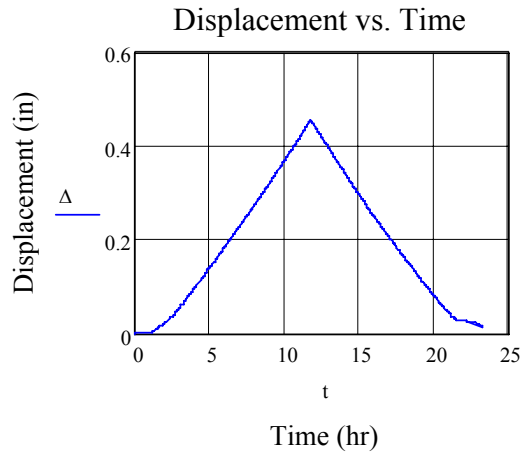
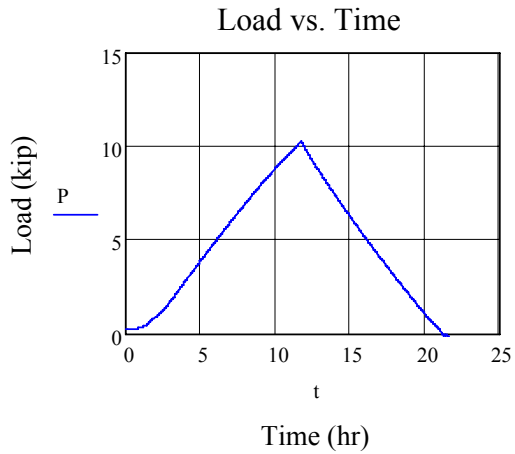


Figure A-4. Shape factor 24, 0.5 ksi compression, 12 hour test 2 data. The stress at 50% shear strain was calculated from a 2nd order curve fit on the ascending portion of the graph.

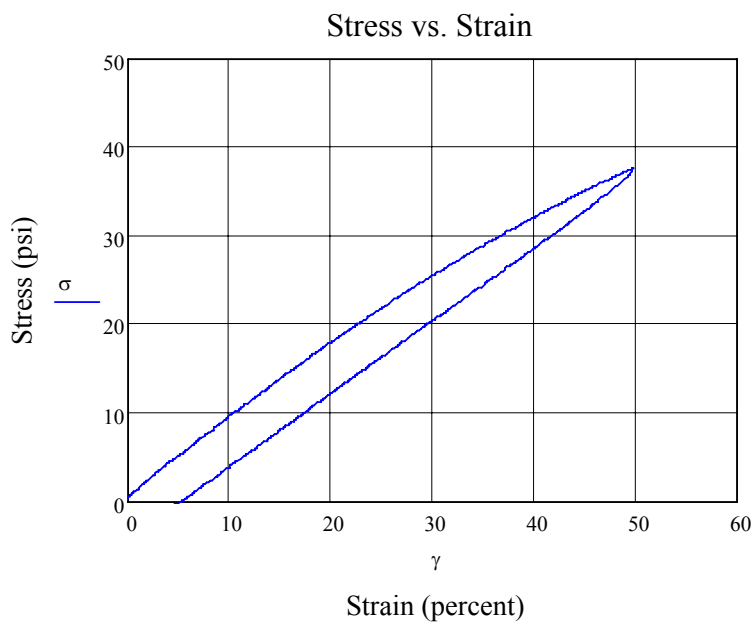
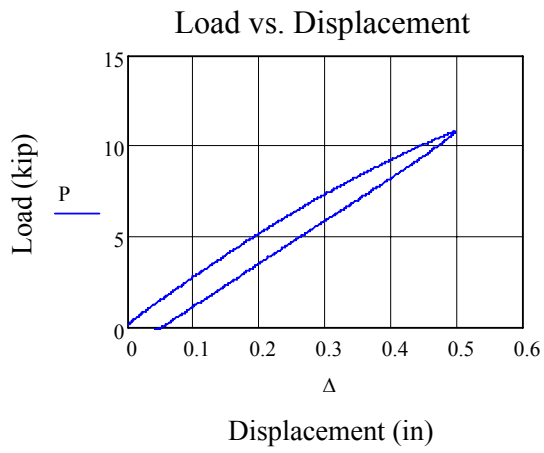
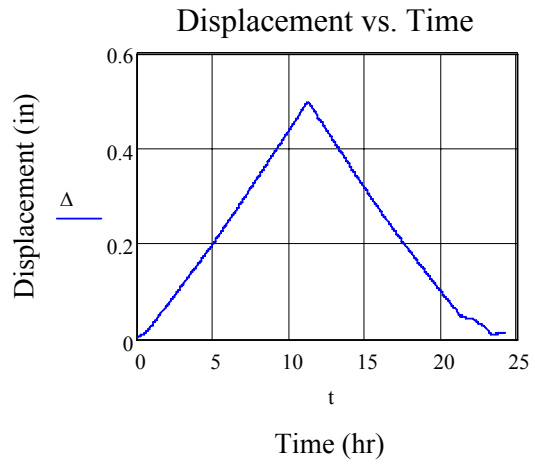
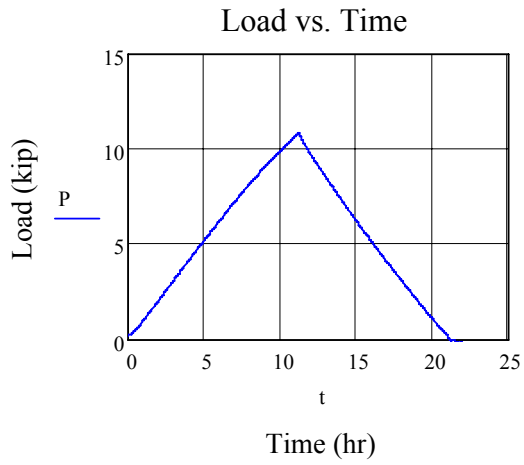


Figure A-5. Shape factor 24, 0.5 ksi compression, 12 hour test 3 data

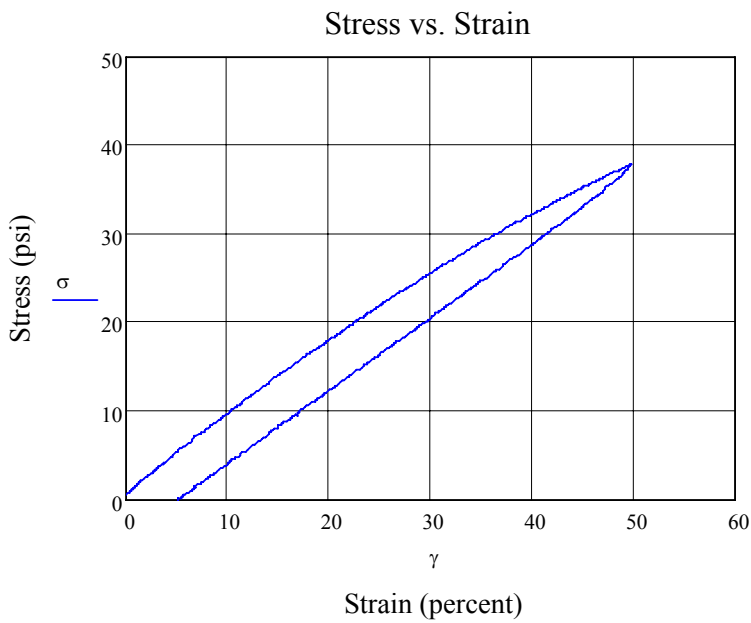
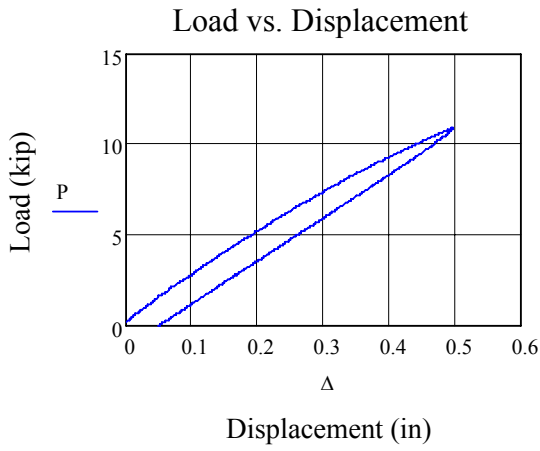
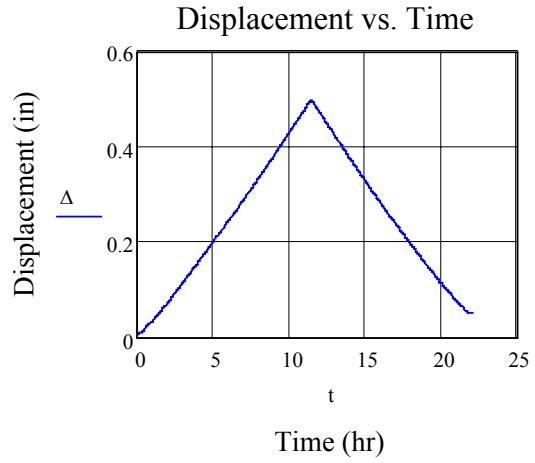
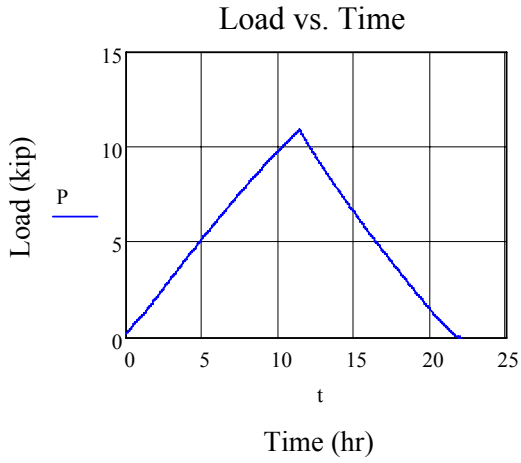


Figure A-6. Shape factor 24, 1.0 ksi compression, 12 hour test 1 data

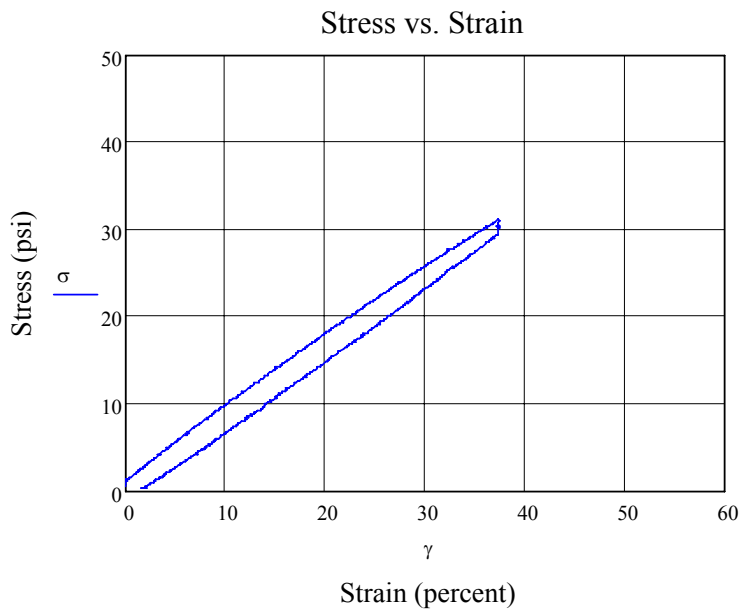
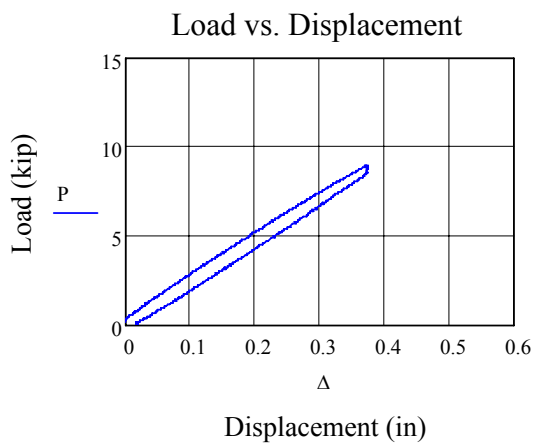
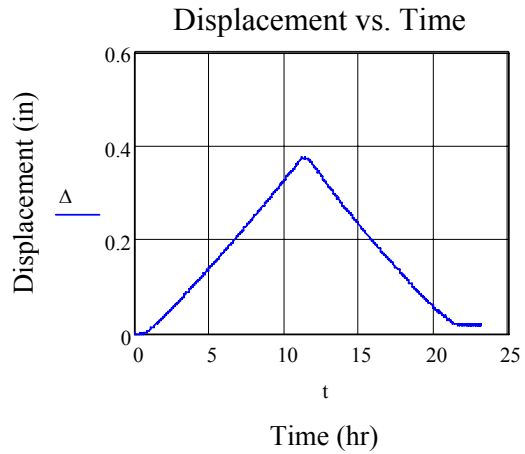
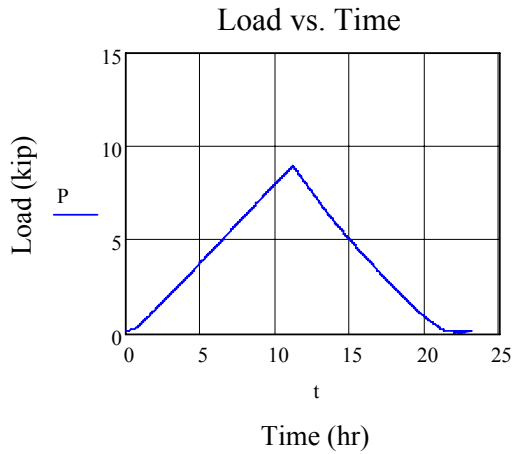


Figure A-7. Shape factor 24, 1.0 ksi compression, 12 hour test 2 data. : The stress at 50% shear strain was calculated from a 2nd order curve fit on the ascending portion of the graph.

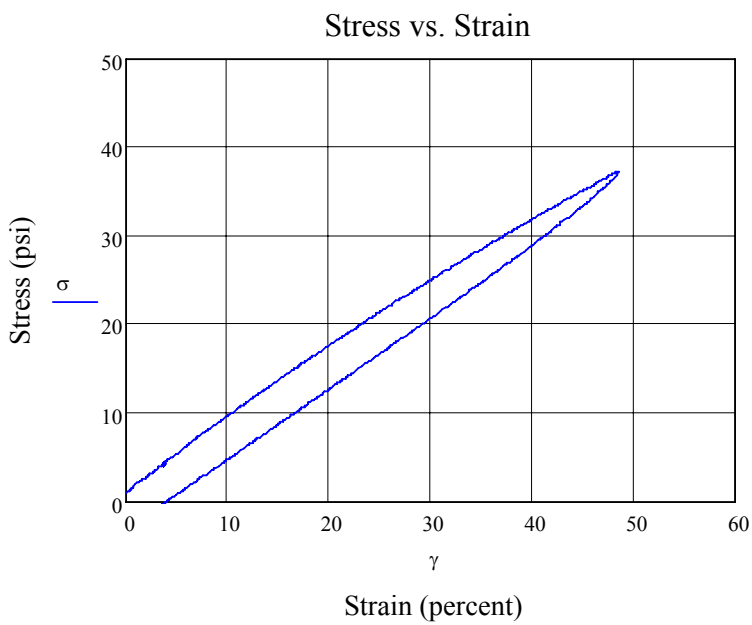
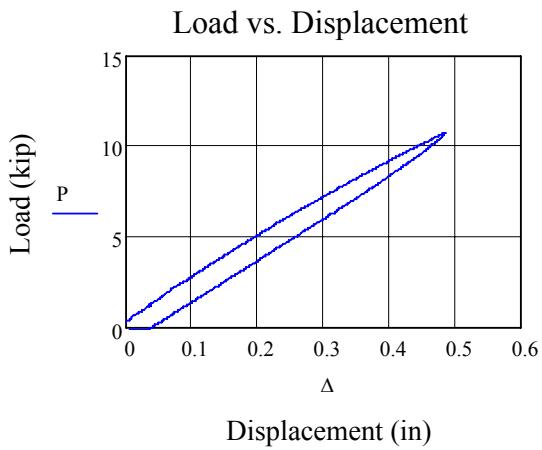
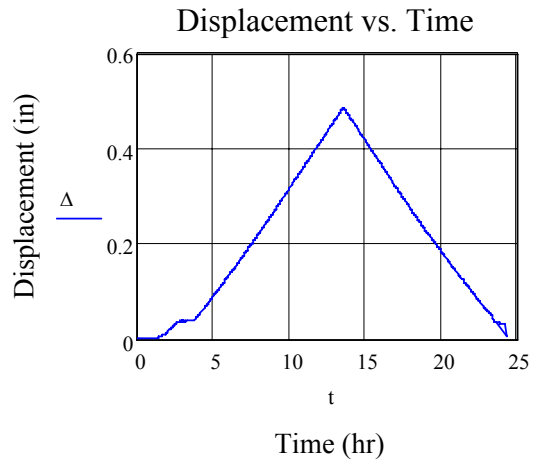
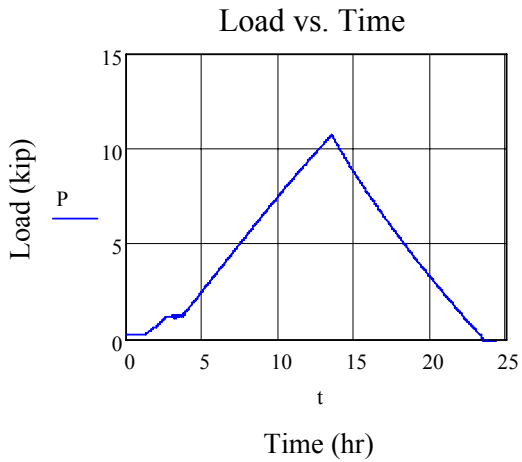


Figure A-8. Shape factor 24, 1.4 ksi compression, 12 hour test data

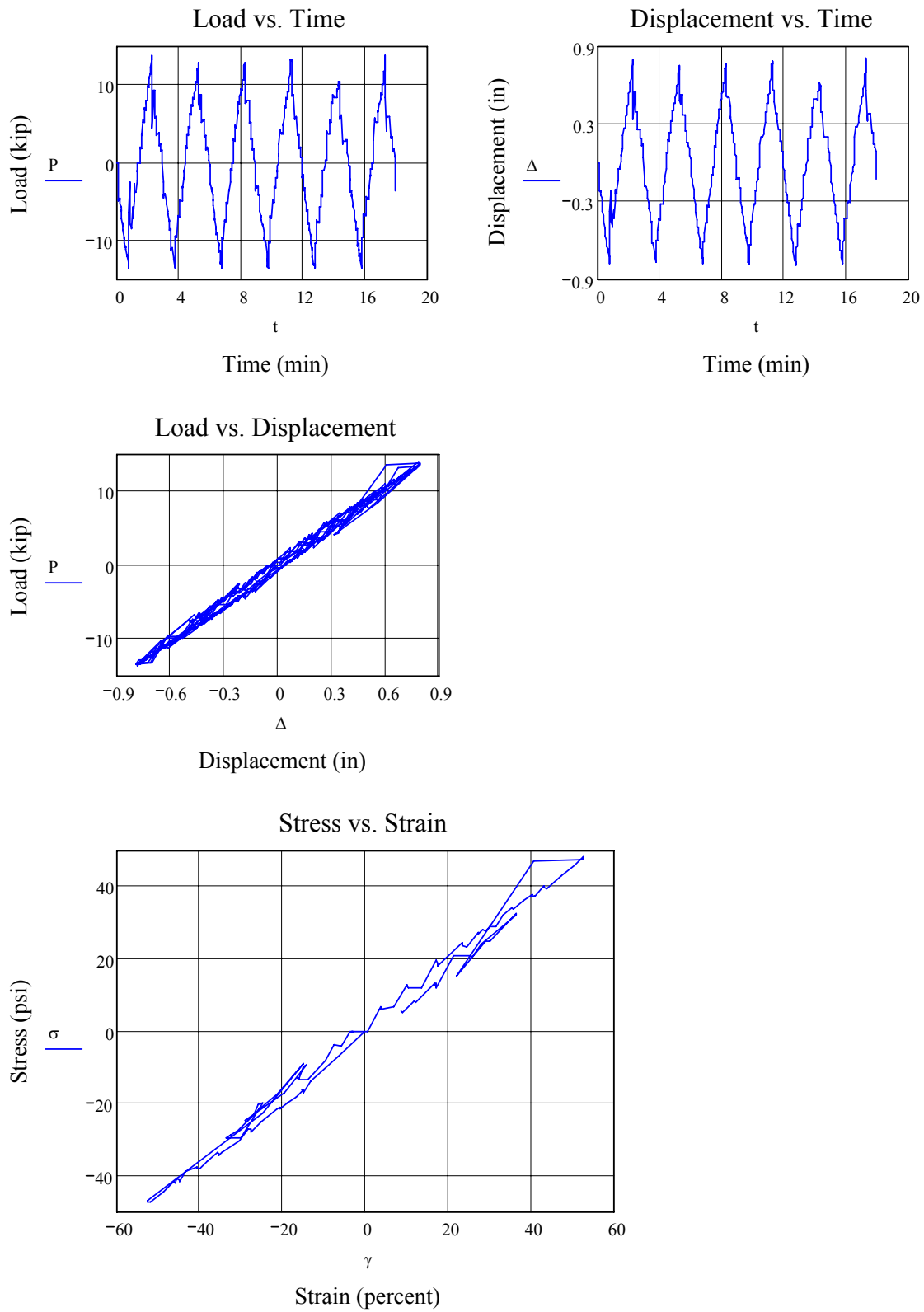


Figure A-9. Shape factor 16, 1.0 ksi compression, 45 second test new pad (start) data

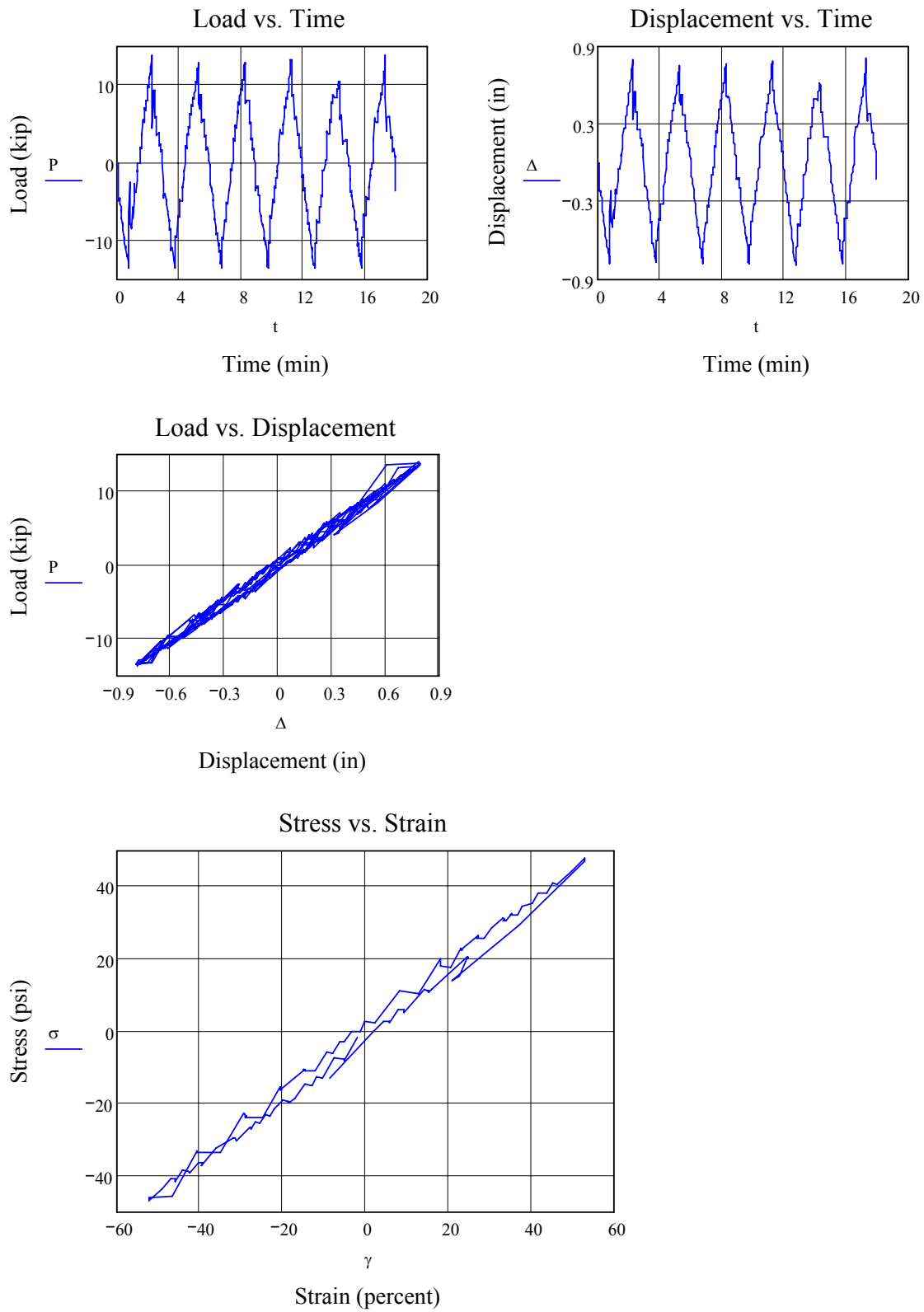


Figure A-10. Shape factor 16, 1.0 ksi compression, 45 second test (end) data

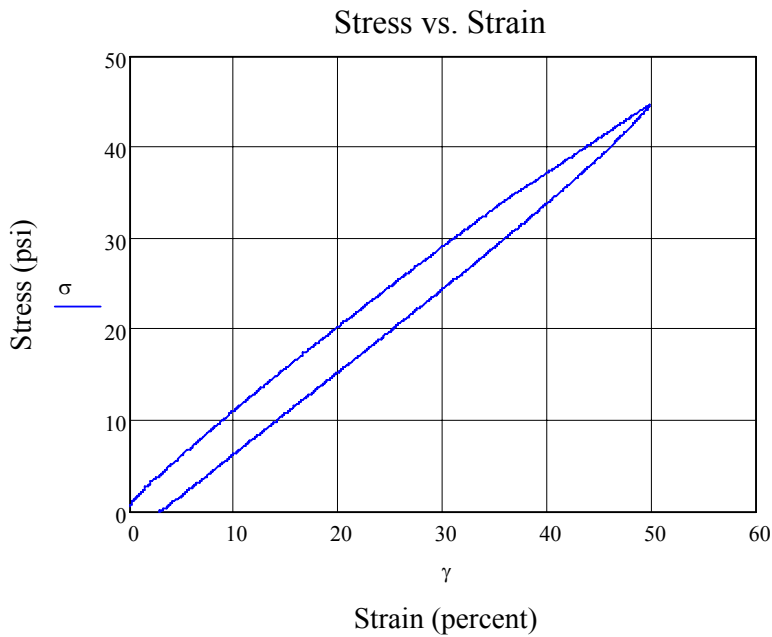
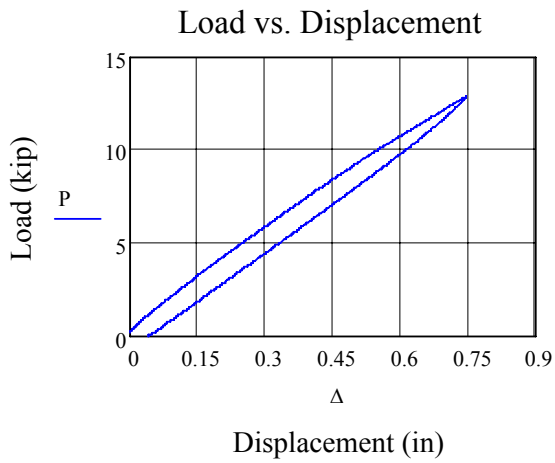
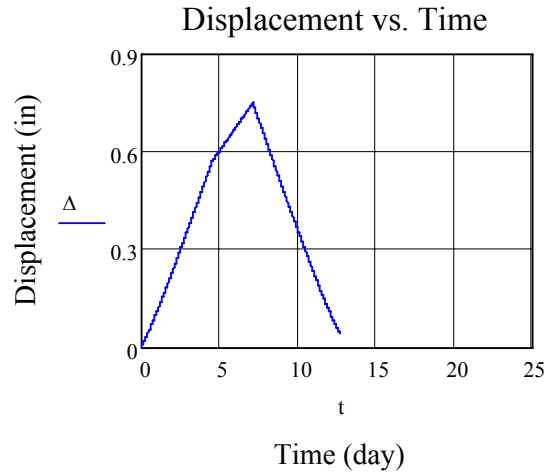
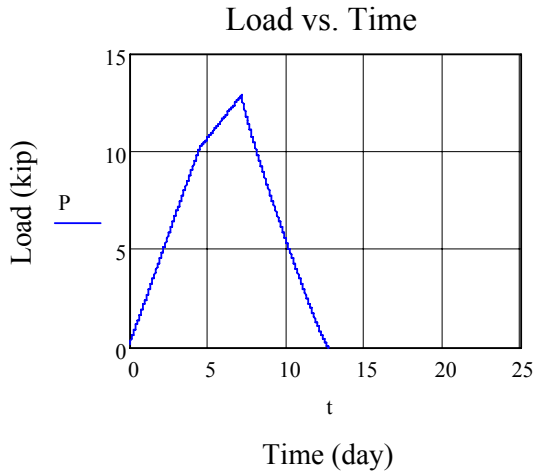


Figure A-11. Shape factor 16, 1.1 ksi compression, 7.2 hour test new pad data

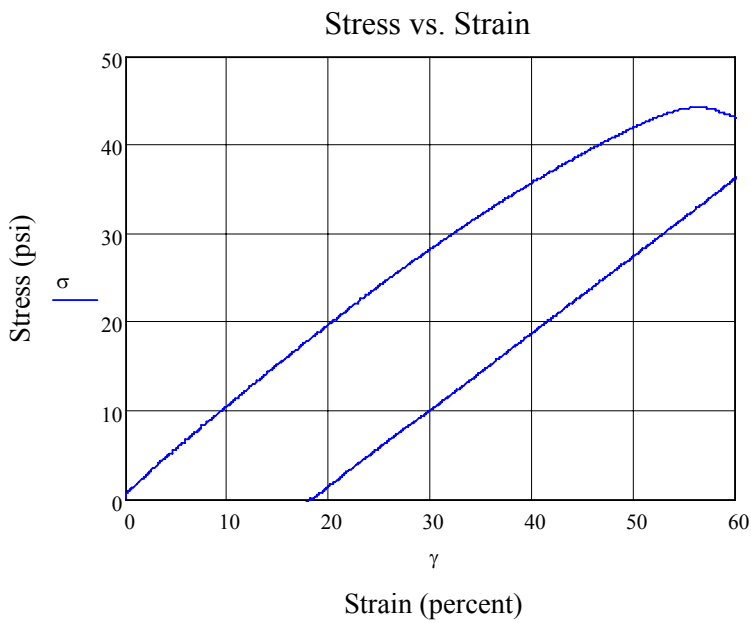
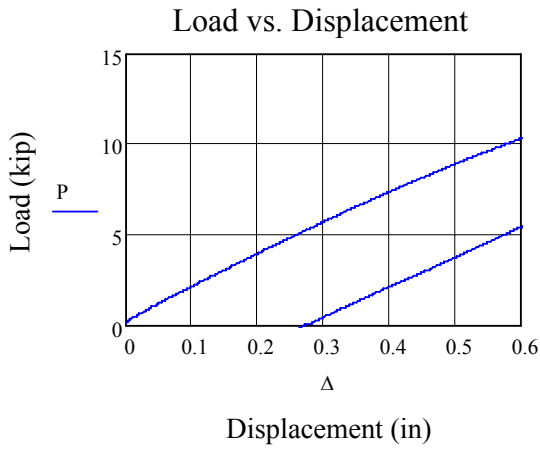
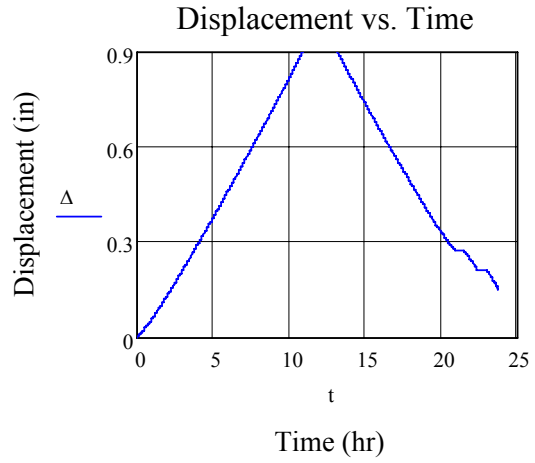
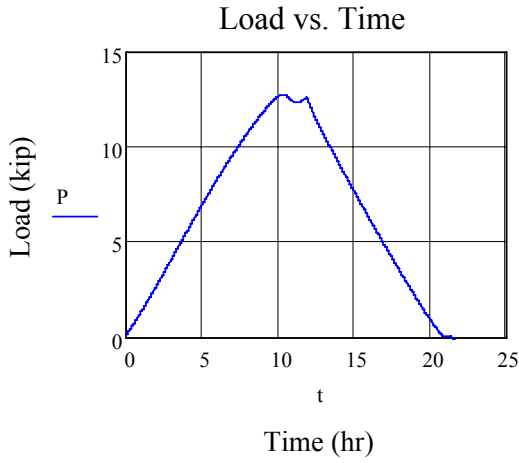


Figure A-12. Shape factor 16, 0.5 ksi compression, 9.5 hour test data

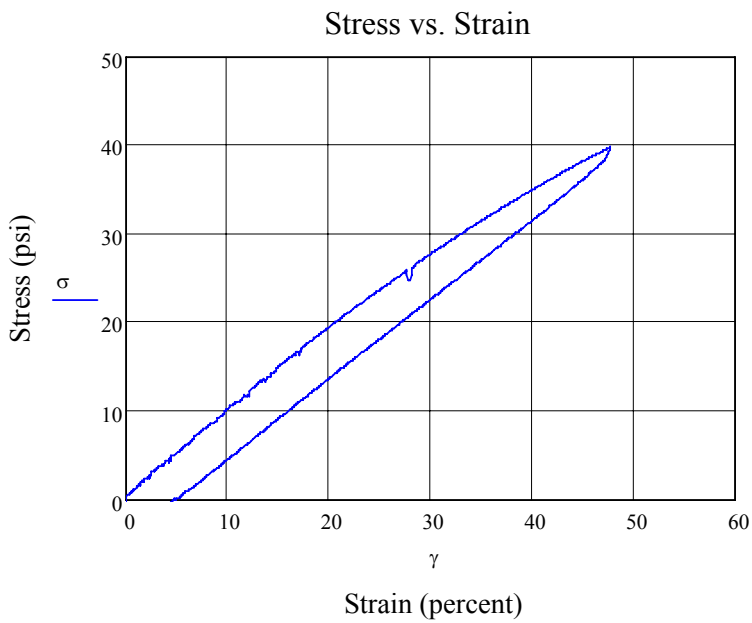
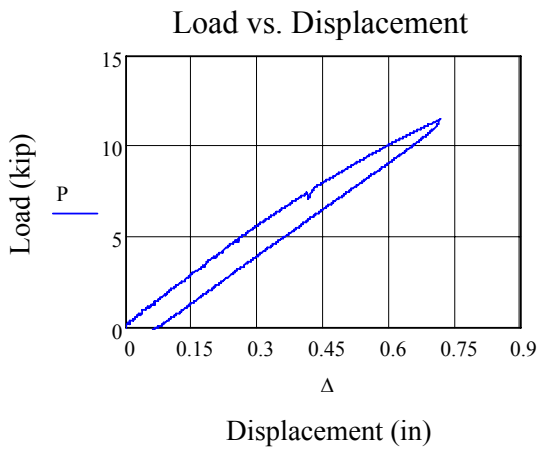
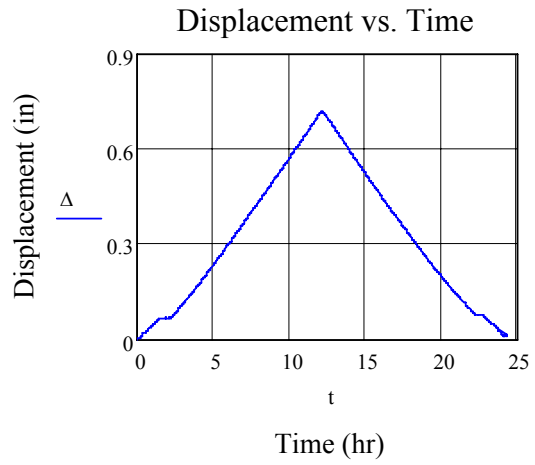
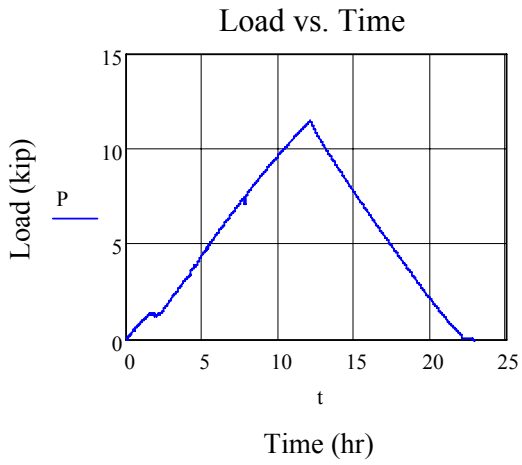


Figure A-13. Shape factor 16, 0.5 ksi compression, 12 hour test 1 data

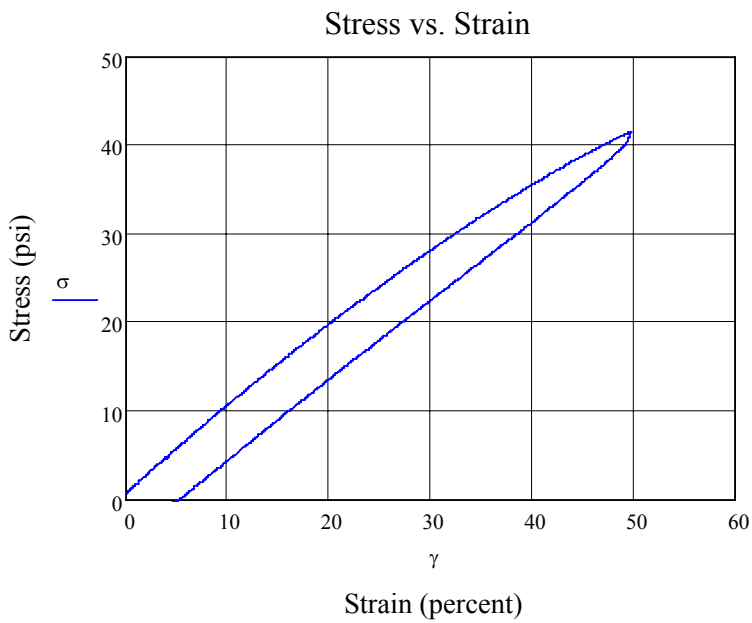
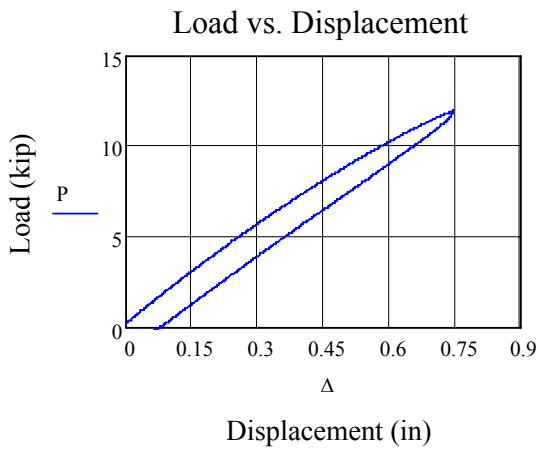
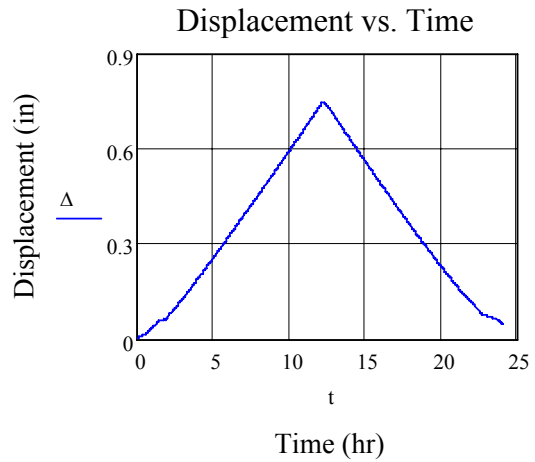
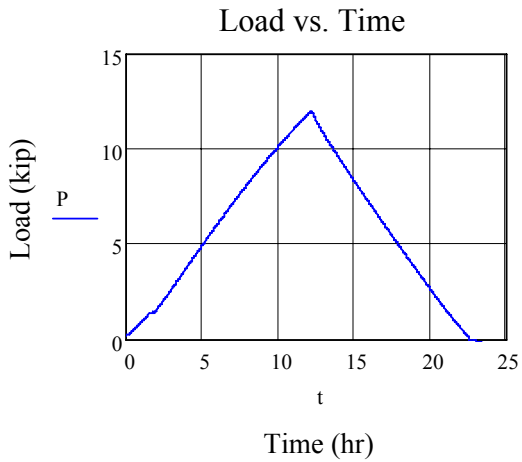


Figure A-14. Shape factor 16, 0.5 ksi compression, 12 hour test 2 data

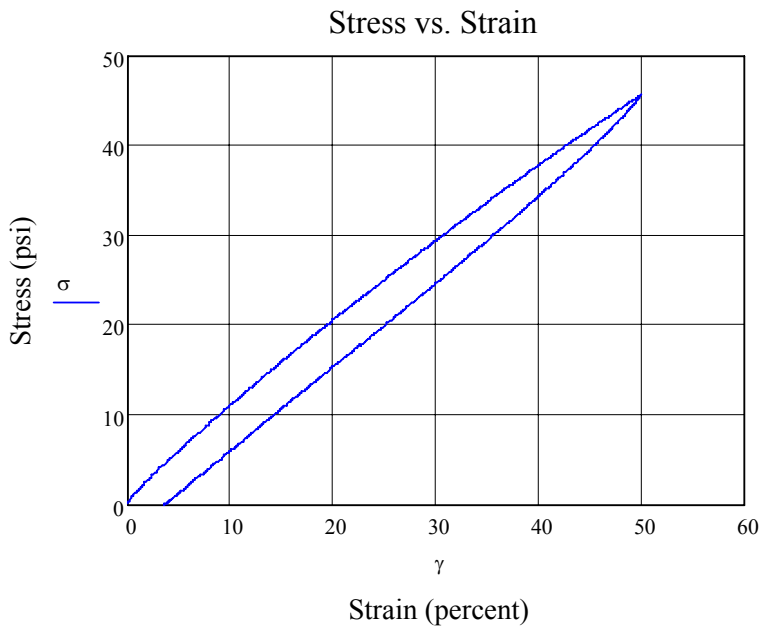
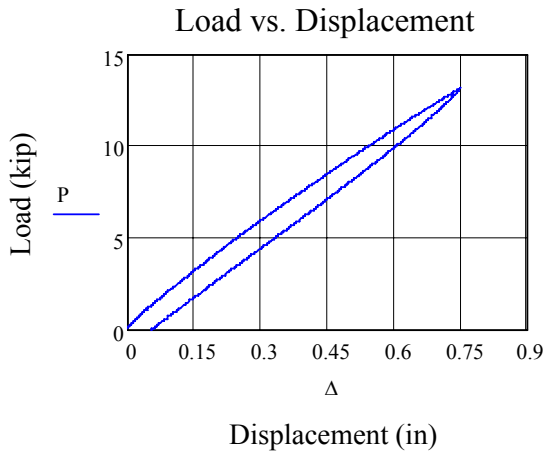
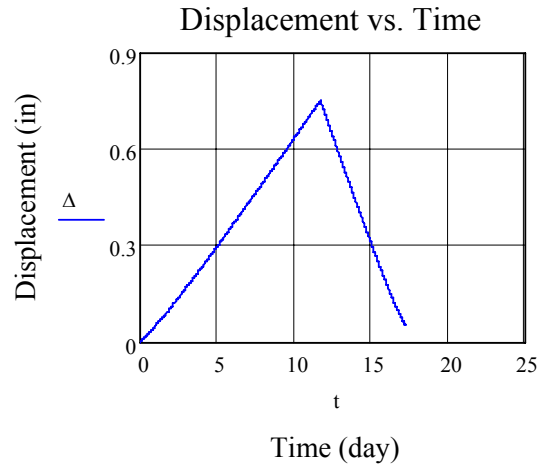
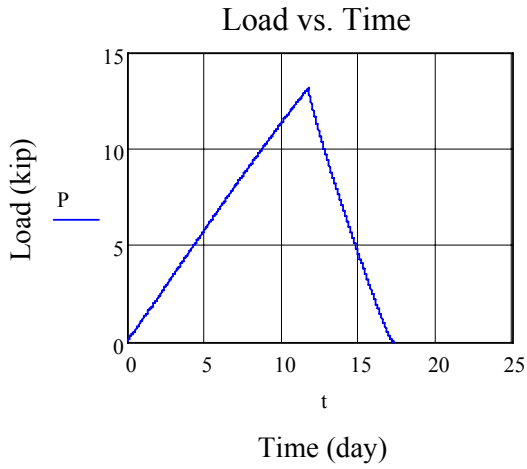


Figure A-15. Shape factor 16, 1.0 ksi compression, 12 hour test 1 new pad data

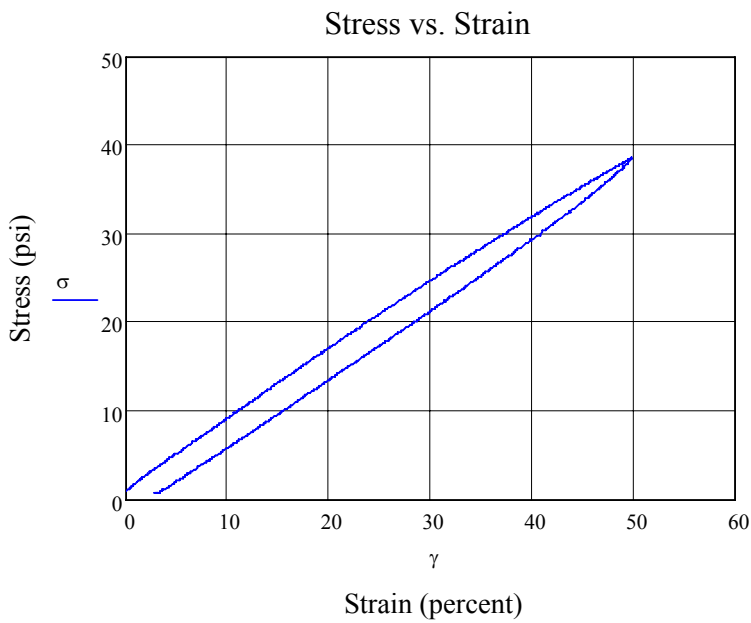
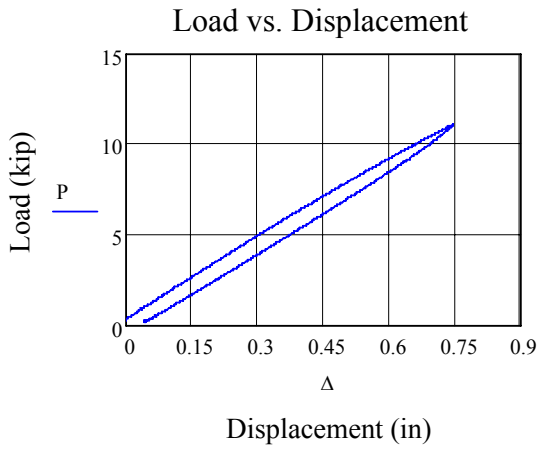
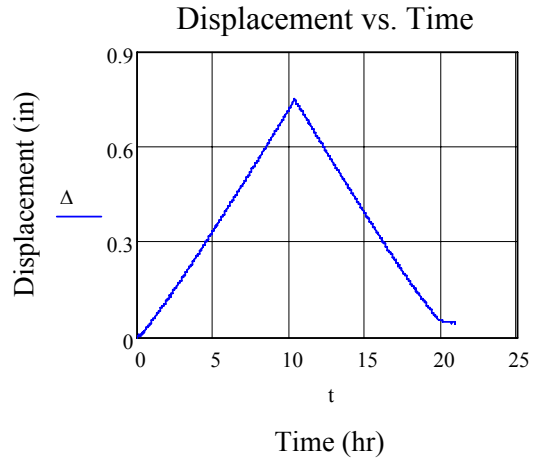
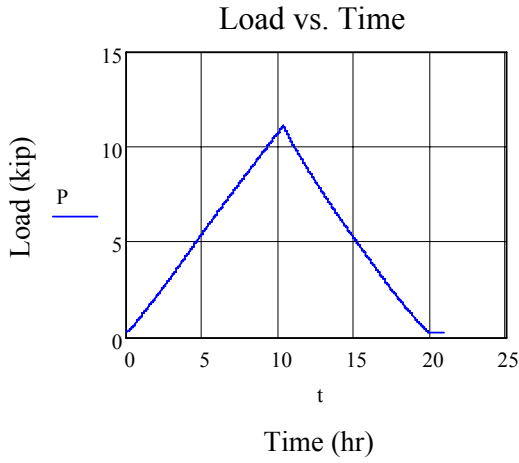


Figure A-16. Shape factor 16, 1.0 ksi compression, 12 hour test 1 data

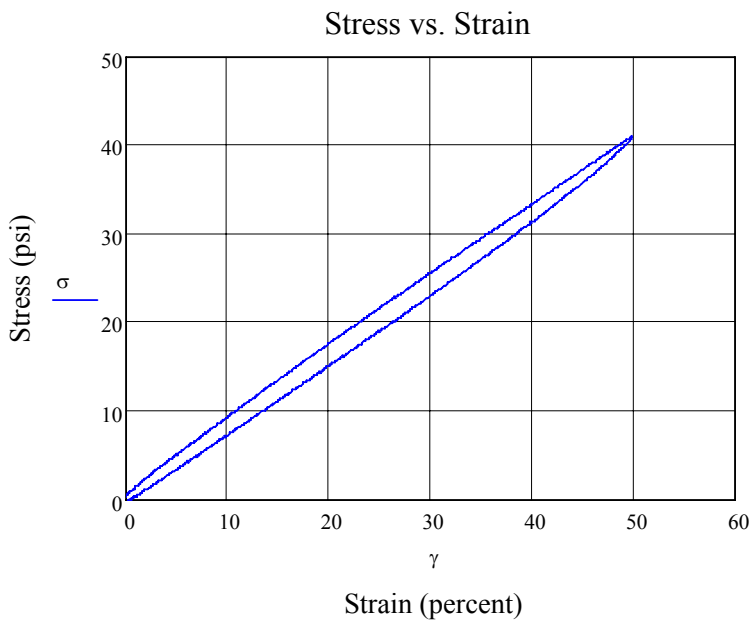
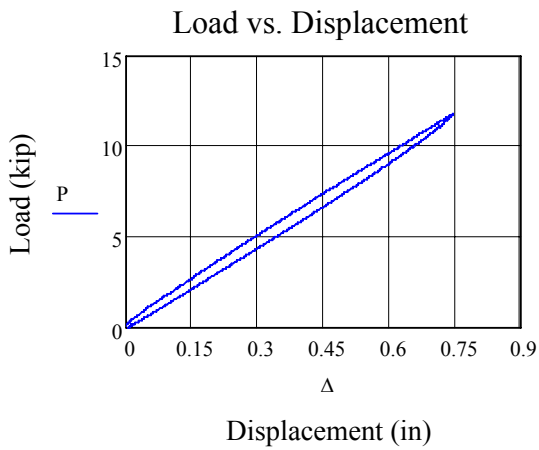
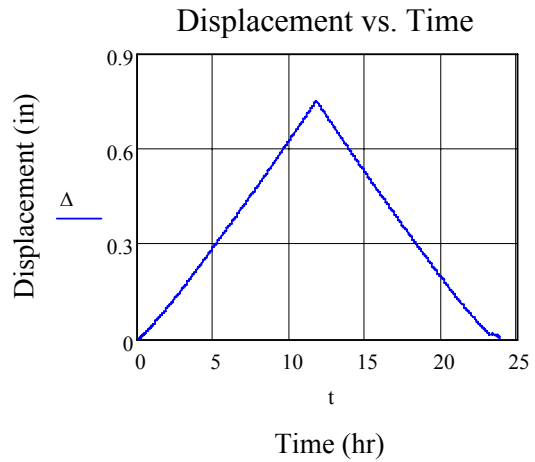
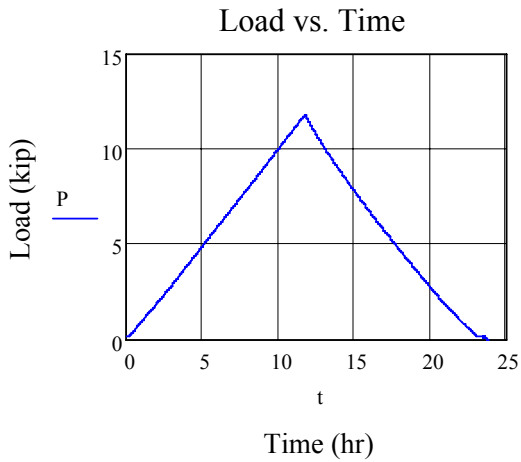


Figure A-17. Shape factor 16, 1.0 ksi compression, 12 hour test 2 data

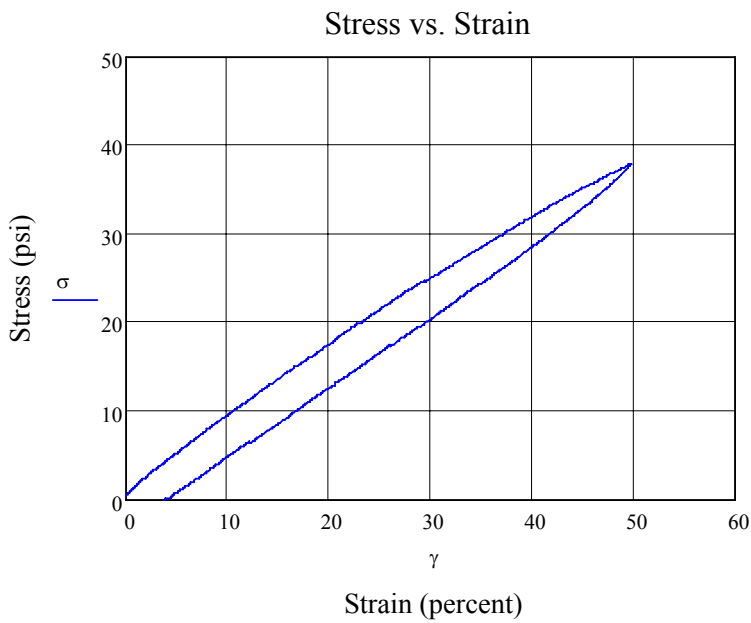
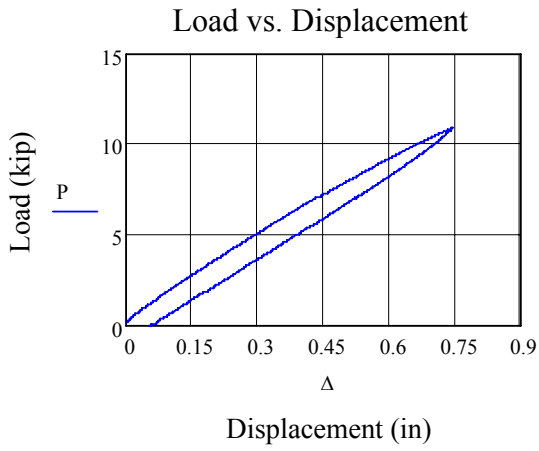
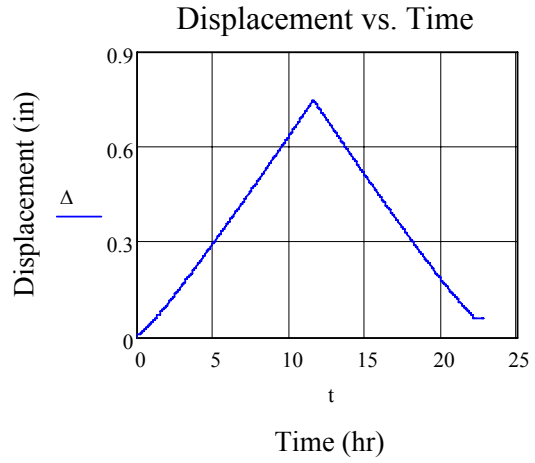
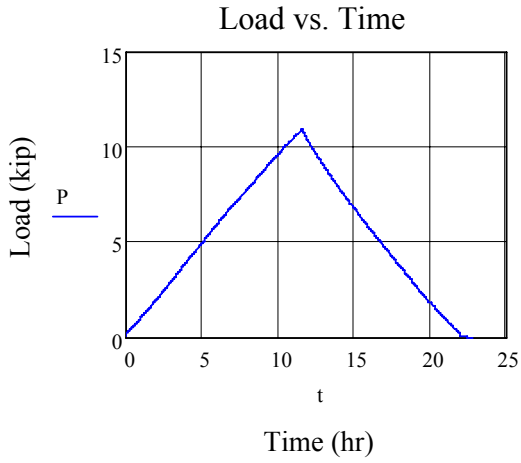


Figure A-18. Shape factor 16, 1.0 ksi compression, 12 hour test 3 data

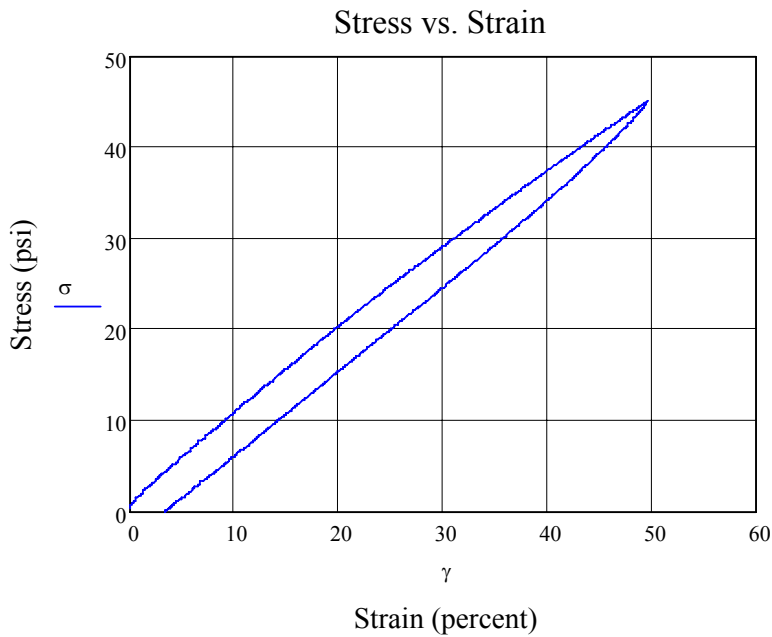
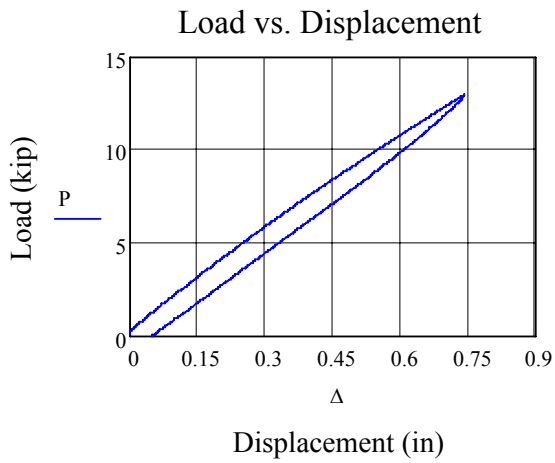
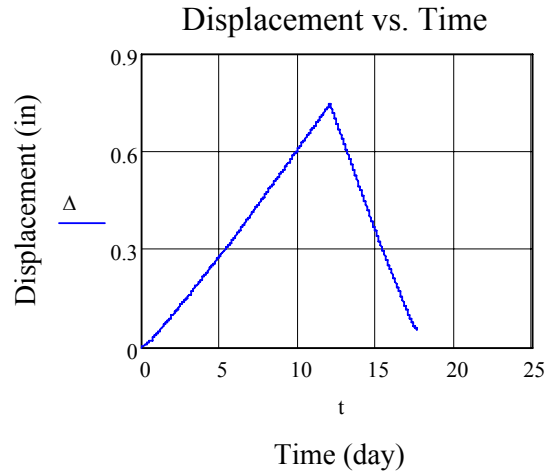
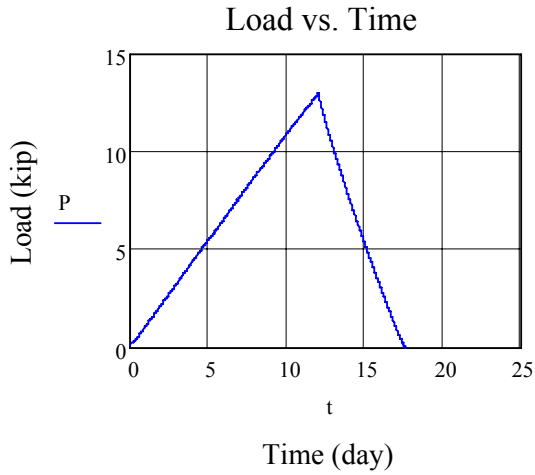


Figure A-19. Shape factor 16, 1.0 ksi compression, 12 hour test 2 new pad data

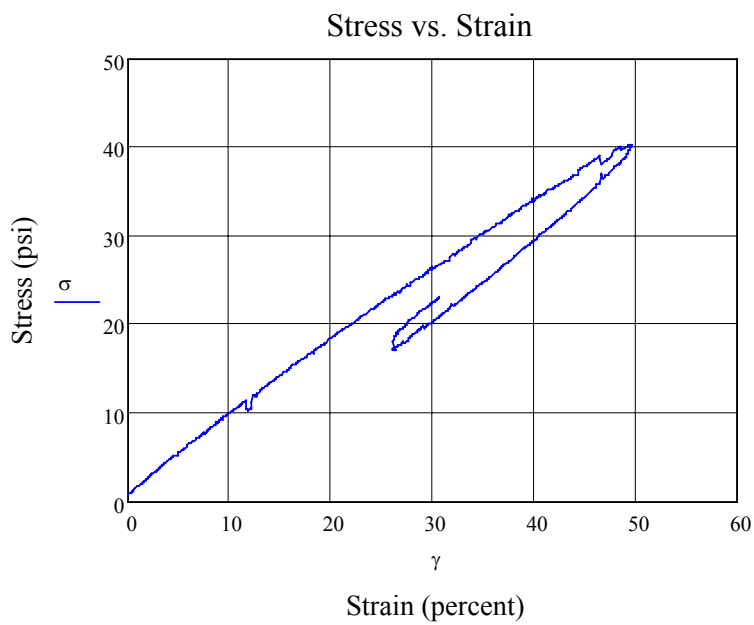
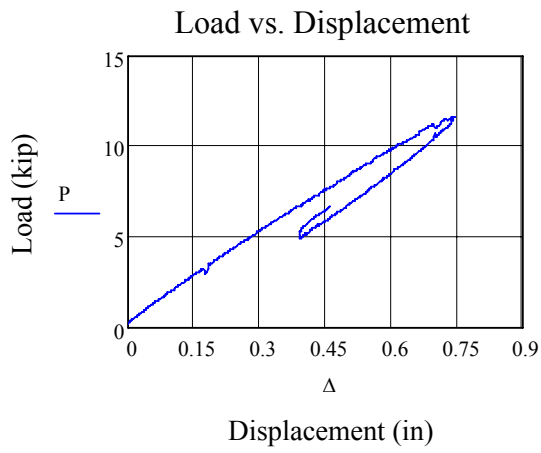
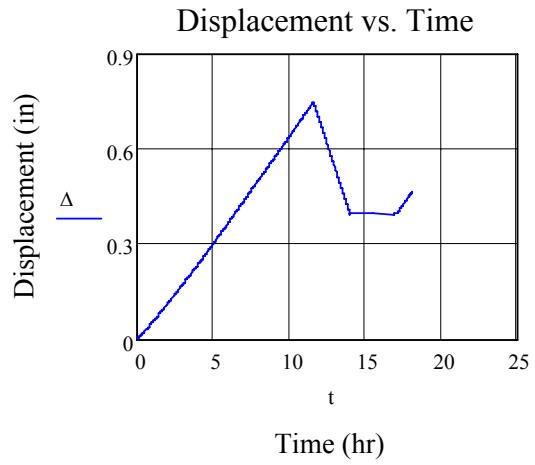
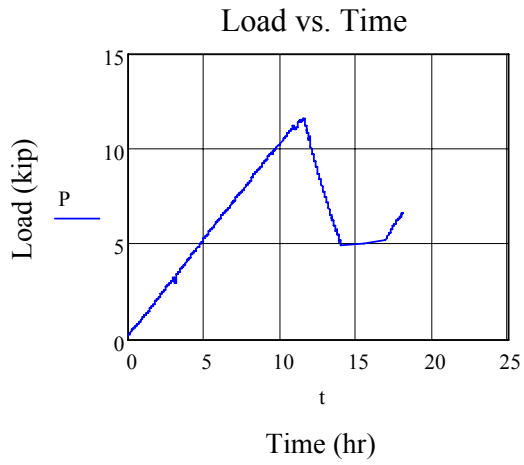


Figure A-20. Shape factor 16, 1.5 ksi compression, 12 hour test data

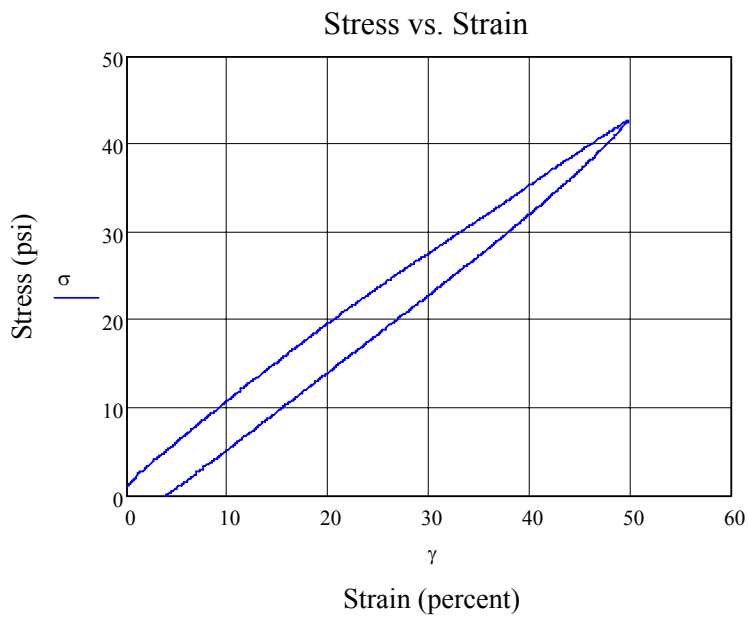
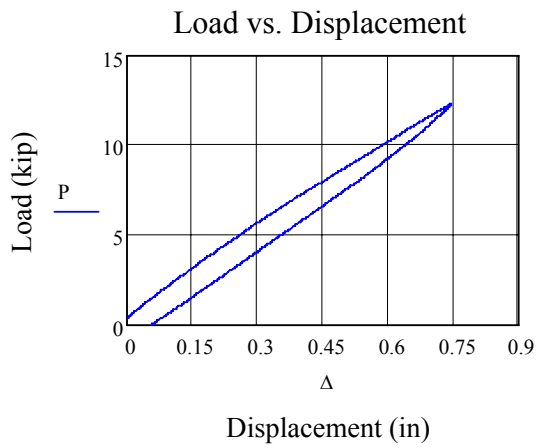
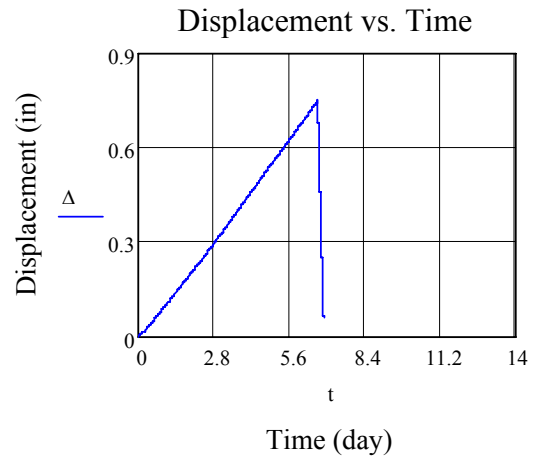
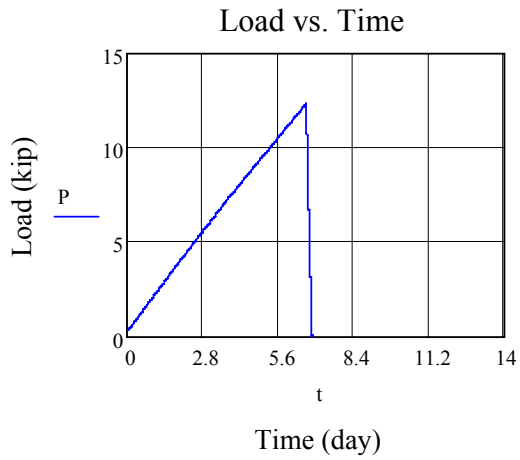


Figure A-21. Shape factor 16, 1.0 ksi compression, 7 day test new pad data

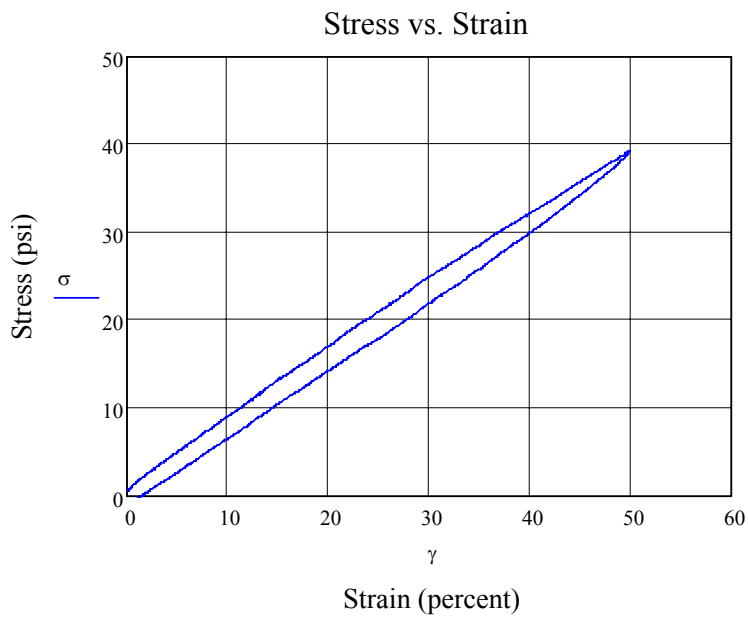
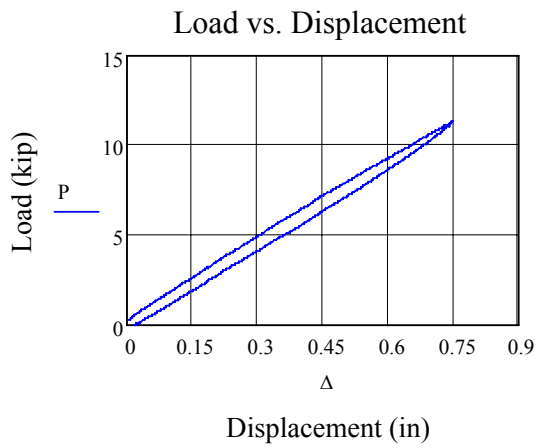
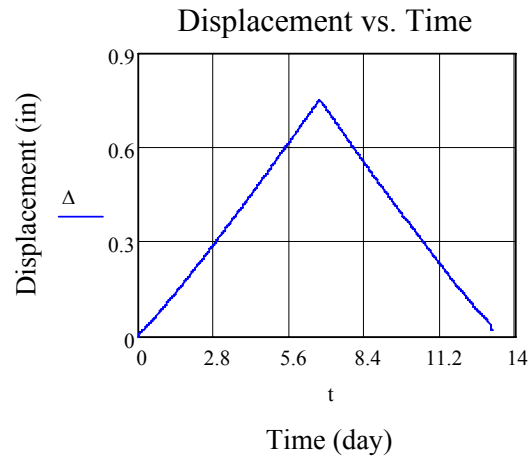
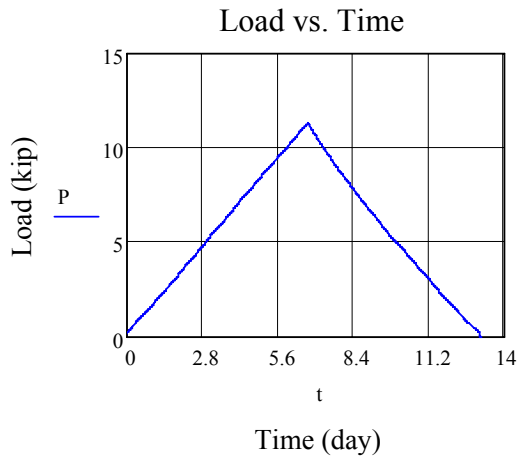


Figure A-22. Shape factor 16, 1.0 ksi compression, 7 day test data

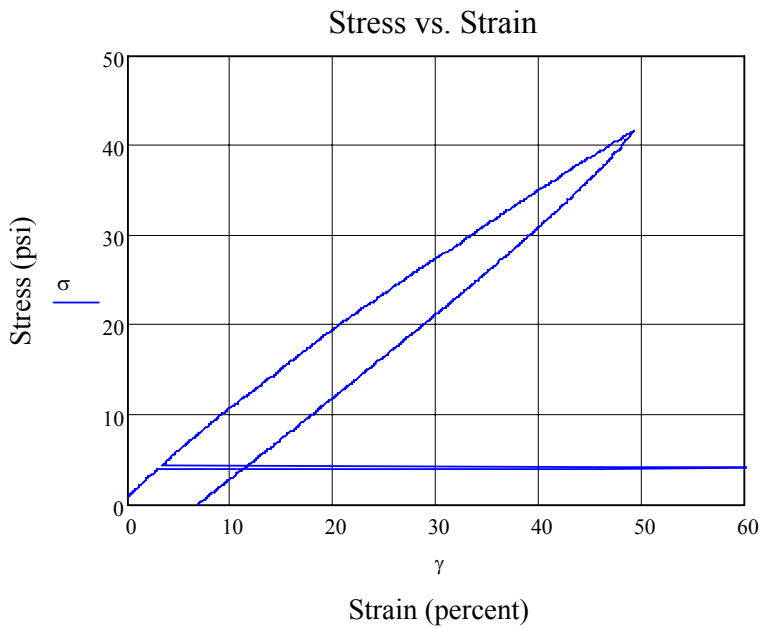
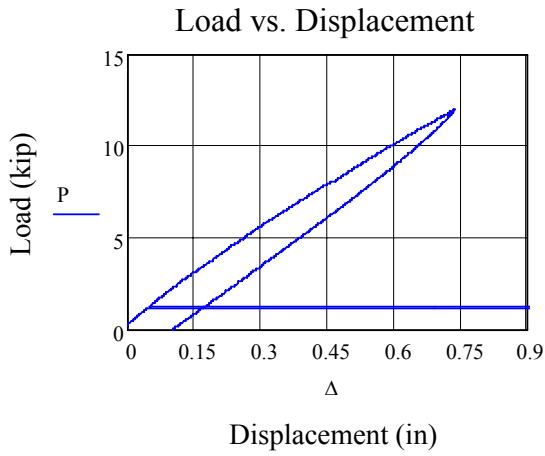
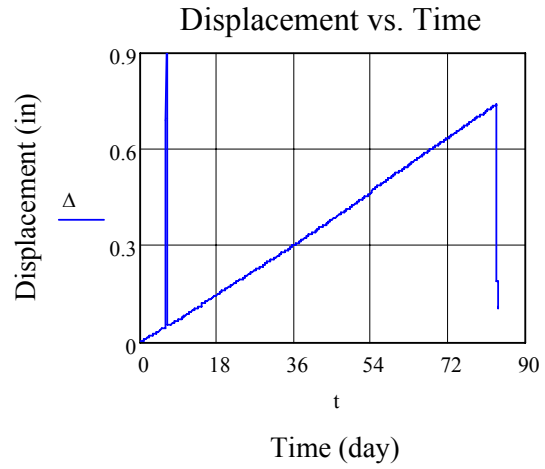
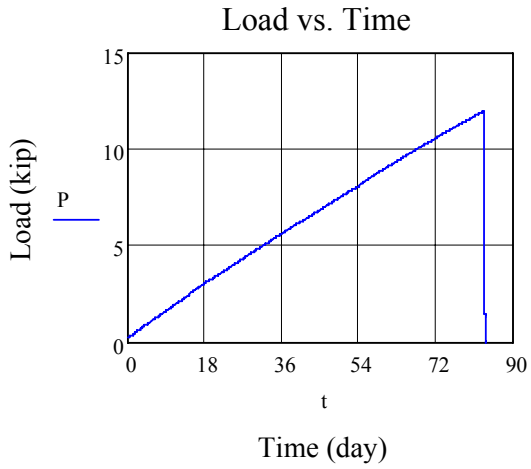


Figure A-23. Shape factor 16, 1.0 ksi compression, 90 day test new pad data

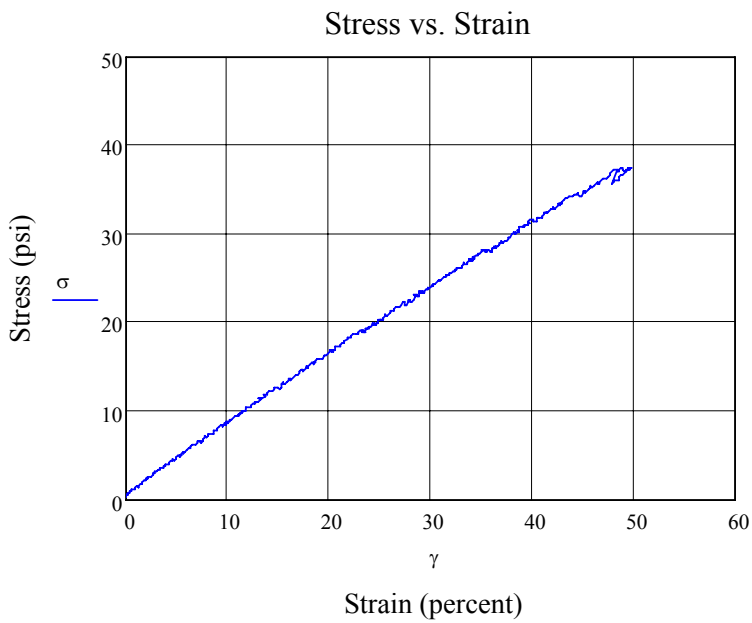
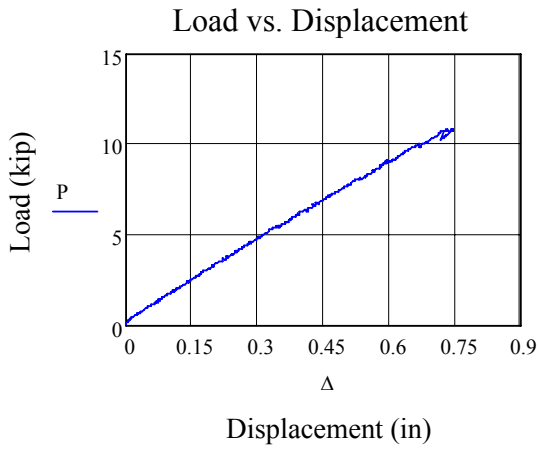
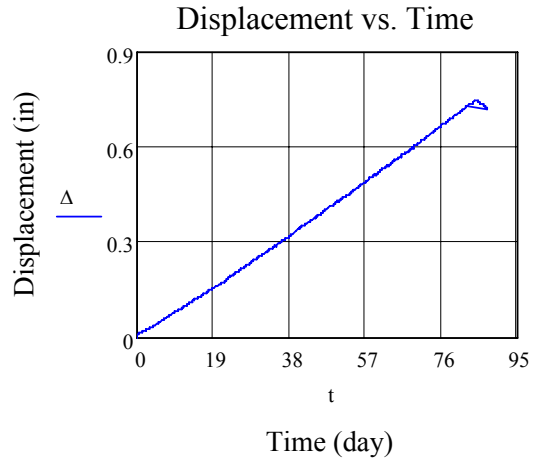
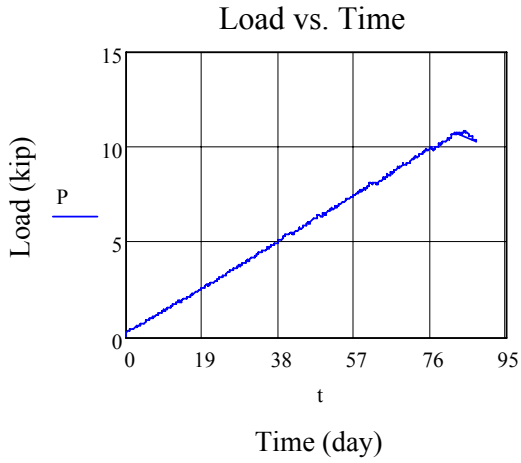


Figure A-24. Shape factor 16, 1.1 ksi compression, 90 day test data

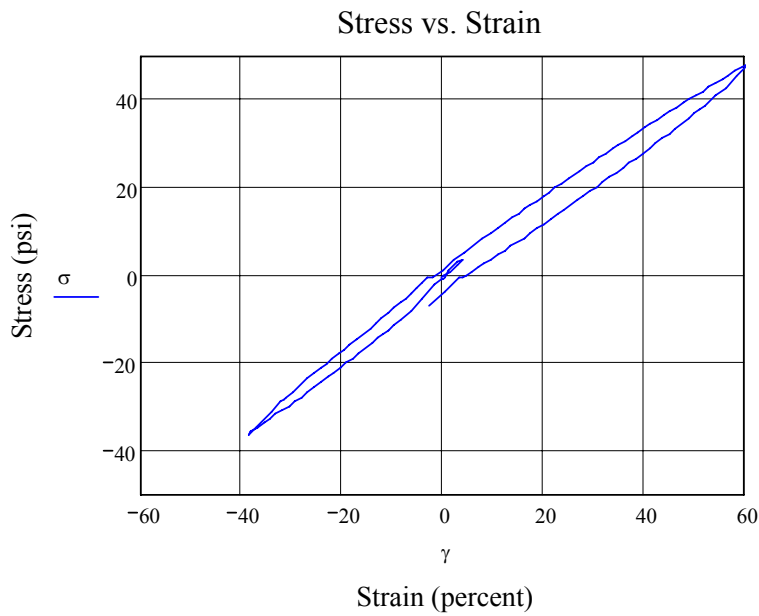
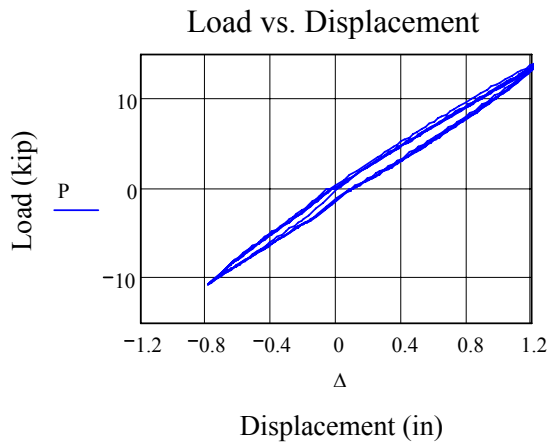
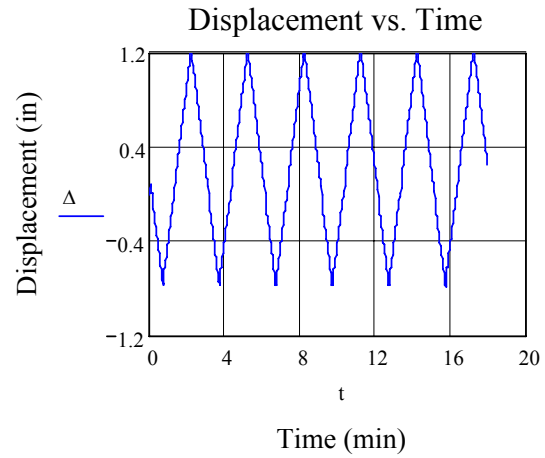
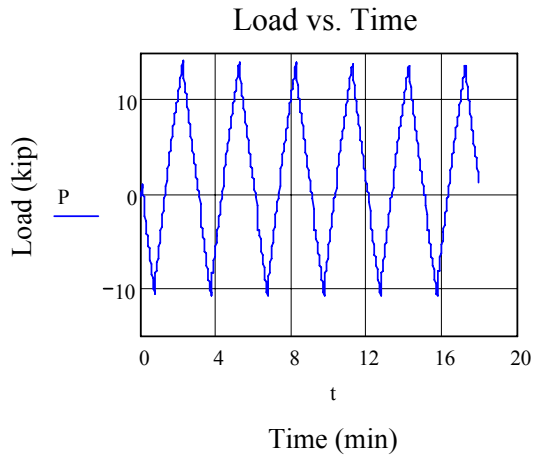


Figure A-25. Shape factor 12, 1.0 ksi compression, 45 second test new pad (start) data

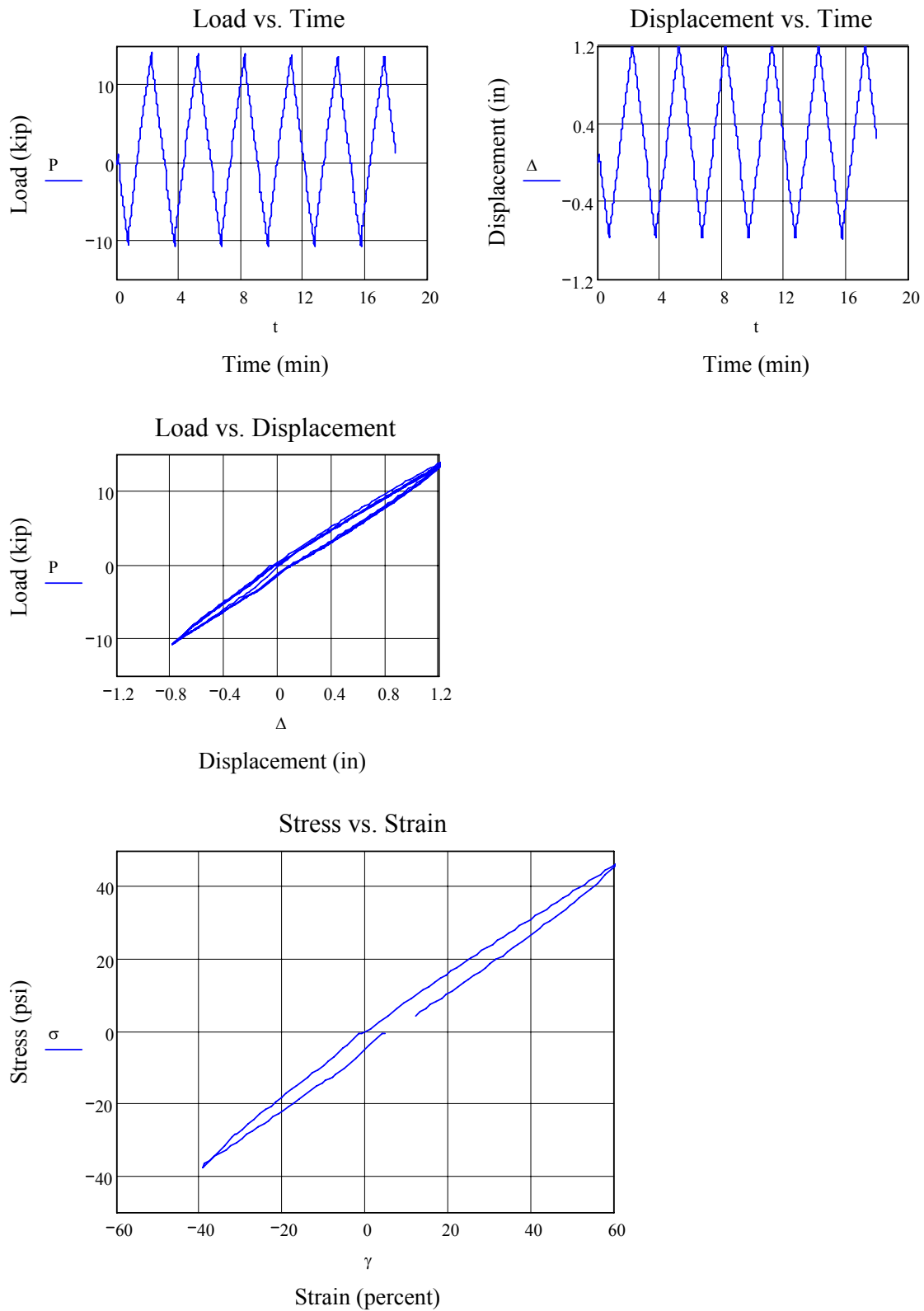


Figure A-26. Shape factor 12, 1.0 ksi compression, 45 second test (end) data

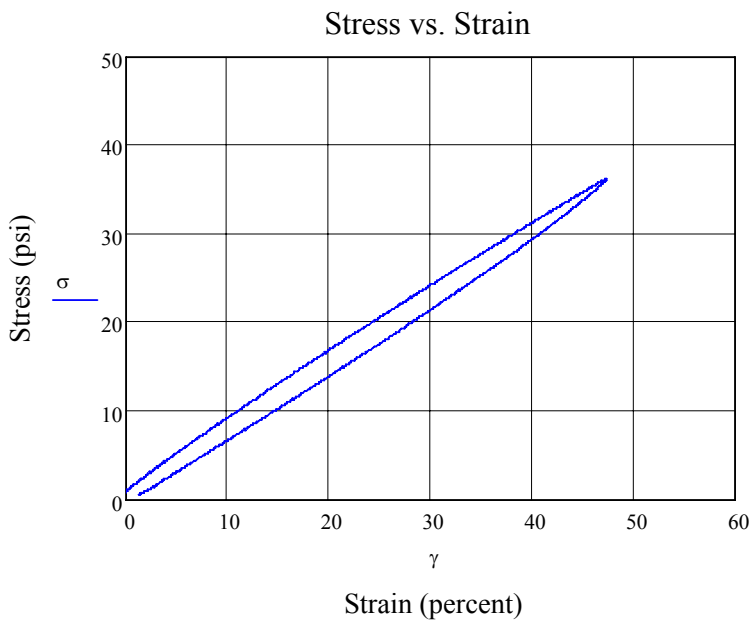
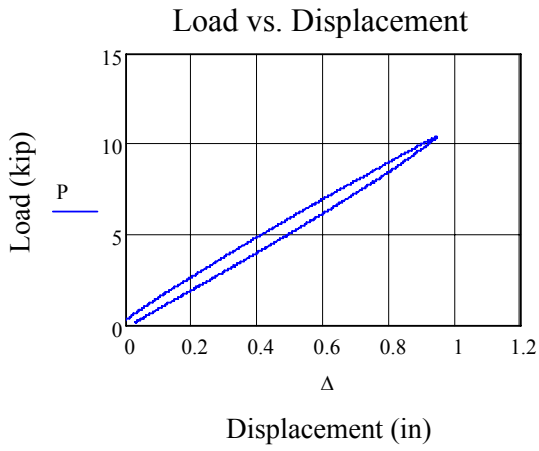
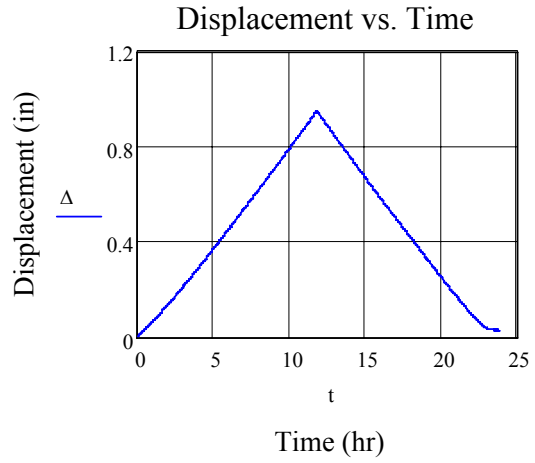
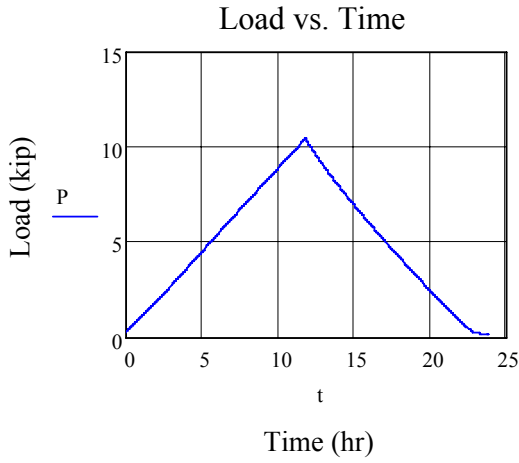


Figure A-28. Shape factor 12, 1.0 ksi compression, 12 hour test 1 data

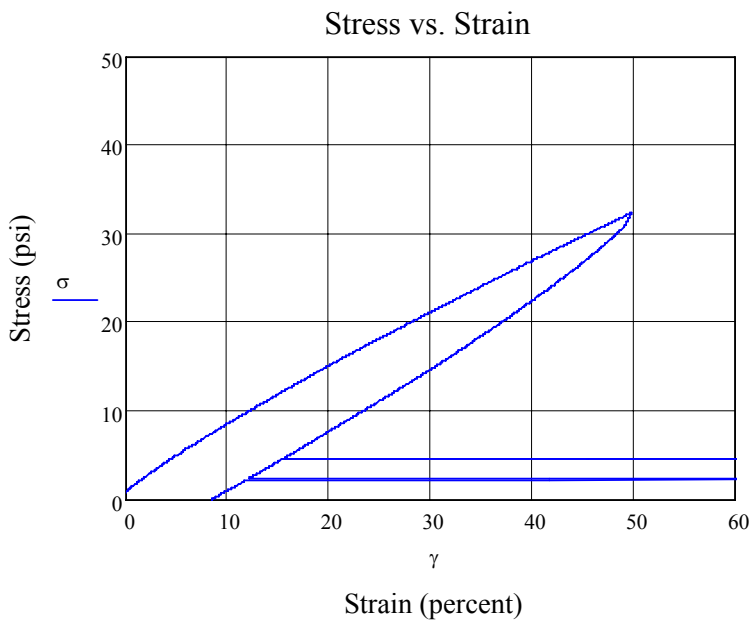
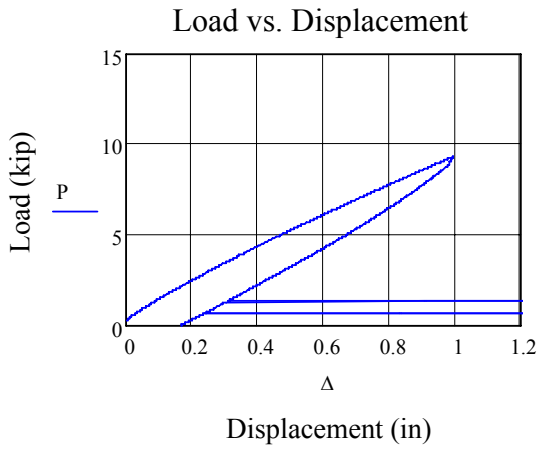
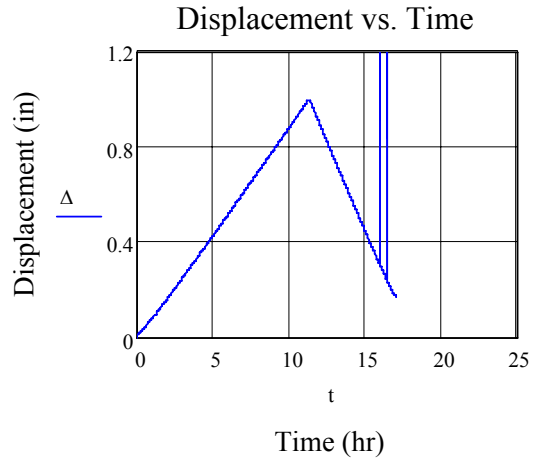
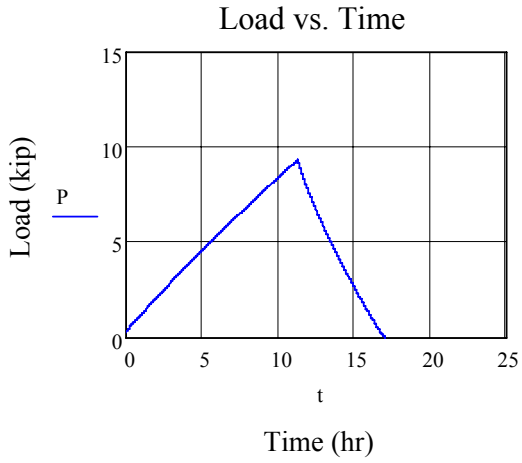


Figure A-30. Shape factor 12, 1.5 ksi compression, 12 hour test 1 data

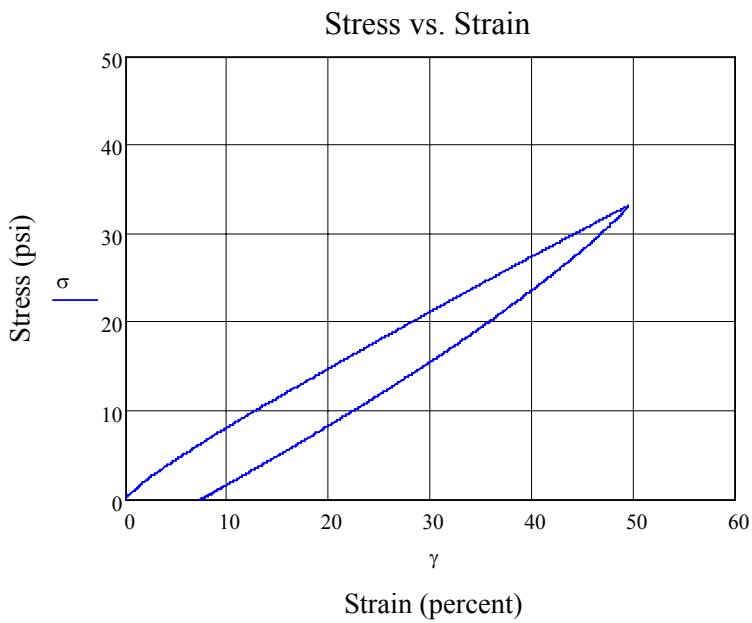
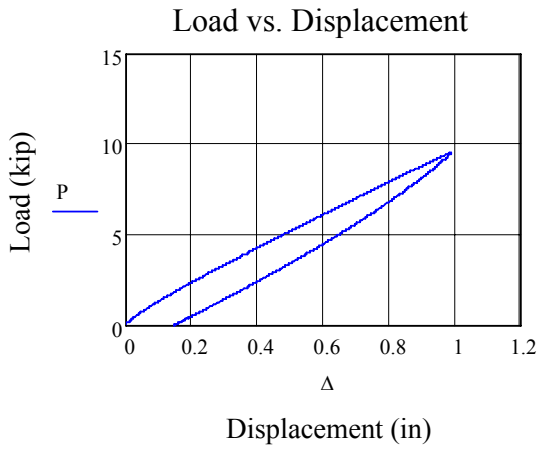
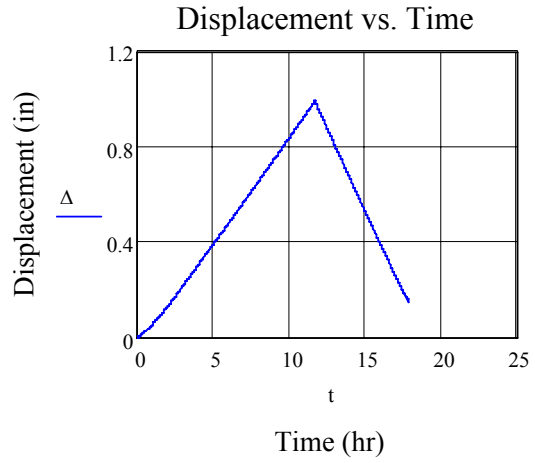
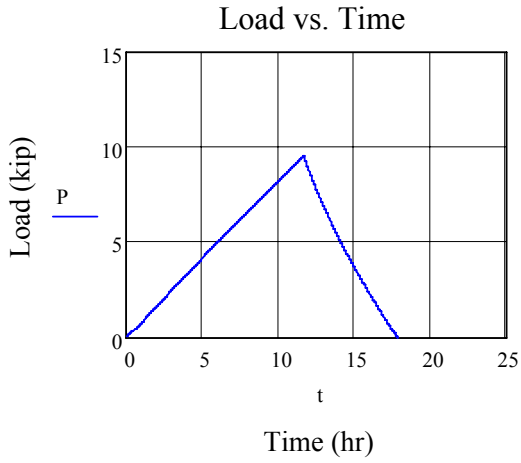


Figure A-31. Shape factor 12, 1.5 ksi compression, 12 hour test 2 data

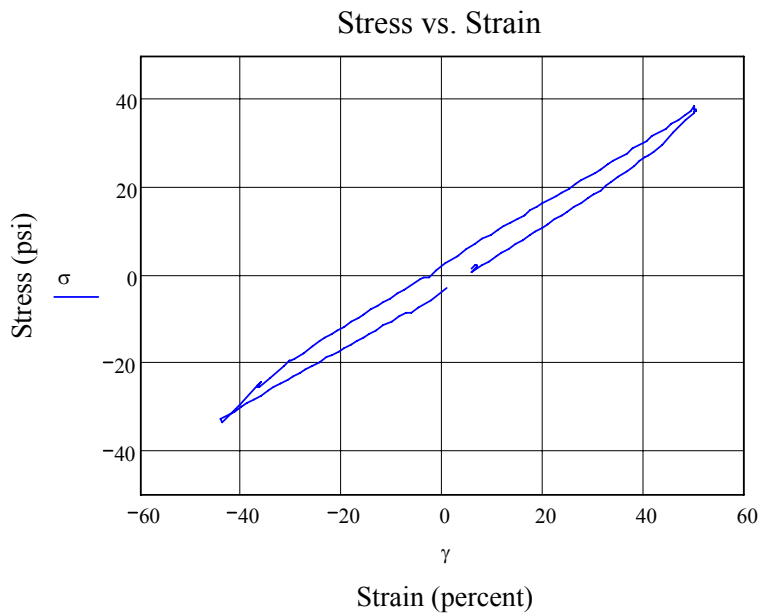
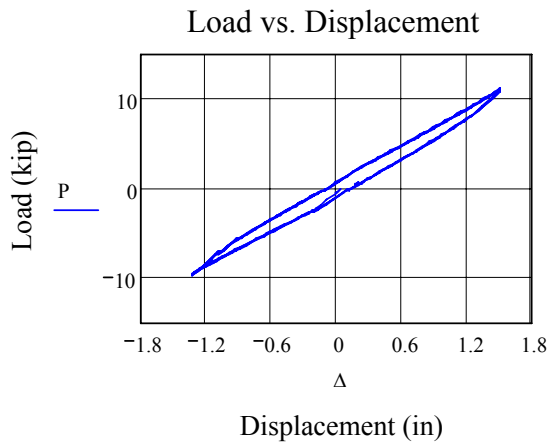
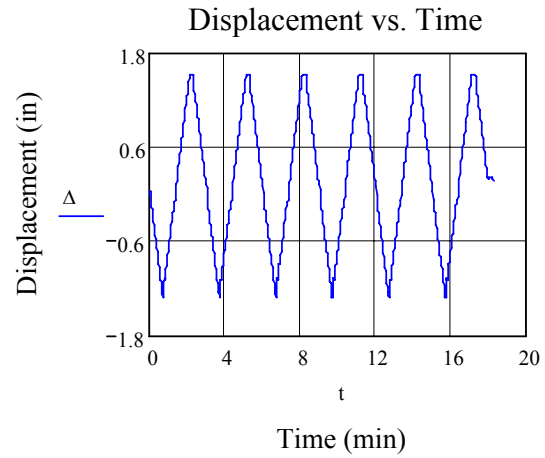
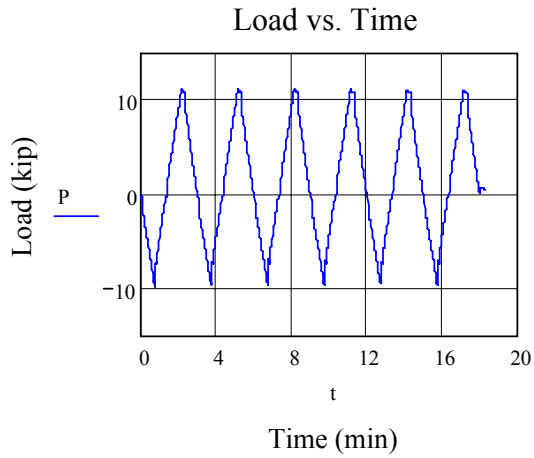


Figure A-32. Shape factor 8, 1.0 ksi compression, 45 second test 1 (end) data

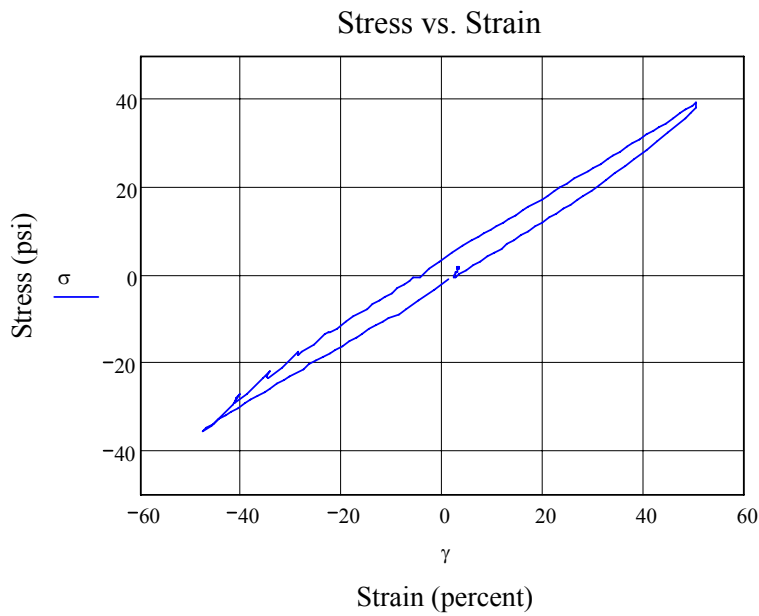
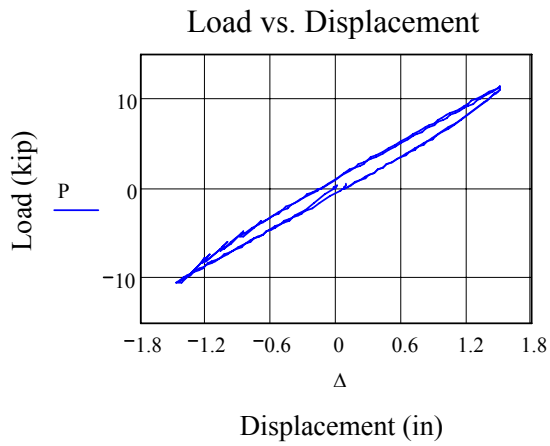
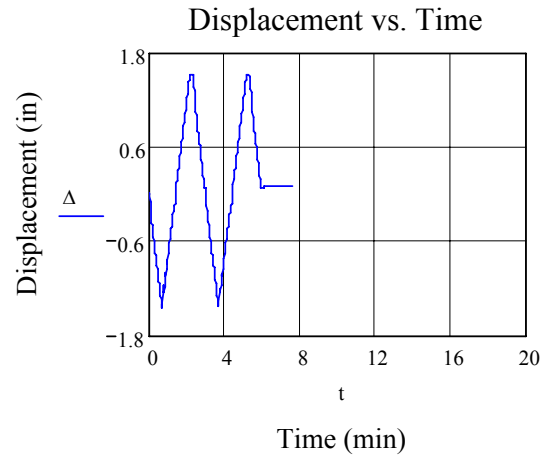
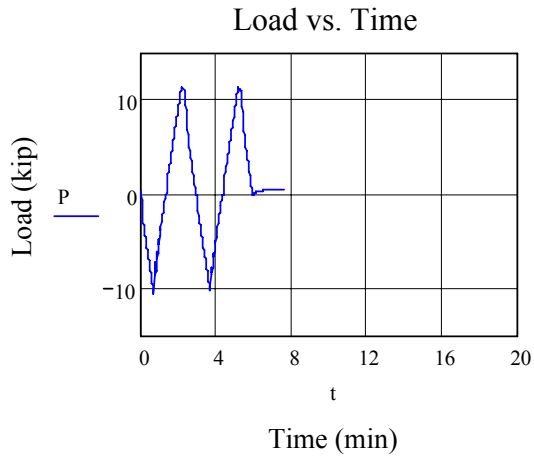


Figure A-33. Shape factor 8, 1.0 ksi compression, 45 second test 2 (end) data

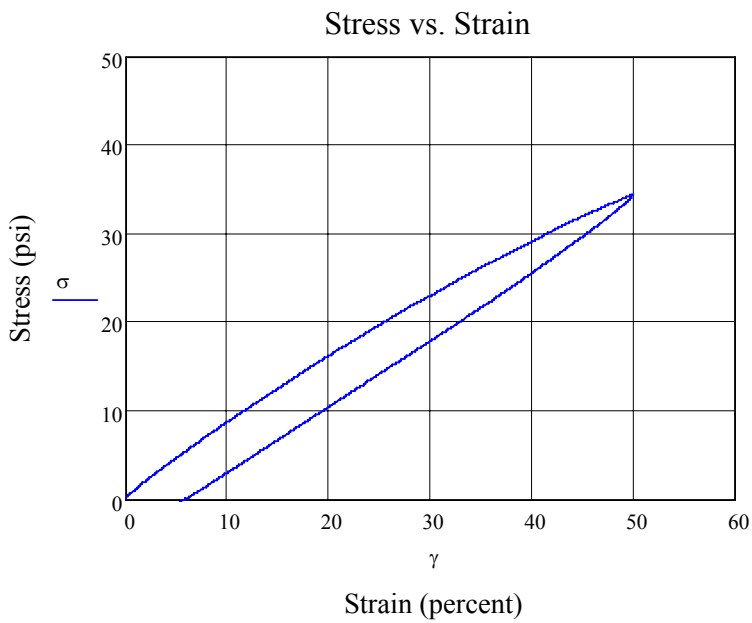
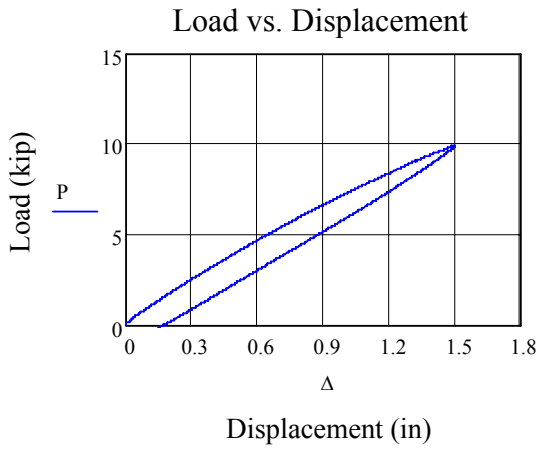
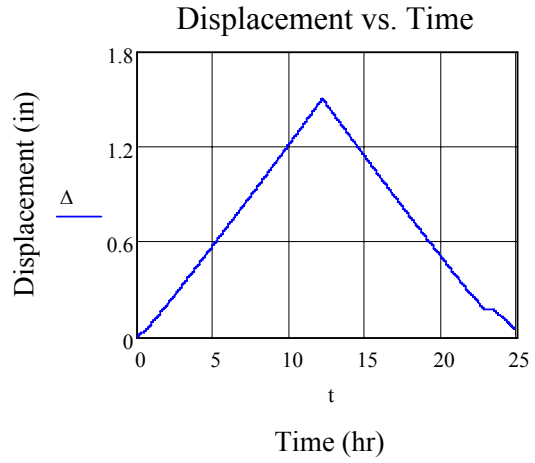
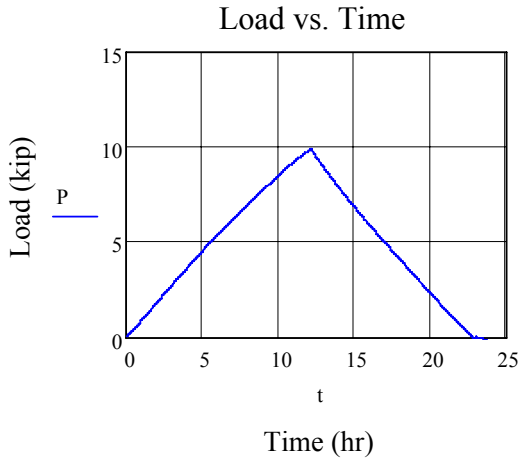


Figure A-34. Shape factor 8, 0.5 ksi compression, 12 hour test data

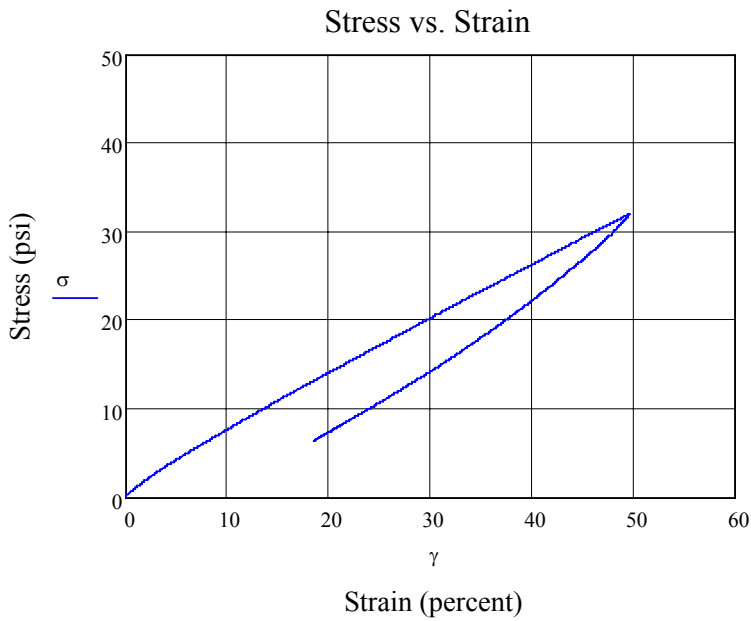
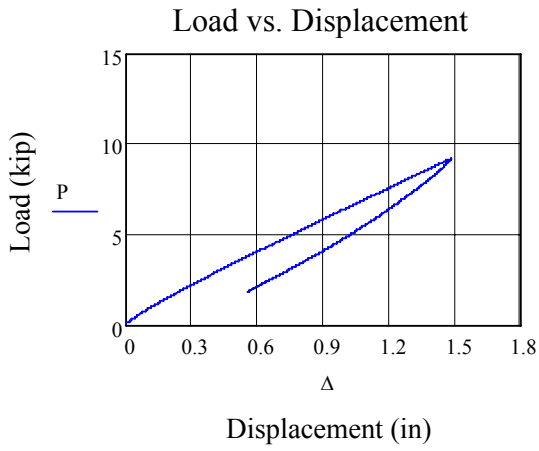
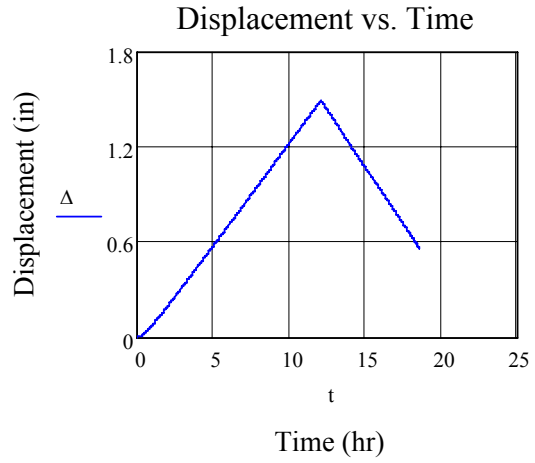
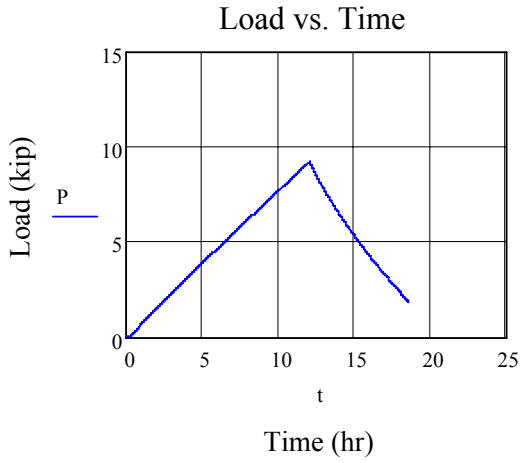


Figure A-35. Shape factor 8, 0.9 ksi compression, 12 hour test 1 data

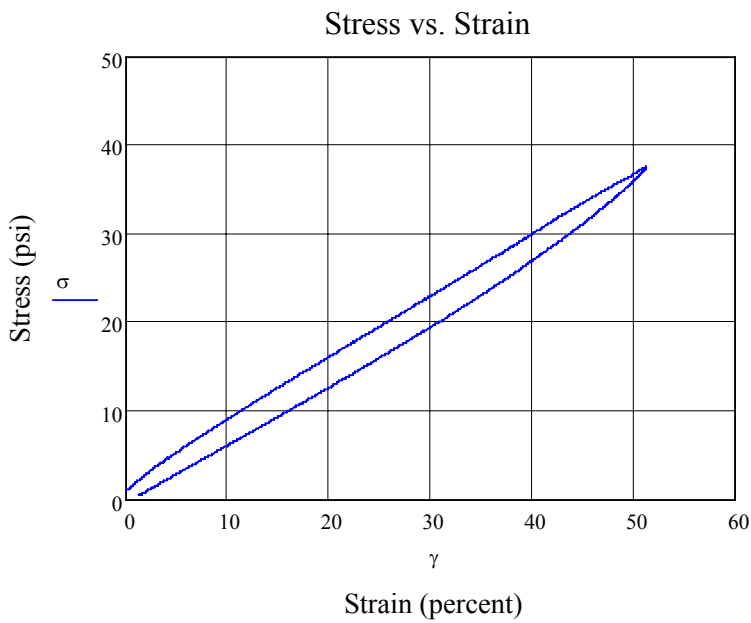
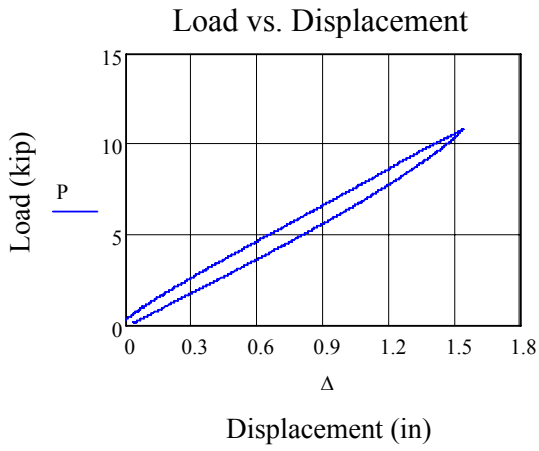
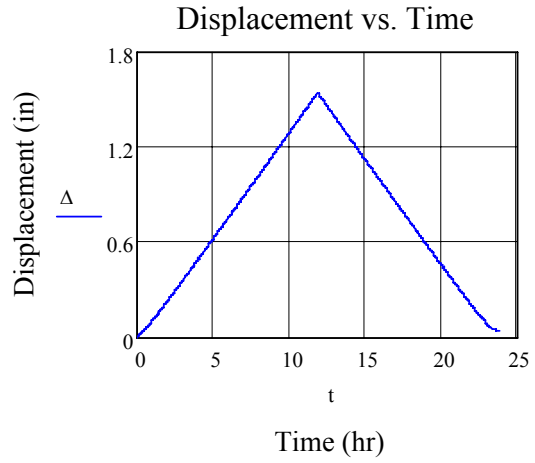
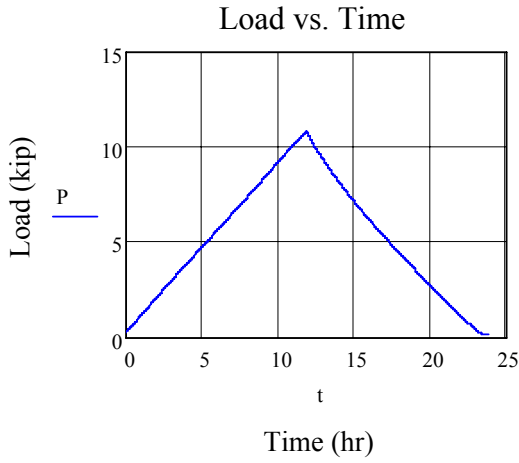


Figure A-36. Shape factor 8, 1.0 ksi compression, 12 hour test 2 data

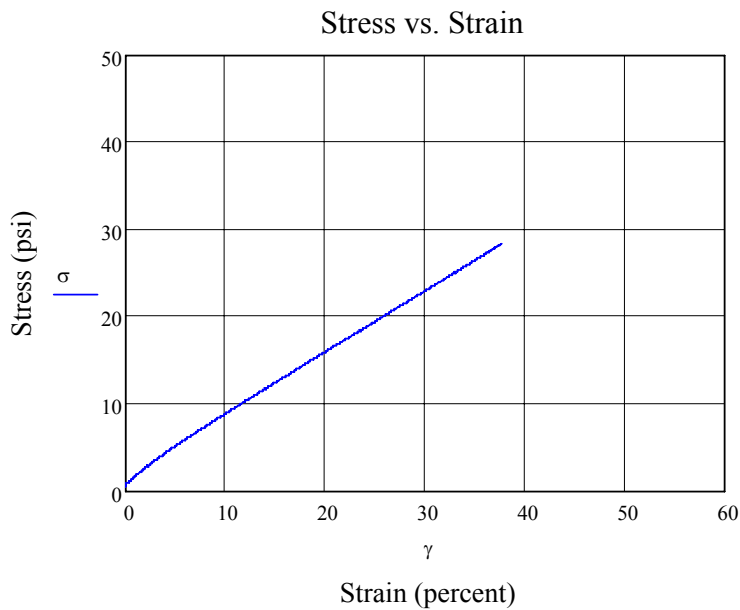
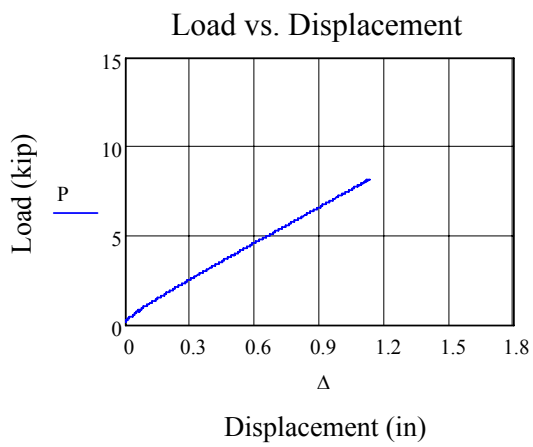
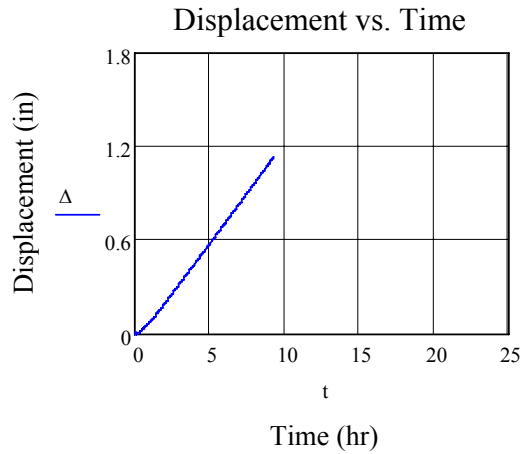
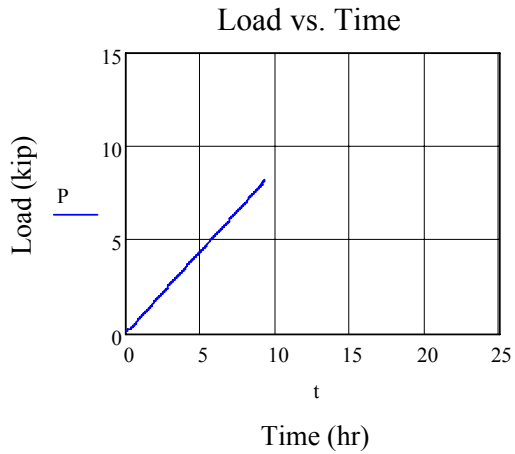


Figure A-37. Shape factor 8, 1.0 ksi ksi compression, 12 hour test 3 data. The stress at 50% shear strain was calculated from a 2nd order curve fit on the ascending portion of the graph.

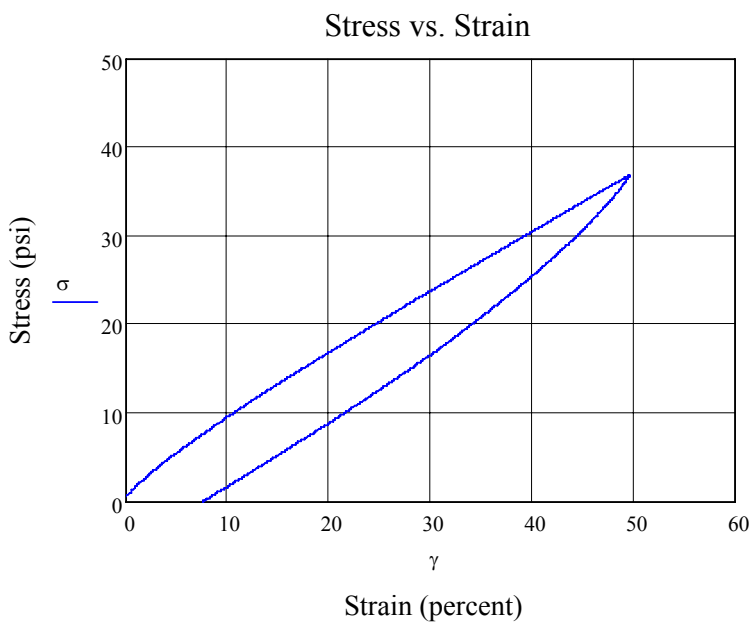
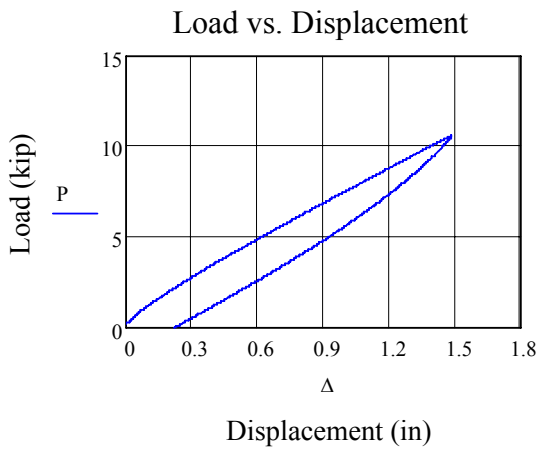
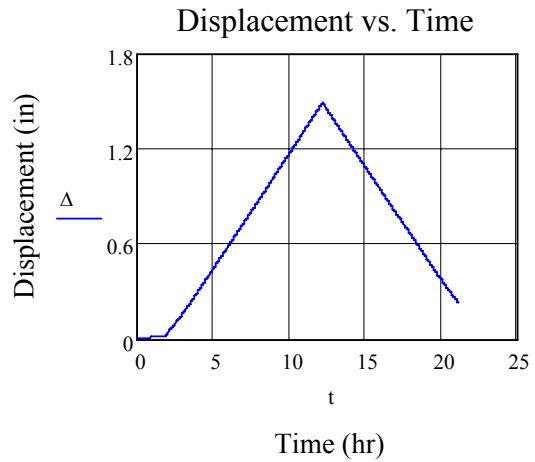
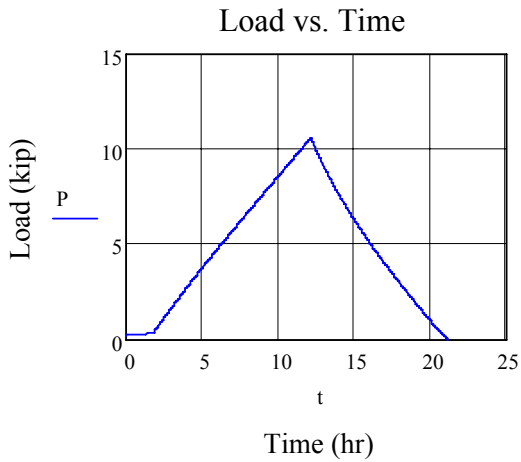


Figure A-38. Shape factor 8, 1.1 ksi compression, 12 hour test new pad data

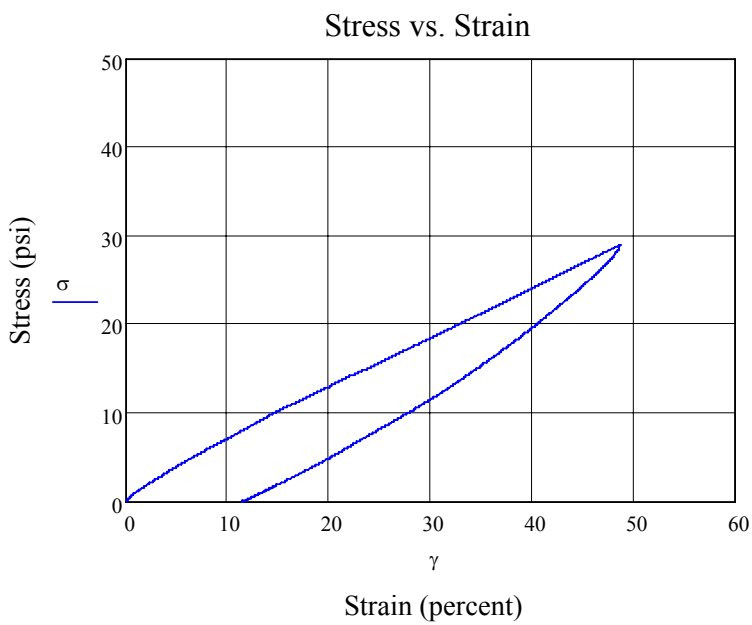
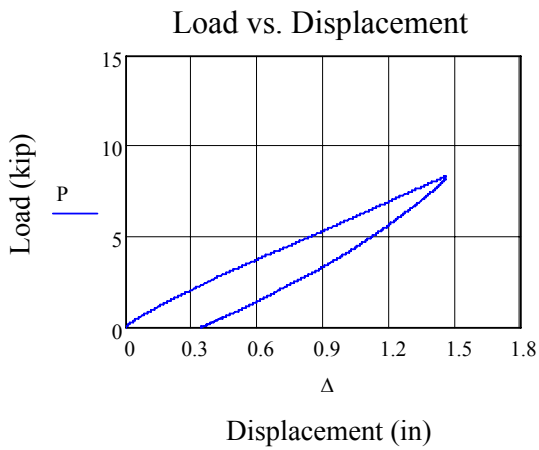
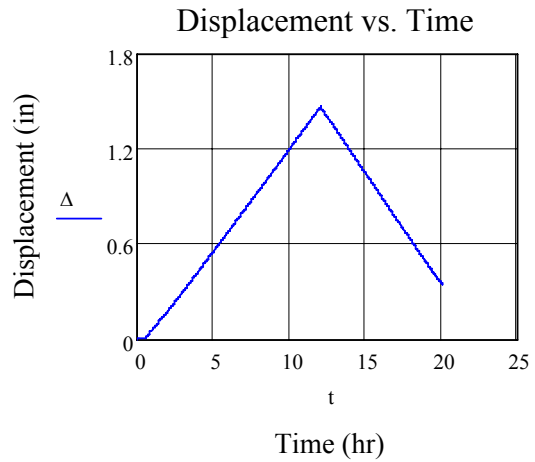
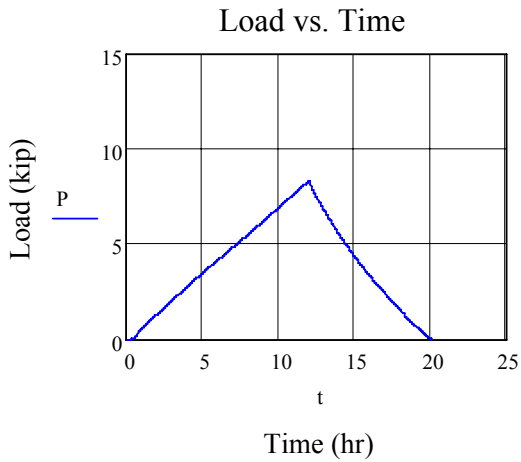


Figure A-39. Shape factor 8, 1.2 ksi compression, 12 hour test 1 data

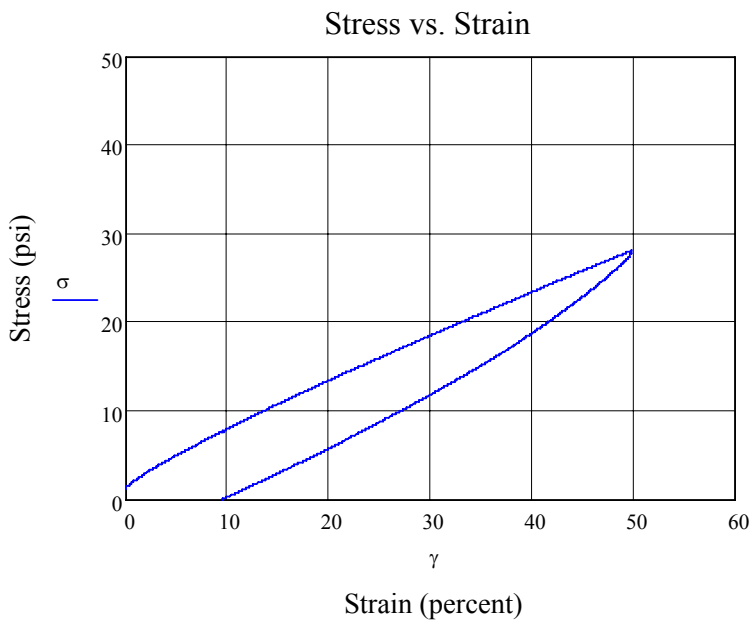
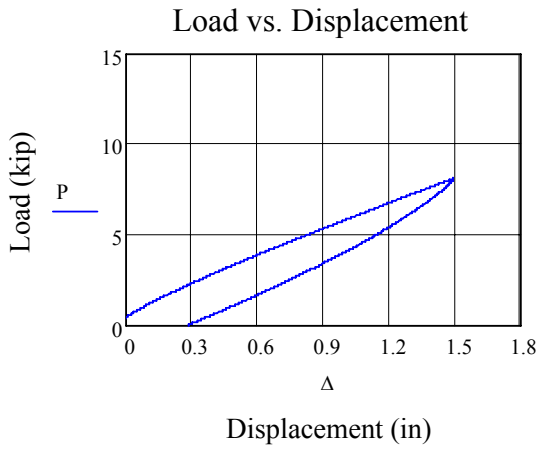
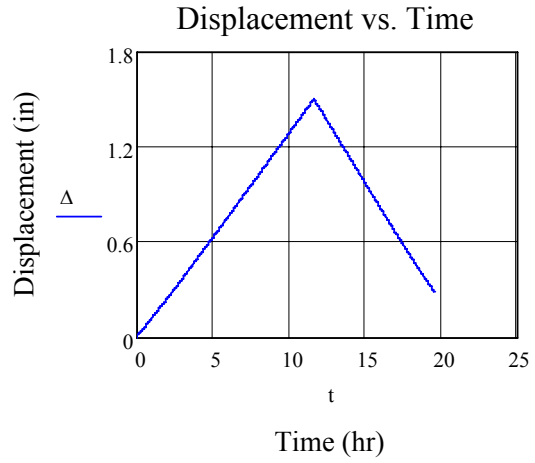
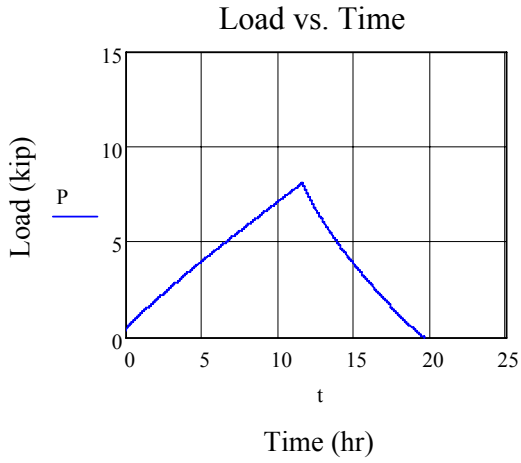


Figure A-40. Shape factor 8, 1.2 ksi compression, 12 hour test 2 data

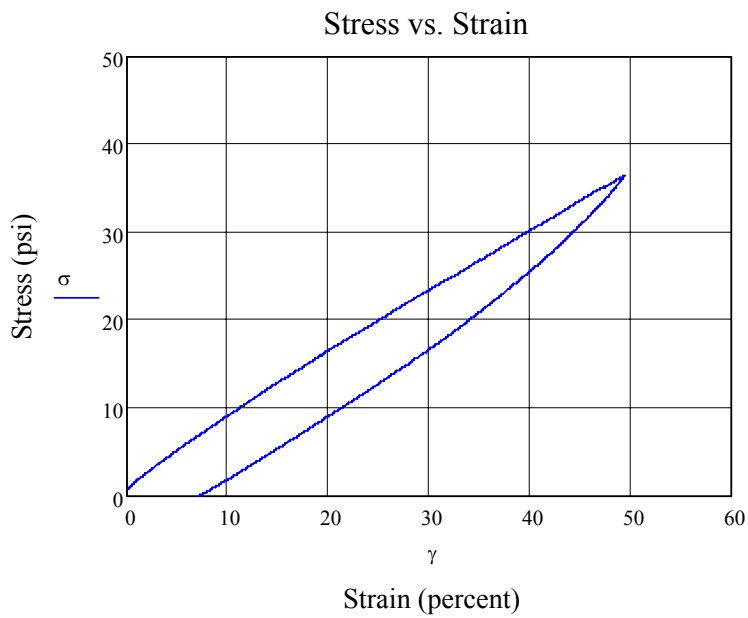
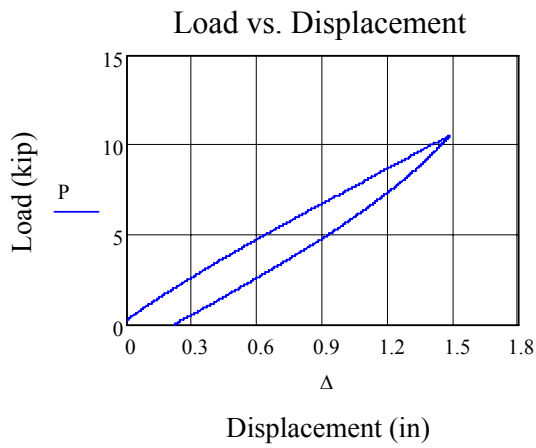
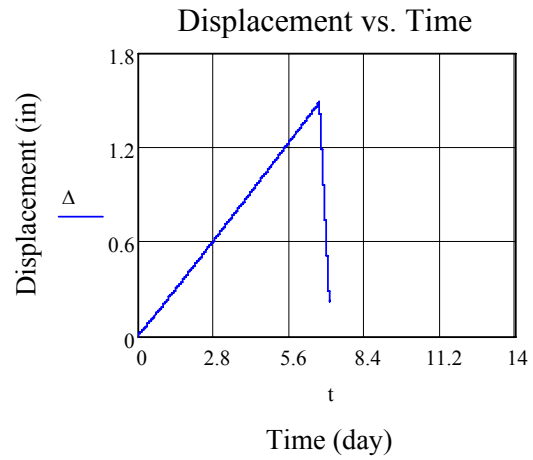
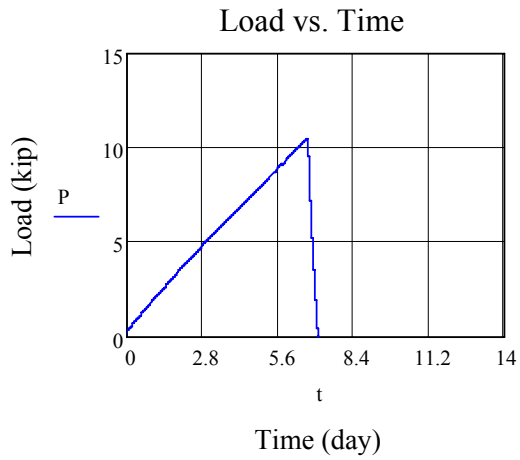


Figure A-41. Shape factor 8, 1.1 ksi compression, 7 day test new pad data

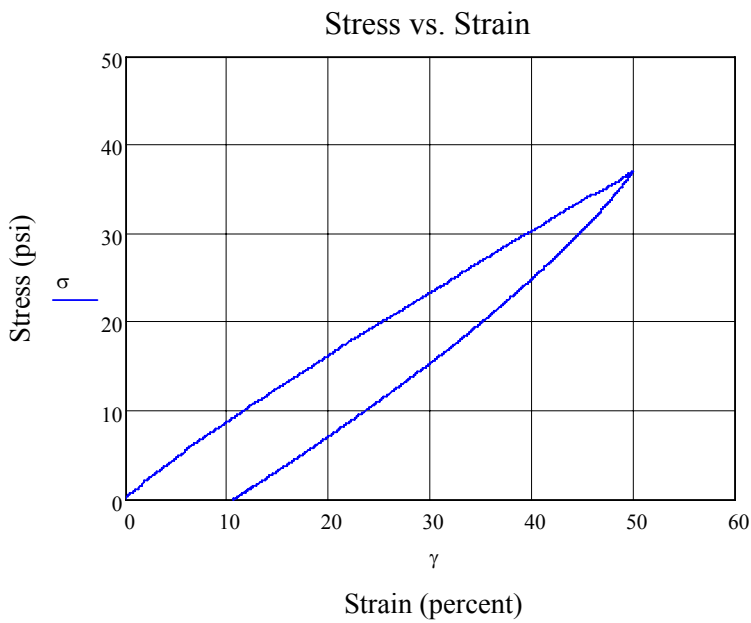
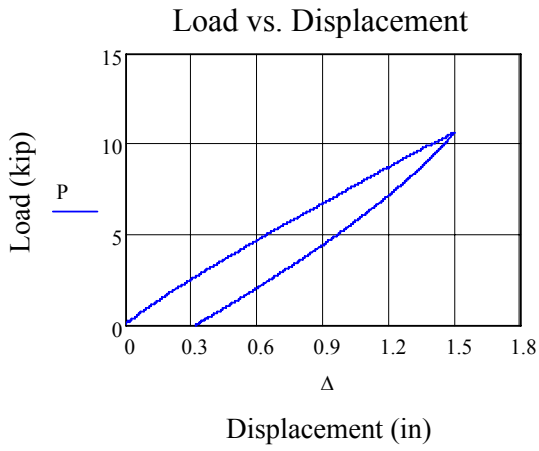
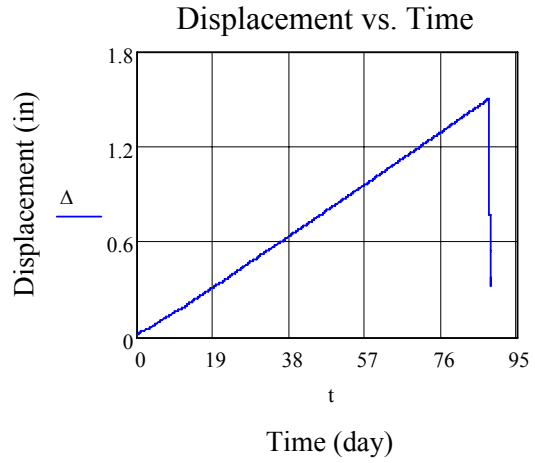
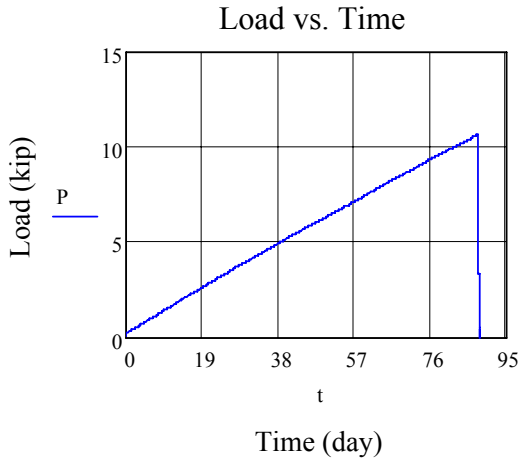


Figure A-42. Shape factor 8, 1.0 ksi compression, 90 day test new pad data

APPENDIX B ADDITIONAL LITERATURE REVIEW

B.1 Additional Literature Summary

It should be noted that not all of the literature reviewed was directly related to the research objective and some was redundant. The literature that fell within these categories is found here.

B.1.1 Elastomeric bearings: state-of-the-art

Roeder and Stanton^[44] reviewed the uses of elastomeric bearings and provide a brief description of the state of the practice with regards to this type of bearing. This includes a discussion of both theoretical and experimental research on elastomeric bearings, this was updated in 1991^[12].

B.1.2 Effect of bearing pads on prestressed concrete bridges

Yazdani, Eddy, and Cai^[45] wrote about the potential benefits of restraining forces coming from elastomeric bearing pads in the design of bridge beams. For the source of these restraint effects Yazdani, Eddy, and Cai noted when properly designed these bearing pads transmit only 5% of the shear due to live loads to the substructure, (cited from AASHTO 1996a). This transmission of live load, however, has a corresponding restraining effect on the beams. In the article they report the results of modeling AASHTO Type III and V beams in two simply supported Florida bridges using a finite element program using modeled after bearing pads vs. rollers. The article provides reports on actual field test results of the shear stiffness of existing bridges vs. the predicted stiffness of those bridges. It reviews previous papers citing stiffening of neoprene pads due to low temperatures and aging of pads. Yazdani, Eddy, and Cai conclude that bridge beams could in some cases have lower midspan moments due to these end restraints. These end restraints provide resistance to the rotation of the beams when they are loaded by

creating a resisting moment. However, using these reductions in design would require a high level of knowledge about the amount these pads restrain the bridge girders.

B.1.3 Restraint effect of bearings

Sen and Spillett^[46] reported on the effects of bearing restraint at temperatures ranging from -2°F to 109°F. For a bridge constructed at 80°F they found that the restraint effect of the bearings reduced the maximum midspan moment of the bridge by 15% at the lowest temperature. Figure B-1 illustrates these restraining effects. Their conclusion included verification of AASHTO predictions of the load distribution.

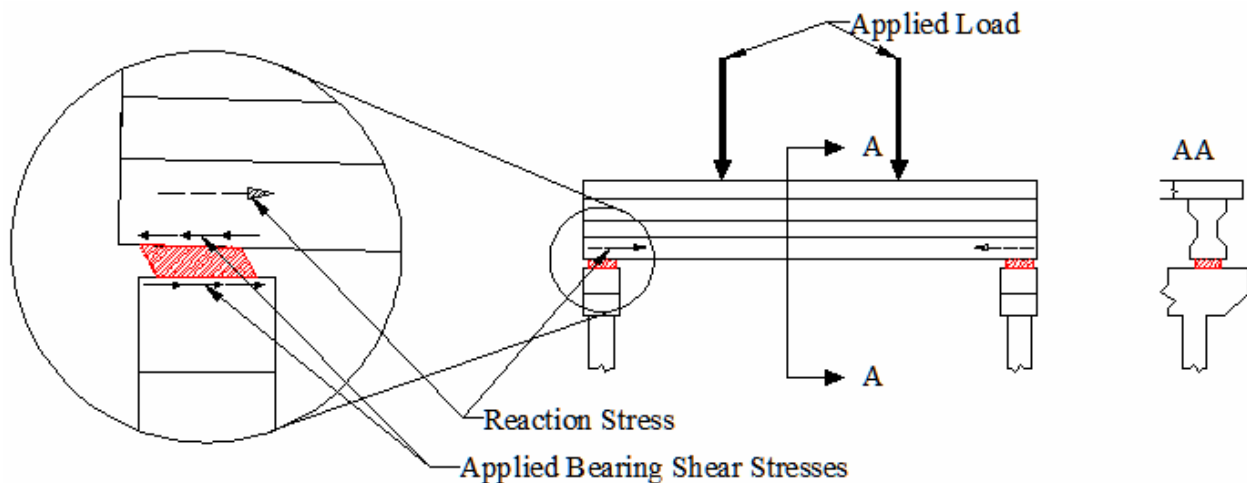


Figure B-1. Expansion restraint – reduction in moment.

B.1.4 Load-deformation characteristics of elastomeric bridge bearing pads

Clark and Moulthrop^[47] reported on a comparison study of three different elastomers: neoprene, butyl rubber and chlorinated butyl rubber (chlorobutyl). This comparison included low temperature effects, accelerated aging and room temperature as control for both shear loading and compression loading. Shear loadings were conducted at a variety of compressive loads and appeared to be a precursor to NCHRP Report 109^[13]. This paper contained data on these various tests, however, in that data it appeared that all samples exhibited creep in both shear and compression. The apparent creep showed up as an increase of deflection over time

once the addition of loading had ceased. The reported data appeared to display creep that increased at a logarithmically decreasing rate over time.

B.1.5 Rotational effects on elastomeric bearings

Both Elastomeric Bearing Pads Under Combined Loading^[48] and NCHRP 12-68^[8] report on the effect of rotation on shear capacity of bridge bearing pads. Both papers tested and modeled a variety of types of elastomeric bearings to develop design procedures with new rotational and compressive limits for AASHTO.

B.1.6 Influence of compression upon the shear properties of bonded rubber blocks

Porter and Meinecke^[49] looked at the contribution of the compressive load to shearing with a sample having a shape factor of 0.625. By taking into account the compressive strain, which increases the effective shear strain and the internal moment induced by eccentric compressive load Porter and Meinecke were able to correct the shear stress-strain to match an uncompressed condition.

The article provides an example based on a circular pad put into compression then sheared. The circular pads were chosen due to the uniform bulge of the pad under compression. Porter and Meinecke provided a description of how the compression of the pads increases the effective shear area. This increased area increases the required force necessary to shear the compressed pad. Additionally it was noted that as the pads decreased height due to their compression a fixed shear displacement would equate to an increase shear strain. The effect of compression, however, was noted as also reducing the shear force needed due to the vector contribution of the compressive force. These effects are described in the following equations:

$$A_s = (1.2 + 2/3u)^2 \pi \tag{B-1}$$

This effective shear area (A_s) is based on an assumed parabolic bulge with Porter and Meinecke citing “Handbook of Chemistry and Physics” the Chemical Rubber Company, 45th edition 1963.

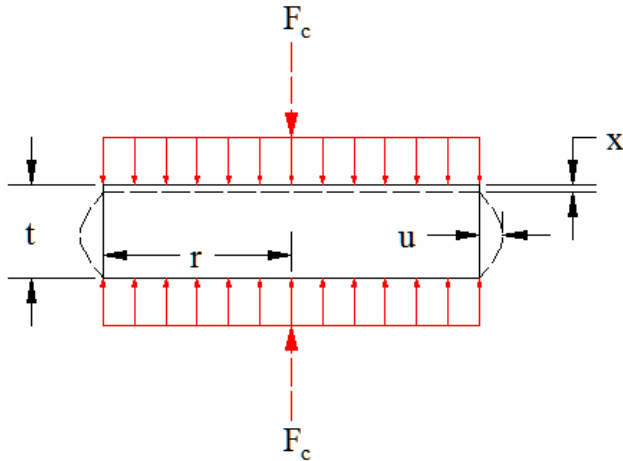


Figure B-2. Pad bulging under compression.^[49] (Source: Figure 1 pp. 1134)

where

$$u = 3rx/(4t)$$

(B-2)

Where u is the peak distance that the pad bulges out (Figure B-2).

x is the compressive deflection

r is the radius of the pad

t is the original thickness of the pad

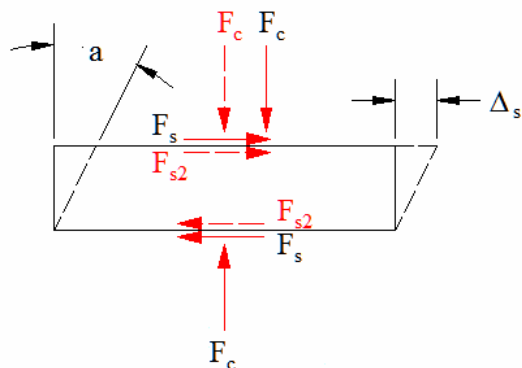


Figure B-3. Pad in original position and in sheared position with shear strain equal to “ a .”^[49] (Source: Figure 4 pp. 1136)

Unfortunately, the bulge equation does not apply to all shapes of bearing pads.

Porter and Meinecke define the compression contribution to the shear force due to the internal moment induced by the offset compression load shown in Figure B-3 as the following:

$$F_{s2} = F_c \sin a \quad (B-3)$$

where

F_{s2} is added to the externally applied shear force to come up with the total shear loading

F_c is the compressive force

$$a = \Delta_s / (t - x) \quad (B-4)$$

Δ_s is the shear displacement

B.1.7 Compression, bending, and shear of bonded rubber blocks

Gent and Meinecke^[50] also make the assumption that the shape of the bulge of a pad under compression is parabolic and provided a reference to the Proceedings of the Cambridge Philosophical Society (1954).

Although Gent and Meinecke do not deal with the combination of compression and shear they do explore the effects of pads bulging on the compressive stiffness of the pad. The following equations are presented:

$$F = f_c A E e \quad (B-5)$$

where

e is the compressive strain

A is the uncompressed cross-sectional area

E is the Young's modulus

$$f_c = f_{c1} + f_{c2} \quad (B-6)$$

where

$$f_{c1} = \frac{4}{3} - \frac{2}{3} (ab + h^2) / (a^2 + b^2 + 2h)^2 \quad (B-7)$$

a and b are the lengths of the sides

h is the original height of the pad

$$f_{c2} = F_2 / A E e \quad (B-8)$$

Where F_2 is derived based on the relationship between compressive strain and maximum bulge displacement k_x . This relationship is a function of the excess hydrostatic pressure due to the restraining effects of the bonded surfaces (Figure B-4). Equation B-9 is the maximum outward displacement of the plane at x . Equation B-11 is generalized for a finite length.

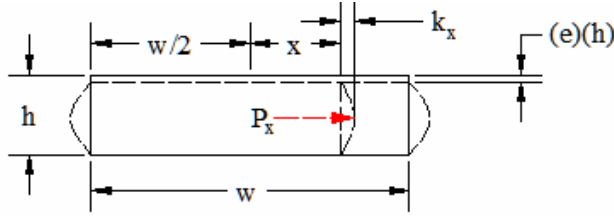


Figure B-4. Cross section of an infinite strip of an elastomer bulging under compression. ^[50]
 (Source: Figure 1 pp. 49)

$$k_x = \frac{3}{2} ex \quad (\text{B-9})$$

$$dP_x = \frac{-8}{3} (Ek_x / h^2) dx \quad (\text{B-10})$$

$$F_2 = \iint P dx dy \quad (\text{B-11})$$

where

P_x is the excess hydrostatic pressure

B.1.8 Behavior of elastomeric bridge bearings: computational results

Hamezeh, Tassoulas and Becker^[51] use finite element models to investigate the shear stiffness of both flat and tapered bearings. These results from finite element modeling including the redistribution of the compressive stress under shear loading. The models revealed that under a shear load the compressive stress redistributes to shift the centroid of the compressive load to mitigate the internal moment in the pad. After this redistribution there is negligible internal moment.

B.1.9 The compression of bonded rubber blocks

Gent and Lindley^[52] review existing theory and conduct experiments to determine the relationship between the shape factor, the addition of carbon black and the Young's modulus of rubber. Based on test using cylindrical disks they concluded that as more carbon black was added the effect of the shape factor on the Young's modulus diminished ultimately reaching half of the theoretical value. This relationship was strictly empirical and based on compressive strains of less than 5%. No additional explanation was provided.

B.1.10 Engineering with rubber

In Engineering with Rubber^[53] (a text by the same name as the Mullins^[10] article) it was noted that the thixotropic or “stress softening” effect is suspected to recover over time. Additionally, stress softening was said to increase with the amount of carbon black used and the amount of carbon black is increased in order to increase an elastomer’s shear modulus. This results in a more pronounced Mullins effect in neoprene with higher shear moduli. The increase of shear modulus in neoprene compared to the amount of the filler carbon black used is shown in Table B-1.

Table B-1. Effect of carbon black on shear modulus of neoprene^[53]

Carbon black (*phr)	25	50	75
Shore A hardness	53	64	78
Shear modulus (psi)	145	180	225
Tensile strength (psi)	325	340	385
Breaking elongation (%)	400	350	300

*phr – Parts by weight per 100 parts by weight of neoprene (Source: pp. 32)

The section of the text about Design of Components noted that there are other relationships that affect the shear stiffness, in particular a correlation between apparent shear modulus, shape factor, and compressive strain. The relationship was presented in the form of the graph in Figure B-5. In the figure, an oval surrounds the part of the graph that most of this study will be dealing with.

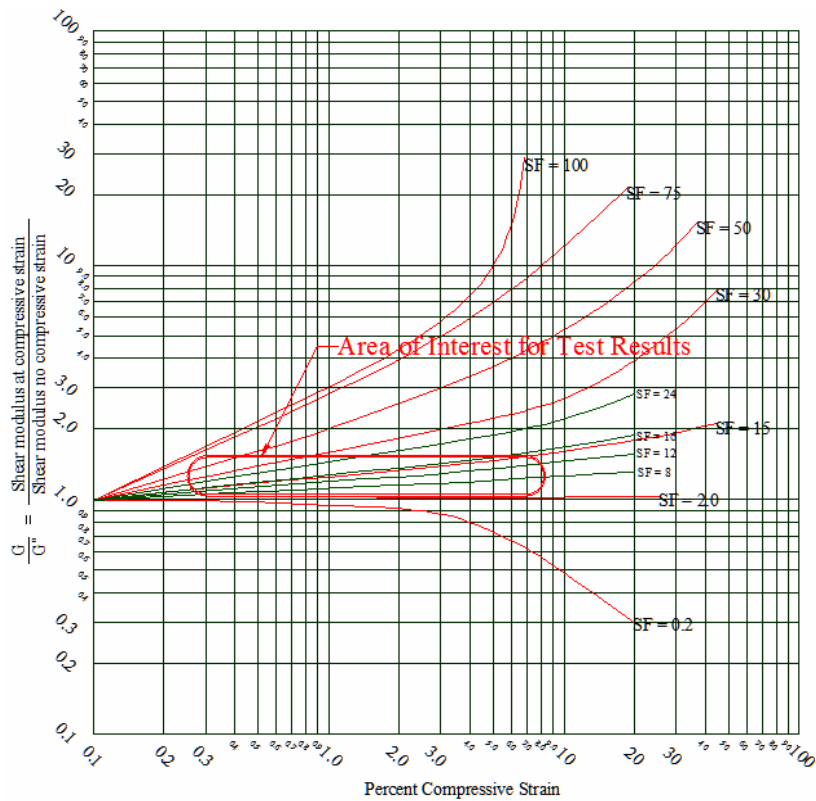


Figure B-5. Relationship between compressive strain, shape factor and apparent shear modulus.^[53] (Source: Figure 8.3 pp. 228)

The author of this portion of the text was contacted to determine the methodology used to develop this graph; the author’s response was that the information is propitiatory. Figure B-5 is to be used in conjunction with Table B-2 and Equation B-12. The Equation B-12 is the effective Young’s modulus^[53].

Table B-2. Coefficient table^[53]

Shear modulus G (kPa)	Young’s modulus E ₀ (kPa)	Bulk modulus E _b (MPa)	Material compressibility coefficient ϕ
296	896	979	0.93
365	1158	979	0.89
441	1469	979	0.85
524	1765	979	0.80
621	2137	1007	0.73
793	3172	1062	0.64
1034	4344	1124	0.57
1344	5723	1179	0.54
1689	7170	1241	0.53
2186	9239	1303	0.52

Note: (Source: Table 8.1 pp. 229)

$$E_c = E_0(1 + 2\phi S^2) \quad (\text{B-12})$$

S is the shape factor of the sample

ϕ is a coefficient provided by Gent to fit data

B.1.11 Stress analysis of rubber blocks under vertical loading and shear loading

Suh^[54] looked at both theoretical and FEA calculations for both bonded rubber and rubber held in place with frictional forces alone. The samples used in testing were chosen to have a small hysteresis and the calculations were based on the assumption of elastic material properties. The conclusions for large shear strains include that the internal normal stresses are in tension throughout the material based on the elastic and incompressible assumption. Suh goes on to state that these stresses are markedly affected by the shape of the free surfaces in the undeformed state.

B.1.12 Hydrostatic tensile fracture of a polyurethane elastomer

Lindsey^[55] investigated the fracture of polymeric materials in hydrostatic tensile fields. In this investigation Lindsey used energy methods of fracture analysis, but there were problems duplicating the ideal boundary conditions imposed by the mathematical treatment.

B.1.13 Steel bridge bearings

Both Roeder and Stanton^[56] as well as Bradberry, Cotham, and Medlock^[57] provide guidelines for designing bearings, including elastomeric bearings, for steel bridges including steel box girders. However, for the shear modulus of neoprene bearing these design guidelines duplicate those found in AASHTO specifications.

B.1.14 Earthquake isolation

References Imbimbo and Kelly^[58], Dicleli^[59], Makris and Zhang,^[60] Tsai and Kelly^[61], Kelly^[62] and Maleki^[63] all report on the use of elastomeric bearings for seismic isolation of structures. All but one of these ignore details of the shear modulus of the elastomer and that

one^[58] treats the elastomer as nonlinear but this is over a shear strain range of up to 500%. The reported nonlinearity was shown using experimental results where the secant shear modulus was seen to drop to approximately half at around 200% shear strain, from 111 psi to 60.5 psi, then rise to approximately double, 215 psi, at 500% shear strain.

B.1.15 Effects of axial load on elastomeric isolation bearings

Koh, and Kelly^[64] investigate the dynamic properties of elastomeric isolation bearings. These include effects of compression on the behavior on the bearings.

B.1.16 Stability of elastomeric isolators: critical load tests and computations

Nagarajaiah and Buckle^[65] looked at the effect of shear displacement had on the critical buckling load in isolation bearings.

B.1.17 Evaluation of low-temperature test methods for elastomeric bridge bearings

Yakut and Yura^[66] review existing test procedures for elastomeric bearings and make recommendations about eliminating and modifying of various tests. These modifications included changing both the AASHTO M251 and ASTM D1043 low temperature tests to more closely reflect the actual conditions that bearings would experience in service.

B.1.18 Parameters influencing performance of elastomeric bearings at low temperatures

Yakut and Yura^[43] investigated the effect of cyclic compression, cyclic shear, rate of loading, type of elastomer compound, temperature history, creep and the slip coefficient. In neoprene, tests run with cyclic compression resulted in a lower compressive modulus if there was a variable temperature history, however, at a constant temperature cyclic compression increased the effective compression modulus. These effects were much less pronounced in natural rubber. In both elastomeric types a slower shear loading rate resulted in a lower shear modulus. The coefficient of friction varied but did not seem to have a significant trend with temperature. This value had a coefficient of variation of 0.07 with the lowest reported value of

0.29. Compressive creep in all samples, as reported as a percentage of initial displacement, increased with decreasing temperature. It was noted that only some of the results of their research were presented in this article while others were presented in other collaborative papers.

B.1.19 Elastomeric bearing design, construction, and materials

Stanton and Roeder^[67] review research on the materials, mechanics, experimental work and design pertaining to elastomeric bearings and elastomers.

B.1.20 Natural rubber structural bearings

Lindley^[68] provides a brief overview of a variety of properties of natural rubber bearings including aspects of their manufacture, variations of stiffness with filler such as carbon black and the effects of dynamic stiffening.

APPENDIX C
RECOMMENDED ADDITIONAL AASHTO LANGUAGE

The following provides a recommended addition to Section 14.7.5.2 of AASHTO LRFD Design Specifications. The addition should be inserted after the second paragraph of Section 14.7.5.2.

CODE	COMMENTARY
<p>Bearings designed using Method B shall be permitted to use a reduction in shear stiffness due to applied compression stress.</p> $G_{eff} = G_0 - \frac{\sigma_s}{\frac{h_T}{2h_r} \left\{ \sqrt{1 + \frac{12If_r}{A_s} \left(\frac{\pi}{h_r} \right)^2} - 1 \right\}} \quad (14.7.5.2-1)$ <p>where:</p> <p>G_e = shear modulus under compression G_0 = shear modulus specified by the designer σ_s = compressive service load on the bearing h_T = total bearing thickness (including steel) A_s = shear area of bearing f_r = ending stiffness coefficient = $1.0 + 0.575 S^2$ I = moment of inertia of the shear area h_r = total elastomer thickness</p> <p>Lateral load calculations shall take into account the variation in the shear modulus due to cycling and strain rate by using equation 14.7.5.2-2.</p> $G_{eff} = G_e \alpha \beta \delta \quad (14.7.5.2-2)$ <p>where:</p> <p>G_e = specified shear modulus of the elastomer under compression</p> <p>$\alpha = 1.12$ for the first five years $\alpha = 1.00$ for cycles after five years</p> <p>$\beta = 0.93$ strain rate effect for shear strains other than those due to impact</p> <p>$\delta = 1.15$ maximum shear modulus modifier $\delta = 0.85$ minimum shear modulus modifier</p>	<p>This accounts for the buckling contribution to the reduction in shear stiffness in steel reinforced elastomeric bearings, Muscarella and Yura (1995). The theoretical basis of this equation limits its use to flat bearings.</p> <p>These provide the two extreme values of shear modulus for calculating the loads induced into the substructure due to super structure lateral movement.</p> <p>Lack of previous shear cycling increases the shear modulus over the reported ASTM value. After repeated cycling this increase in the shear modulus dissipates.</p> <p>An elastomer is required to be within $\pm 15\%$ of the specified shear modulus according to ASTM D4014.</p>

LIST OF REFERENCES

1. *AASHTO Bridge Design Specifications Customary U.S. Units Third Edition 2004*, American Association of State Highway and Transportation Officials, Sections 14.7.5, 14.7.6, 3.4.1.
2. *AASHTO Bridge Construction Specifications Customary U.S. Units Third Edition 2004*, American Association of State Highway and Transportation Officials, Sections 18.1, 18.2.
3. *Structure Specifications for Road and Bridge Construction, 2004*, Florida Department of Transportation, Section 932, Tallahassee, FL.
<http://www2.dot.state.fl.us/SpecificationsEstimates/Implemented/2004Bk/2004Bk.aspx>
Accessed Jan 17, 2006.
4. *Structures Design Office English Standard Drawings, 2005.2*, Florida Department of Transportation, Last revised March 17, 2005, Tallahassee, FL.
<http://www.dot.state.fl.us/structures/CADD/standards/standards.shtm>
Accessed Jan 17, 2006.
5. *Plain and Laminated Elastomeric Bridge Bearings, AASHTO Designation: M 251-06*, American Association of State Highway and Transportation Officials, Washington, DC.
6. *Standard Specification for Plain and Steel-Laminated Elastomeric Bearings for Bridges, ASTM Standard D 4014*, American Society for Testing and Materials, 1995 Annual Book of ASTM Standards, Vol. 04.03, p. 409, Philadelphia, PA.
7. Roeder, C. W., Stanton, J. F., Taylor, A. W., *Performance of Elastomeric Bearings*, National Cooperative Highway Research Program Report 298, University of Washington, Seattle, Washington, 1987.
8. Stanton, J. F., Roeder, C. W., Mackenzie-Helnwein, P., White, C., Kuester, C., Craig, B., *Rotational Limits for Elastomeric Bearings*, NCHRP 12-68, Seattle, WA. December 2006.
9. Meinecke, E. A., Comparing the Time and Rate Dependent Mechanical Properties of Elastomers, The University of Akron, Institute of Polymer Science, Akron, Ohio 44325, Presented at a meeting of the Rubber Division, American Chemical Society, Las Vegas, Nevada, May 20-23, 1980.
10. Mullins, L., *Engineering with Rubber*, Chemtech, December 1987, pp. 720-727.
11. Maguire, C. A. et al, Neoprene Elastomeric Bearings- Ten Years Experience Proves their Importance, *Civil Engineer-ASCE*, November 1967. pp. 37-39
12. Roeder, C. W., Stanton, J. F., Elastomeric Bearings: State-of-the-Art *Journal of Structural Engineering*, Vol. 109 No. 12, December 1983, pp. 2853-2871.

13. Minor, J. C., and Egen, R. A., *Elastomeric Bearing Research*, National Cooperative Highway Research Program Report 109, Battelle Memorial Institute, Columbus, Ohio, 1970.
14. Bell, L. W., Shloss, A. L., Subramanian, N. S., *Additional Design Data Based on Full-Size Bridge Bearing Pads of Neoprene*, Presented to the World Congress on Joint Sealing and Bearing Systems for Concrete Structures. September 28, 1981.
15. Podolny, W. Jr., Muller, J. M., *Construction and Design of Prestressed Concrete Segmental Bridges*, John Wiley & Sons, New York, 1982.
16. Rejcha, C., Design of Elastomeric Bearings *PCI Journal*, October 1964, pp. 62-78.
17. Topkaya, C., Yura, J. A., Test Method for Determining the Shear Modulus of Elastomeric Bearings, *Journal of Structural Engineering*, June 2002, pp. 797-805.
18. Yura, J., Kumar, A., Yakut, A., Topkaya, C., Becker, E., Collingwood, J., *Elastomeric Bridge Bearings: Recommended Test Methods*, , National Cooperative Highway Research Program Report 449, University of Texas, Austin, Texas, 2001.
19. Haringx , J. A., On Highly Compressible Helical Springs and Rubber Rods, and Their Application for Vibration-free Mountings, I. *Philips Research Reports*, 3, 1948 pp. 401-449.
20. Haringx , J. A., On Highly Compressible Helical Springs and Rubber Rods, and Their Application for Vibration-free Mountings, II. *Philips Research Reports*, 4, 1949 pp. 49-80.
21. Haringx , J. A., On Highly Compressible Helical Springs and Rubber Rods, and Their Application for Vibration-free Mountings, III. *Philips Research Reports*, 4, 1949 pp. 206-220.
22. Gent, A. N., 1964, Elastic Stability of Rubber Compression Springs, *Journal Mechanical Engineering Science*, Vol. 6 No. 4, pp. 318-326.
23. Muscarella, J. V., Yura, J. A., *An Experimental Study of Elastomeric Bridge Bearings with Design Recommendations*. Publication FHWA/TX-98/1304-3, Texas Department of Transportation, October 1995.
24. McDonald, J., Heymsfield, E., Avent, R. R., Slippage of Neoprene Bridge Bearings, *Journal of Bridge Engineering*, August 2000, pp. 216-233.
25. English, B. A., Klingner, R. E., Yura, J. A., *Elastomeric Bearings: Background Information and Field Study*. Publication FHWA/TX-95/1304-1, Texas Department of Transportation, June 1994.
26. Heymsfield, E., McDonald, J., Avent, R. R., Neoprene Bearing Pad Slippage at Louisiana Bridges, *Journal of Bridge Engineering*, January/February 2001, pp. 30-36.

27. Malvern, L. E., *Introduction to the Mechanics of a Continuous Medium*, Prentice-Hall, Inc., Upper Saddle River, NJ, 1969.
28. Findley, W. N., Lai, J. S., Onaran, K., *Creep and Relaxation of Nonlinear Viscoelastic Materials with an Introduction to Linear Viscoelasticity*, North-Holland Publishing Company, Amsterdam, New York, 1976.
29. Smith, T. L., Viscoelastic Behavior of Polyisobutylene under Constant Rates of Elongation, *Journal of Polymer Science*, Vol. XX, 1956, pp. 89-100.
30. Yin, T. P., Pariser, R., Dynamic Mechanical Properties of Neoprene Type W *Journal of Applied Polymer Science* Vol. 7, 1963 pp. 667-673.
31. Ronan, S., Alshuth, T., Jerrams, S., An Approach to the Estimation of Long-Term Stress Relaxation in Elastomers, *KCK*, October 2007, pp. 559-563.
32. Green, M. S., Tobolsky, A. V., A New Approach to the Theory of Relaxing Polymeric Media *The Journal of Chemical Physics*, Vol. 14 No 2, February 1946, pp. 80-92.
33. Adkins, J. E., *Some General Results in the Theory of Large Elastic Deformations* Proceedings of the Royal Society of London. Series A, Mathematical and Physical Sciences, Vol. 231, No. 1184, Jul. 19, 1955, pp. 75-90.
34. Schapery, R. A., An Engineering Theory of Nonlinear Viscoelasticity with Applications *International Journal of Solids and Structures*, Vol. 2, 1966, pp. 407-425.
35. Bergström, B., Constitutive Modeling of the Large Strain Time-Dependent Behavior of Elastomers, *Journal of Mechanical and Physics of Solids*, Vol. 46, 1998 pp. 931-954.
36. Arruda, E. M. and Boyce, M. C., A three-dimensional constitutive model for the large stretch behavior of rubber elastic materials, *Journal of the Mechanics and Physics of Solids*, Vol. 41, Issue 2, February 1993, pp. 217-412.
37. Bloch, R., Chang, W. V., Tscgoegl, N. W., The Behavior of Rubberlike Materials in Moderately Large Deformations, *Journal of Rheology* Vol. 22 No. 1, 1978 pp. 1-32.
38. Qi, H. J., Boyce, M. C., Constitutive model for stretch-induced softening of stress-stretch behavior of elastomeric materials, *Journal of the Mechanics and Physics of Solids*, Vol. 52, Issue 10, October 2004, pp. 2187-2205.
39. *Nonlinear Finite Element Analysis of Elastomers – Technical Paper*, MSC Software Corporation, 2000, pp. 1-62.
40. Ferry, J. D., *Viscoelastic Properties of Polymers*, John Wiley & Sons, Inc., London, New York, 1980.

41. Roeder, C. W., Stanton, J. F., Feller, T., *Low Temperature Behavior and Acceptance Criteria for Elastomeric Bridge Bearings*, National Cooperative Highway Research Program Report 325, University of Washington, Seattle, Washington, 1989.
42. Yakut, A., *Performance of Elastomeric Bridge Bearings at Low Temperatures*, Ph.D. Dissertation, University of Texas at Austin, May 2000.
43. Yakut, A., Yura, J. A., Parameters Influencing Performance of Elastomeric Bearings at Low Temperatures *Journal of Bridge Engineering*, August 2002, pp. 986-994.
44. Roeder, C. W., Stanton, J. F., State of the Art Elastomeric Bridge Bearing Design, *ACI Structural Journal*, January-February 1991, pp. 31-41.
45. Yazdani, N., Eddy, S., Cai, S. C., Effect of Bearing Pads on Precast Prestressed Concrete Bridges, *Journal of Bridge Engineering*, August 2000, pp. 224-232.
46. Sen, R. and Spillett, K., *Restraint Effect of Bearings (Phase I)*, A Report on a Research Project Sponsored by the Florida Department of Transportation in cooperation with the U.S. Department of Transportation, January 1994.
47. Clark, E. V., Moulthrop, K., Load Deformation Characteristics of Elastomeric Bridge Bearing Pads, *Highway Research Record #34*, Highway Research Board Washington D.C., 1966, pp. 91-116.
48. Mtenga, P. V., *Project Title: Elastomeric Bearing Pads Under Combined Loading*, FDOT-FHWA Sponsored Research Project, Florida Department of Transportation, March 2007
49. Porter, L. S., Meinecke, E. A., Influence of Compression upon the Shear properties of Bonded Rubber Blocks, Presented at a meeting of the Rubber Division, American Chemical Society, Las Vegas, Nevada, May 20-23. 1980.
50. Gent, A. N., Meinecke, E. A., Compression, Bending, and Shear of Bonded Rubber Blocks, *Polymer Engineering and Science* January 1970, Vol. 10 No 1, pp. 48-53.
51. Hamzeh, O. N., Tassoulas, J. L., Becker, E. B., Behavior of Elastomeric Bridge Bearings: Computational Results, *Journal of Bridge Engineering*, August, 1998.
52. Gent, A. N., Lindley, P. B., The Compression of Bonded Rubber Blocks, *Proceedings / Institution of Mechanical Engineers*, Vol. 173 No 3 1959.
53. Champion, R. P., Ellul, M. D., Finney, R. H., Gent, A. N., Hamed, G. R., Hertz, Jr., D. L., James, F. O., Lake, G. J., Miller, T. S., Scott, K. W., Sheridan, P. M., Sommer, J. G., Stevenson, A., Sueyasu, T., Thomas, A. G., Wang, C., Yeoh, O. H., *Engineering with Rubber ed. 2*, Hanser Publishers, Munich, 2001.
54. Suh, J. B., *Stress Analysis of Rubber Blocks under Vertical Loading and Shear Loading*, Ph.D. Dissertation, Dept. of Mechanical Engineering, University of Akron, August, 2007.

55. Lindsey, G. H., *Hydrostatic Tensile Fracture of a Polyurethane Elastomer*, Ph.D. Dissertation, California Institute of Technology, December 1966.
56. Roeder, C. W., Stanton, J. F., *Steel Bridge Bearing Selection and Design Guide* American Iron and Steel Institute, Highway Structures Design Handbook, Vol. 2, Chapter 4, 1997.
57. Bradberry, T. E., Cotham, J. C., Medlock, R. D. Elastomeric Bearings for Steel Trapezoidal Box Girders Bridges, In *Transportation Research Record: Journal of the Transportation Research Board, No. 1928*, Transportation Research Board of the National Academies, Washington D.C., 2005, pp. 27-38.
58. Imbimbo, M., Kelly, J. M., Influence of Material Stiffening on Stability of Elastomeric Bearings at Large Displacements, *Journal of Engineering Mechanics*, September 1998, 1045-1049.
59. Dicleli, M., Seismic Design of Lifeline Bridge using Hybrid Seismic Isolation *Journal of Bridge Engineering*, March/April 2002, pp. 94-103.
60. Makris, N., Zhang, J., Seismic Response Analysis of Highway Overcrossing Equipped with Elastomeric Bearings and Fluid Dampers, *Journal of Structural Engineering*, June 2004, pp. 830-845.
61. Tsai, H.-C., Kelly, J. M., Stiffness Analysis of Fiber-Reinforced Rectangular Seismic Isolators, *Journal of Engineering Mechanics*, April 2002, pp. 462-470.
62. Kelly, J. M., Tension Buckling in Multilayer Elastomeric Bearings, *Journal of Engineering Mechanics*, December 2003, pp. 1363-1368.
63. Maleki, S., Effect of Side Retainers on Seismic Response of Bridges with Elastomeric Bearings, *Journal of Bridge Engineering*, January/February 2004, pp. 95-100.
64. Koh, C. G., Kelly, J. M., *Effects of Axial Load on Elastomeric Isolation Bearings*, Earthquake Engineering Research Center, UBC/EER-86/12, November 1987.
65. Nagarajaiah, S., Buckle, I., *Stability of Elastomeric Isolators: Critical Load Tests and Computations*, MCEER Bulletin, Vol. 16, No.1, Spring/Summer 2002.
66. Yakut, A., Yura, J. A., Evaluation of Low-Temperature Test Methods for Elastomeric Bridge Bearings, *Journal of Bridge Engineering* January/February 2002, pp. 50-56.
67. Stanton, J. F., Roeder, C. W., *Elastomeric Bearing Design, Construction, and Materials*, NCHRP Report 248, Seattle, WA., August 1982.
68. Lindley, P. B., *Natural Rubber Structural Bearings*, ACI, SP70-20 Vol. 70, January 1981.